Ocular Blast Trauma: Mechanisms of Degeneration and a Potential Therapeutic Strategy

By

Courtney Bricker-Anthony

Dissertation

Submitted to the Faculty of the

Graduate School of Vanderbilt University

in partial fulfillment of the requirements

for the degree of

DOCTOR of PHILOSOPHY

in

Neuroscience

December, 2016

Nashville, Tennessee

Approved:

David J. Calkins, Ph.D.

Tonia S. Rex, Ph.D.

Rebecca M. Sappington, Ph.D.

Kevin L. Schey, Ph.D.

To my incredible husband, Christopher, you're the best.

ACKNOWLEDGMENTS

I want to begin by thanking my advisor, Dr. Tonia Rex, for her guidance throughout my training. Dr. Rex is a tenacious and accomplished young investigator. When I first met Dr. Rex five years ago at the University of Tennessee Health Science Center in Memphis, her passion for science was palpable. Her compassion for wounded veterans is a constant reminder of why our work is so important. My committee has also provided invaluable advice throughout my dissertation research. Dr. David Calkins, the chair of my committee, was an excellent mentor and was always willing to provide advice. Both Dr. Rebecca Sappington and Dr. Kevin Schey challenged me to think about my project in new and different ways. I am immensely grateful for the time and effort my committee put into shaping my project and helping me mature as a scientist.

My experiences with the Rex lab members, both past and present, challenged me to become a better researcher. Jessica Hines-Beard trained me on numerous techniques necessary for my project. I was frequently inspired by her meticulous research and drive to understand the etiology of complex ocular diseases. Dr. Ana de Lucas Cerrillo broadened my understanding of molecular biology and patiently mentored me during my time as a rotation student in the lab. Kristi Wynn helped me gather data and took beautiful OCT images for my project. Dr. Patty Washington helped my project grow and constantly encouraged me with her optimism and fresh new ideas. Dr. Wesley Bond challenged me to think critically about science and to never take anything at face value. Lorraine Kasmala provided beautiful optic nerve and retinal histology for my project. Finally, John Shula, Navya Nadimpalli, Minhee Jo, Addie Clark

and Jackie Cruz (all talented and intelligent undergraduates) assisted me with imaging and quantification.

I am also eternally grateful to my previous mentor at Tennessee Tech University, Dr. Linda Giesbrecht-Bettoli. Dr. GB taught me experimental design in psychology and encouraged me to pursue my interest in research. I will always remember her wonderful advice and equally wonderful dry wit. I am also incredibly indebted to the faculty of the TTU psychology department, Dr. Shannon Morgan, Dr. Matthew Zagumny, Dr. Zachary Wilcox and Dr. Kevin Harris, for their guidance and support.

Finally, I would have never made it through graduate school without the love and support of my family and friends. My wonderful spouse, Chris Anthony, cheered me on and bolstered my confidence in rough times. My amazing mother-in-law, Mary Anthony, let me cook away my first year stress in her kitchen and has supported my endeavors throughout. Wendall and Holly Bricker, my amazing parents, encouraged me to work hard and fight for my dreams from an early age. My parents pushed me to succeed in all of my endeavors, large and small, but never tried to force me into a specific mold or career path. Their loving support and willingness to allow me to find my own way in the world shaped me into the person I am today.

TABLE OF CONTENTS

LIST OF FIGURES

LIST OF TABLES

CHAPTER 1

INTRODUCTION[1]

The prevalence of blast injuries

Blast trauma has become increasingly commonplace over the past several decades. According to the RAND Database of Worldwide Terrorism Incidents (http://www.rand.org/nsrd/projects/terrorism-incidents.html), the number of terrorist bombings increased from 1,190 in the 1970's to 15,239 in the 2000's. Collectively, these explosive attacks injured 118,018 people and killed 36,518 people worldwide. In the United States alone, 28,529 bombings injured 5,931 people and killed 699 people within a 20 year period (Kapur et al., 2005).

Blast trauma is also the hallmark injury of recent conflicts in Iraq and Afghanistan, accounting for 80% of all injuries reported to the Joint Theater Trauma Registry (Bass et al., 2012). Ocular blast injuries are common among blast-exposed veterans, with over 186,000 veterans diagnosed with ocular injuries over a ten year period (Hilber, 2011). Ocular blast injury is also a common comorbid condition with traumatic brain injury and was estimated to affect 66% of veterans with mild traumatic brain injury (Weichel et al., 2009). Ocular blast trauma encompasses a wide variety of clinical and pathological manifestations, which is likely due to the multiple injurious components of explosive devices (DePalma et al., 2005; Scott, 2011).

[1] Portions of this chapter were published as Bricker-Anthony, C (2014). Ocular blast trauma: models, mechanisms, and a potential therapeutic strategy. VRN 6.

Categorizing blast injuries

Blast injuries are split into four major categories: primary, secondary, tertiary and quaternary (Scott, 2011). Explosive devices emit a shockwave or overpressure airwave upon detonation that causes primary blast injuries. Computer modeling of primary ocular blast injuries predicts sharp increases in intraocular pressure, tissue strain and reflection and amplification of pressure waves within the orbit upon exposure to a blast wave (Rossi et al., 2012). Clinically, primary ocular blast injuries are indistinguishable from those caused by blunt force trauma, as both injury mechanisms can cause cataracts, vitreous hemorrhage, retinal edema and traumatic optic neuropathy (Scott, 2011).

Shrapnel and other flying debris from an explosion cause secondary ocular blast injuries (Scott, 2011). Secondary ocular blast injuries include perforations, contusions, lacerations and corneal or intraocular foreign bodies. Pathological features of secondary ocular blast injury include corneal abrasions, damage to structures of the anterior chamber (iris, ciliary body, trabecular meshwork, lens), hyphema, commotio retinae, globe rupture and traumatic optic neuropathy (Scott, 2011).

The remaining two categories of blast injury, tertiary and quaternary, are caused by being thrown against objects and chemical/thermal burns, respectively (Scott, 2011). Tertiary ocular blast trauma can manifest as Purtscher's retinopathy, a condition characterized by vaso-occulsion and hemorrhages in the retinal vasculature (Scott, 2011). Chemical and thermal burns typically damage the sclera, corneal epithelium and conjunctiva.

Categorizing ocular blast trauma

Given the complex nature of explosions, it is no surprise that ocular blast injuries vary widely in severity and visual prognosis from one individual to the next (Erdurman et al., 2011; Phillips et al., 2013; Weichel et al., 2009). These diverse injuries are further classified as either closed globe injuries (contusions and lamellar lacerations) or open globe injuries (Scott, 2011). Both closed and open globe injuries negatively impact vision, but open globe injuries are typically associated with poorer visual outcomes (Erdurman et al., 2011).

Despite occupying different categories, closed and open globe injuries share much common pathology. Both can cause corneal abrasions, hyphema, cataracts, retinal detachment, optic neuropathy and retinal pigment epitheliopathy (Alam et al., 2012; Cockerham et al., 2011; Erdurman et al., 2011; Phillips et al., 2013; Thach et al., 2008). The main difference between the two injury types is the physical disruption of ocular immune privilege with open globe injuries.

The eye is a tightly regulated, immune privileged space that works in concert with the spleen to preserve the integrity of the visual axis (Streilein, 2003). Ocular immune privilege consists of both physical barriers and a complex signaling cascade known as anterior chamber-associated immune deviation (ACAID). Immune privilege within the eye exists to provide controlled responses to infection and injury, avoiding excessive production of inflammatory cytokines that can lead to corneal and lens opacification, as well as retinal edema (Streilein, 2003). Loss of immune privilege and the ensuing inflammation likely contributes to vision loss after blast-induced open globe injuries.

Modeling ocular blast trauma: differences in murine and human ocular anatomy

Every model of human injury or disease confronts several common limitations. Species differences are a substantial challenge for every researcher wishing to mimic any disease or injury in a controlled environment. As with most pre-clinical research, *in vivo* ocular blast injury models are currently limited to rodents (Hines-Beard et al., 2012; Mohan et al., 2013; Por et al., 2016; Wang et al., 2014; Zou et al., 2013). Numerous transgenic and knockout mice are commercially available to study human genetic diseases, which gives mice a slight advantage over rats. In terms of basic anatomy, the eyes of mice and rats are quite similar to human eyes, with some exceptions. Since mice are the most commonly used animals in ocular blast models, I will focus on this species.

Humans have a well-defined lamina cribrosa, a meshwork of elastin and collagen fibers through which the retinal ganglion cell axons converge and exit the eye (Hernandez, 1992). In contrast, mice lack an identifiable lamina cribrosa and instead have a glial lamina composed of astrocytes (Tansley, 1956). Pathological changes in the lamina cribrosa are associated with several forms of glaucoma, especially primary open-angle glaucoma (Hernandez, 1992). At the present time, it is not clear how much stress ocular blast trauma exerts upon the optic nerve head and lamina cribrosa in the patient population. Potentially, mechanical stress from blast exerted upon the human lamina cribrosa could cause the elastin and collagen fibers to physically impinge upon the retinal ganglion cell axons, causing direct injury. Injury to the human lamina cribrosa could also cause increased secretion of matrix metalloproteinases from reactive astrocytes over time, leading to damaging, long-term structural changes (Agapova et

al., 2001). In the mouse glial lamina, mechanical stress could lead to reactive gliosis of the astrocytes, ultimately also leading to pinching of the retinal ganglion cell axons. Blast could also stretch the axons and cause direct injury.

Another key species difference between rodents and humans is the lens. The lens is a translucent structure in the anterior chamber of the eye, composed primarily of α-A and B crystallins (Bloemendal et al., 2004). The structure and conformation of the crystallins contributes to the refractive index of the eye (Bloemendal et al., 2004). While the proteins within the lens are largely the same between species, the shape and size of the lens vary, which results in differences in how light travels through the lens. Mouse and rat lenses are spherical in shape and take up a substantial amount of space within eye, when compared to the human lens (Lei and Yao, 2006). This difference in lens size between mice, rats and humans may pose an issue for models of ocular blast trauma. A larger lens may result in higher numbers of traumatic cataracts, which only occurred in 6% of Veterans in a recent study (Cockerham et al., 2011). Using a porcine model instead of a rodent model may be better for lens research in ocular blast trauma, as the porcine lens is similar in shape and size to the human lens (Lei and Yao, 2006).

Additional differences include the structure and photoreceptor populations of the retina. The ratio of rods to cones varies between the human and mouse retina, with 95% rods to 5% cones in the human retina (Curcio et al., 1990) and 97% rods and 3% cones in the mouse retina (Carter-Dawson and Lavail, 1979). Humans are also trichromats, with short, medium and long wavelength cones, while mice are dichromats and only have short and medium wavelength cones (Huberman and Niell, 2011). The human retina contains a foveal pit densely and exclusively packed with cone

photoreceptors. The fovea is important for high acuity vision, which is created by low convergence of cones to retinal ganglion cells (1:1) and downstream magnification of the foveal representation within the visual cortex (Curcio and Allen, 1990). In contrast, there is no analogous structure to the fovea in the mouse retina. Instead, cones in the mouse retina are segregated by wavelength in the dorsal and ventral retina (Szel et al., 1993). Cockerham and colleagues reported macular damage in 15% of veterans with ocular blast trauma (Cockerham et al., 2011). A recent finite element model of human ocular blast trauma also predicted significant strain on the macula (Rossi et al., 2012). In order to appropriately model visual deficits created by damage to the macula, an alternative to the mouse is required. One of the few other species with a macula and fovea is the non-human primate. Other smaller mammalian alternatives include the cat and the ferret, which lack a fovea and macula but have an area centralis, a region in the central retina specialized for high acuity vision (Rapaport and Stone, 1984).

Even though mice lack some important ocular anatomical structures seen in humans, the structure and function of the anterior chamber of the eye (cornea, iris, aqueous humor, angle, ciliary body) are largely the same in both species. Furthermore, the cell biology of the retina is highly conserved between the two species. Much of our understanding of phototransduction comes from studies conducted in mouse models (Calvert et al., 2000; Humphries et al., 1997). While mice rely heavily upon olfaction to learn about their environment, they also have well-characterized responses to tests of visual function, including visual acuity, contrast sensitivity and evoked potentials (Douglas et al., 2005; Hetling and Pepperberg, 1999). Thus, despite some limitations, a

mouse model is appropriate for studying basic biological responses and changes in retinal cell physiology following ocular blast trauma.

Current models of ocular blast trauma

To date, most ocular blast trauma models only manage to reproduce certain aspects of the plethora of possible pathologies. Additionally, there are no models of open globe blast injury. Current models of ocular blast injury include the shock tube (Mohan et al., 2013; Por et al., 2016; Wang et al., 2014), trinitrotoluene (Zou et al., 2013) and modified paintball marker (Hines-Beard et al., 2012).

Shock tube model

The shock tube model is a two-chambered apparatus divided by a mylar membrane. Compressed air is pumped into one chamber until the mylar membrane ruptures and releases an overpressure airwave into the neighboring chamber, which contains a rat or mouse. Animal placement and restraints vary among researchers and range from full head exposure with body shielding to full body exposure. The shock tube produces low-level overpressure waves ranging from 9.9-20 psi; 20psi is the minimum pressure level for damaging air-filled organs such as the ears and lungs in humans (DePalma et al., 2005). However, repeated exposure to blast pressures as low as 6psi is associated with abnormal changes in visual field and cell loss within the cornea in soldiers during breacher training (Capó-Aponte et al., 2015), so the eye is potentially more vulnerable to low-level blasts. These low-level blasts produce a mild injury phenotype with corneal inflammation and neutrophil infiltration (Por et al., 2016), cell

death within the inner retina and optic nerve pathology (Mohan et al., 2013; Wang et al., 2014), reduced nerve fiber layer thickness (Mohan et al., 2013), acute increases in oxidative stress and degenerative markers and a reduction in pattern electroretinogram (pERG) amplitude (Mohan et al., 2013).

Corneal damage (Por et al., 2016) is consistent with previous findings in blast-exposed individuals (Capó-Aponte et al., 2015; Cockerham et al., 2013; Yonekawa et al., 2014). Transient potential vanilloid 1 channel, endothelin 1, calcitonin gene-related peptide and substance P increases in the cornea (Por et al., 2016) are unsurprising, given the well-established roles of these proteins in nociception (Julius and Basbaum, 2001; Plant et al., 2007). Ocular discomfort is common complaint in blast-exposed patients (Cockerham et al., 2013), so targeted antagonists for nociceptors in the cornea may prove effective at reducing ocular surface pain.

Neutrophil infiltration in the cornea in Por and colleagues' model is important as peripheral immune cell infiltration indicates loss of ACAID in the absence of an open wound. While neutrophils are effective at combating bacterial infections and phagocytosing debris in peripheral sites, they pose a significant threat to the cornea and the rest of the anterior chamber due to their excretion of reactive oxygen species, reactive nitrogen species and inflammatory cytokines (Smith, 1994). Neutrophil-mediated inflammation in the cornea can eventually lead to corneal opacities and blindness (Hall et al., 2001).

Retinal ganglion cell death (Wang et al., 2014), retinal nerve fiber layer thinning (Mohan et al., 2013) and optic nerve degeneration (Mohan et al., 2013; Wang et al., 2014) also align with previously identified pathology in blast-exposed veterans

(Cockerham et al., 2009, 2011; Weichel et al., 2008). The decreased pERG amplitudes and lack of full-field ERG deficits in this model represent the functional outcomes of retinal ganglion cell dysfunction and loss, as the pERG response is specific to retinal ganglion cells (Maffei et al., 1985). Blast-induced optic nerve injury is also associated with poor visual outcomes (Cockerham et al., 2009; Weichel et al., 2008) and is thought to progress in stages (Samardzic et al., 2012).

It is currently postulated that the first stage of traumatic optic neuropathy is mechanical insult to the nerve, such as axonal shearing from globe rotation or a penetrating injury, while the second stage is ischemia in the supporting vasculature (Steinsapir and Goldberg, 1994). These injury phases cause retinal ganglion cell death, inflammation and permanent vision loss in roughly half of patients (Steinsapir and Goldberg, 1994). Unfortunately, the only available treatments are large doses of corticosteroids and decompression surgery (Samardzic et al., 2012; Steinsapir and Goldberg, 1994). These treatment measures are less effective than observation alone (Levin et al., 1999), which suggests that the true molecular mechanisms of traumatic optic neuropathy are still unknown.

Both oxidative stress and beta amyloid are known participants in neurodegenerative changes in several brain and eye diseases and trauma (Dentchev et al., 2003; Ethen et al., 2007; Hardy and Selkoe, 2002; Petersen and Doorn, 2004; Readnower et al., 2010). The presence of 4-hydroxynonenal (4-HNE) in the retina is particularly troubling due to its known cytotoxic effects (Niki et al., 2005). Beta amyloid is also highly toxic to retinal neurons (Jen et al., 1998) and works synergistically with 4-HNE to disrupt cell membrane integrity and neuronal ion homeostasis (Mark et al.,

1997). 4-HNE and beta amyloid were only observed acutely in the shock tube model and likely represent the first phases of blast-induced neurodegeneration (Mohan et al., 2013).

However, the shock tube model does not appear to damage other anterior structures such as the lens, iris and pupil (Mohan et al., 2013; Wang et al., 2014). There are also no reports of gross pathology (edema, hyphema or neovascularization), outer retinal damage (retinal detachments or outer nuclear layer thinning) or pathological changes in the RPE (retinal pigment epitheliopathy or vacuoles). Another potential issue with this model is that the blast is head-directed and not eye-directed. While it may be more valid to opt for full head exposure, it becomes difficult to determine whether the changes in the inner retina and optic nerve are due to ocular injury or brain injury from blast.

A previous study identified axon degeneration in primary visual pathway and inner retinal cell death after a head-directed blast (Koliatsos et al., 2011). Axonal shearing in the optic nerve during blast exposure could initiate Wallerian degeneration of the retinal ganglion cells in the inner retina (Strich, 1961). Currently, the shock tube model is an ideal platform for further characterization of visual deficits in mild traumatic brain injury, but is unlikely to provide specific information about the pathogenesis of ocular blast trauma.

TNT model

While the TNT model of ocular blast trauma also utilizes a whole head exposure approach, it succeeds in inducing some pathology absent in the shock tube model and

accurately recapitulates both primary (overpressure wave) and quaternary (thermal exposure) aspects of blast injury (Zou et al., 2013). This model also incorporates two blast pressures into a single study, including both 70psi and 26psi blasts, which are much higher than the pressures in the shock tube model. A 26psi blast is sufficient to injure the ears, lungs and eyes and possibly the brain and spinal cord, while a 70psi blast can injure nearly every organ in the human body (DePalma et al., 2005). The body is shielded and restrained in this model, which prevents secondary and tertiary injuries, as well as internal organ damage. Unfortunately, the authors did not provide any information regarding the anterior chamber or assess visual function after blast.

In contrast with the shock tube model, the TNT model mainly elicits cell death in the outer retina, as well as increased retinal thickness. The authors also show that increased inducible nitric oxide, aquaporin-4 and vascular endothelial growth factor immunostaining mostly occur within the inner retina, which suggests a significant inflammatory immune response and the potential for future cell death within the inner retina. Additionally, the increased retinal thickness and aquaporin-4 expression imply retinal edema, which is one of the clinical manifestations of ocular blast injury (Abbotts et al., 2007). Surprisingly, the 26psi and 70psi blasts induce similar retinal pathology; this finding suggests that both moderate and high-pressure level blasts are equally damaging when the body is shielded. Overall, the TNT model successfully recapitulates some features of ocular blast injury, but needs further characterization with gross pathology and visual function assessments to determine whether it truly reproduces the injuries observed in clinical settings.

Modified paintball marker

Our laboratory utilizes the modified paintball marker model (Hines-Beard et al., 2012). This model system consists of a paintball marker with a machined barrel that produces overpressure airwaves. C57Bl/6J (Bl/6) mice are secured and completely shielded from the overpressure wave, with the exception of the exposed left eye. This model system is unique because it isolates primary blast trauma to eye alone; this allows us to study the effects of blast exposure on the neural retina and optic nerve without contributions from traumatic brain injury.

Unlike the shock tube model, the modified paintball marker damages multiple anterior structures, including the cornea, lens and extraocular muscles. Intraocular pressure (IOP) decreases significantly over time after blast exposure, which is indicative anterior chamber inflammation and/or injury to the iris or ciliary body (Sanders, SP, 2016). Damage to the anterior chamber is also a significant risk factor for the development of post-traumatic glaucoma (Ozer et al., 2007).

The modified paintball marker also injures the retina. Outer retinal thinning occurs in a small area in the mid-peripheral after injury. Discrete areas of outer retinal thinning (due photoreceptor loss) are commonly observed in commotio retinae and ballistic trauma (Blanch et al., 2012; Blight and Hart, 1977; Sipperley et al., 1978), which suggests the model has a blunt injury component. Blast-exposed individuals also experience retinal thinning in the macula, an area highly enriched with photoreceptors (Phillips et al., 2013).

Additionally, the model induces decreased visual acuity, as measured by optokinectic nystagmus (OKN), in a subset of animals. In a previous study, over 30% of

blast-exposed veterans with ocular injuries had no light perception, while 75% of the veterans with open globe injuries had a final best-corrected visual acuity of 20/200 or less (Weichel and Colyer, 2008). Since we only measured visual acuity in mice without corneal or lens opacities, the changes were likely due to retinal injury. In the mouse, functional directional-selective retinal ganglion cells and starburst amacrine cells are necessary for the OKN response (Yoshida et al., 2001). Therefore, our model system potentially induces both inner and outer retinal injuries.

Given the ability of our model system to recapitulate multiple features of ocular blast injury, we decided to continue characterizing any cellular and molecular changes that occurred after injury. Since ocular blast injuries vary widely in affected individuals, we characterized the injury response in two additional inbred strains of mice, the DBA/2J (D2) and Balb/cJ strains, to determine if different genetic backgrounds would respond uniformly to injury. Following our initial characterization of Bl/6 mice, we chose 26psi as our pressure level of choice moving forward because it consistently induced ocular injuries with a fairly low mortality rate (Hines-Beard et al., 2012).

Summary and specific aims of dissertation

Ocular blast trauma is a persistent threat to vision in both civilian and military populations. There are currently no treatments that can block degeneration of the retina or optic nerve following ocular blast injury. The specific molecular mechanisms underlying ocular blast trauma are also currently unknown. Given our laboratory's ability to effectively recapitulate key features of ocular blast trauma in the mouse (Hines-Beard et al., 2012), we will further characterize the pathological effects of our model system on

the murine retina and optic nerve. Oxidative stress is a common marker of blast trauma, so we will assess the role of oxidative stress in the pathogenesis of ocular blast trauma. Since EPO has both neuroprotective and antioxidant properties, we will evaluate its efficacy for the treatment of ocular blast trauma. We hypothesize that ocular blast trauma causes both acute and long-term neurodegeneration and vision loss that can be blocked by decreasing oxidative stress after blast with EPO treatment. The specific goals of this study are to characterize the progression of neuronal degeneration, test the efficacy of EPO and EPO-R76E at reducing oxidative stress and preserving vision after blast and elucidate the role of oxidative stress.

Aim 1. Determine the progression of neuronal degeneration and vision loss after blast. We will test the hypothesis that ocular blast trauma induces both acute and long-term neuronal injury and vision loss.

We will expose adult Balb/cJ, C57Bl/6J and DBA2/J mice to an eye-directed blast. Assessments of visual function will include optokinetics (OKN) and electroretinogram (ERG). We will collect eyes at 3 days and 1 week (acute) or at 1 month (long-term) post-injury to measure retinal structure. Markers of cell death, lipid peroxidation and nitrosylation will be examined using immunohistochemistry (IHC). Both ipsilateral and contralateral eyes will be examined.

Aim 2. Test the efficacy of EPO-R76E as an antioxidant and neuroprotective agent for blast injury. We will test the hypothesis that acute treatment via EPO protein and

long-term treatment via gene therapy with rAAV2/8.Epo-R76E will protect the retina from blast injury by reducing oxidative stress.

Prior to blast, C57Bl/6J mice will receive an intramuscular injection of viral vector delivering Epo-R76E. Assessments of visual function will include OKN and ERG. We will collect eyes at 28 days and 3 months post-injury to measure retinal structure and cell death. We will perform: 1) *in vivo* imaging to quantify levels of hydrogen peroxide and superoxide, 2) an oxidative stress RT-PCR array, and 3) immunolabeling with markers of lipid peroxidation, nitrosylation, and cell death. Both ipsilateral and contralateral eyes will be examined.

Specific Aim 3: **Determine the role of oxidative stress in neuronal degeneration and vision loss after blast.** We will test the hypothesis that vision loss after blast is mediated by oxidative-stress.

Aim 3A: To test if decreased antioxidant load will exacerbate blast-induced injury, C57Bl/6J mice will be compared to low vitamin C Gulo$^{-/-}$ mice after an eye-directed blast.

Aim 3B: To test if increased antioxidant load will protect the retina from blast injury by decreasing oxidative stress, C57Bl/6J mice will be maintained on a high antioxidant regimen, consisting of dietary supplementation of both vitamin C and E, prior to and following blast.

Assessments of visual function will include OKN and ERG. We will collect eyes at both acute (3 days and 1 week) and long-term (1 month) time points post-injury to measure retinal structure and cell death. We will perform: 1) *in vivo* imaging to quantify

levels of hydrogen peroxide and superoxide, 2) an oxidative stress RT-PCR array, and 3) immunolabeling with markers of lipid peroxidation, nitrosylation, and cell death. Both ipsilateral and contralateral eyes will be examined.

CHAPTER 2

OCULAR BLAST TRAUMA ELICITS RETINAL CELL DEATH, NITROSATIVE STRESS AND VISUAL DEFICITS IN THREE GENETICALLY DISTINCT INBRED MOUSE LINES[2]

Introduction

Genetic susceptibility contributes the pathogenesis of multiple human diseases and injuries, including glaucoma (Libby et al., 2005), age-related macular degeneration (Abecasis et al., 2004), traumatic brain injury (Friedman et al., 1999) and sympathetic ophthalmia (Kilmartin et al., 2001). Several studies have also uncovered varying degrees of genetic susceptibility to ischemia/reperfusion injury (Burne et al., 2000), experimental autoimmune uveitis (Sun et al., 1997) and optic nerve crush (Li et al., 2007) among different strains of inbred mice. Different alleles or even single nucleotide polymorphisms can dramatically alter biological responses to injury or disease. For example, in both Alzheimer's disease and traumatic brain injury, the apolipoprotein E4 allele of the APOE gene reduces amyloid-beta clearance and interferes with phospholipid metabolism, which results in the accumulation of toxic amyloid-beta

[2] Portions of this chapter were published as Bricker-Anthony C, Hines-Beard J and Rex T (2014) Molecular changes and vision loss in a mouse model of closed-globe blast trauma. IOVS 55:4853-4862; Bricker-Anthony C, Hines-Beard J, D'Surney L and Rex TS (2014) Exacerbation of blast-induced ocular trauma by an immune response. J Neuroinflammation 11: 192; Bricker-Anthony C and Rex TS (2015) Neurodegeneration and vision loss after mild blunt trauma in the C57Bl/6J and DBA/2J mouse. PLOS One 10(7); Bricker-Anthony C, Hines-Beard J and Rex TS (2016) Eye-directed overpressure airwave-induced trauma causes lasting damage to the anterior and posterior globe: a model for testing cell-based therapies. J Ocul Pharmacol Ther Epub ahead of print.

plaques, impaired synaptic function and exacerbation of disease or injury (Zhu et al., 2015).

Currently, the role of genetic susceptibility in ocular blast injury is unknown. Responses to ocular blast injury in human patients vary widely in terms of pathological features and visual outcomes (Weichel et al., 2008; Erdurman et al., 2011), but this could due to differences in injury mechanism (e.g., primary vs. secondary blast injury) or severity (closed vs. open globe injury). However, genetic susceptibility should not be ruled out as a contributing factor to the pathogenesis of ocular blast injury, as a simple genetic variant could protect against injury or exacerbate it. Given the genetic heterogeneity of the human population, a single inbred mouse strain is unlikely to capture the full range of potential genetic susceptibility to ocular blast injury. Therefore, we decided to characterize our model of ocular blast injury in three inbred strains of mice commonly used in vision research, including C57Bl/6J (Bl/6) mice, Balb/cJ mice and DBA/2J (D2) mice, which are summarized below.

The Bl/6 is one of the most widely used inbred mouse strains in laboratory research, often serves as the background strain for transgenic and knockout mice and is well-characterized on a wide variety of behavioral assessments (Crawley et al., 1997). The Bl/6 strain is also one of the parental strains (the other parental strain is the D2, described below) for the BXD recombinant inbred mouse line, which is used to map complex genetic traits and explore gene function (Peirce et al., 2004). Among inbred mouse strains, Bl/6 mice are mildly susceptible to both optic nerve injury (Li et al., 2007) and experimental glaucoma (Cone et al., 2010) and are highly resistant to light-induced retinal degeneration (Wenzel et al., 2001). While the genes underlying the Bl/6 mouse's

susceptibility to various ocular insults are still being actively pursued, there is some evidence suggesting that downregulation of crystallin gene expression after optic nerve injury may exacerbate axon loss in the Bl/6 mouse (Templeton et al., 2009). Additionally, a variation in the RPE65 gene in the Bl/6 mouse reduces recycling of rhodopsin in the RPE and reduces light-induced apoptosis of rod photoreceptors (Wenzel et al., 2001). Altogether, the Bl/6 mouse is ideal for characterization of ocular blast injury because it allows for comparison to other models of blast injury using Bl/6 mice, is only mildly susceptible to ocular injury and could be used to explore potential genetic contributors to ocular blast injury.

D2 mice are commonly used in vision research as an animal model of pigmentary dispersion glaucoma (Libby et al., 2005). Mutations in two genes that encode melanosomal proteins, GPNMP and TYRP1, cause leakage of toxic intermediates from melanin production in melanosomes, which leads to inflammation, pigment dispersion and IOP elevation in the D2 mouse (Anderson et al., 2002). The D2 mouse develops glaucoma at approximately 6 months of age (John et al., 1998), but reactive microglia are present in the D2 retina at 3 months of age, indicating a heightened neuroinflammatory state prior to the onset of glaucoma (Bosco et al., 2011). In addition to the glaucoma-related mutations, there are also deletions in the C5 gene and CD94 gene that result in complement component 5 deficiency (Wetsel et al., 1990) and lack of cell surface expression of CD94 (Wilhelm et al., 2003), respectively. C5 is involved in all three complement cascades (classical, alternative and lectin pathways) and is critical for assembly of the membrane attack complex, which forms in the membrane of target cells and initiates lysis (Howell et al., 2013). C5 deficiency makes

the D2 mouse more vulnerable to infection; however, restoration of C5 expression in the D2 exacerbates glaucoma possibly through deposition of the membrane attack complex in diseased retinal ganglion cells (Howell et al., 2013). CD94 is important for induction of anterior chamber-associated immune deviation (ACAID), a molecular cascade that maintains ocular immune privilege in the anterior chamber after infection or injury (He et al., 2008). The lack of CD94 expression in the D2 mouse results in defective ACAID signaling, which allows peripheral immune infiltrate to enter the anterior chamber in response to infection or injury (Chattopadhyay et al., 2008). Surprisingly, despite their susceptibility to glaucoma, D2 mice are highly resistant to optic nerve injury (Li et al., 2007; Templeton et al., 2009). After optic nerve injury, crystallin gene expression increases in the D2 and may exert a protective effect (Templeton et al., 2009). Overall, the D2 mouse is another good candidate for characterization of ocular blast injury because it allows for exploration of altered immune status in an injured state and, like the Bl/6, can also be used to research potential genetic contributors to ocular injury.

Balb/cJ mice are another widely used inbred strain in laboratory research that have been historically used for antibody production and autoimmune research (Pal-Ghosh et al., 2008). When compared to other inbred strains like the Bl/6 and D2, the Balb/cJ strain is highly susceptible to optic nerve injury (Li et al., 2007). The genetic differences underlying the Balb/cJ's susceptibility to optic nerve injury are currently unknown, but several researchers have hypothesized that it is immune-mediated, as the Balb/cJ and Bl/6 vary in their immune responses to experimental autoimmune disease (Li et al., 2007; Kipnis et al., 2001). Other researchers have postulated that downregulation of genes involved in axonal regeneration and synaptic plasticity in the

Balb/cJ after optic nerve injury exacerbate axonal degeneration, but it is unclear if these changes are unique to the Balb/cJ strain (Sharma et al., 2014). The Balb/cJ is also highly susceptible to retinal degeneration induced by light exposure, which is due to genetic variability in the RPE65 gene (Wenzel et al., 2001). Unlike the Bl/6, the Balb/cJ lacks the RPE65 Leu450Met variant and efficiently recycles rhodopsin during light exposure, allowing rhodopsin-mediated apoptosis of photoreceptors to occur (Wenzel et al., 2001). In conclusion, the Balb/cJ mouse is another good candidate for characterizing ocular blast injury as its susceptibility to optic nerve damage may make it useful for studying traumatic neuropathy after blast exposure.

To characterize the progression of ocular blast injury in all three mouse strains, we chose both acute (3 and 7 days) and long-term (1-2 months) time points. At multiple time points, we assessed gross pathology, *in vivo* retinal structure (OCT), visual responses (i.e. optokinetics and electroretinogram), retinal and optic nerve histology, mRNA expression (rt-PCR) and immunohistochemistry to provide a complete characterization of ocular blast injury in each mouse strain.

Materials and Methods

Animals

Three strains of commercially available mice, Bl/6 (n=89), D2 (n=170) and Balb/cJ (n=160) (The Jackson Laboratory, Bar Harbor, ME), between 8-12 weeks of age were used for our characterization studies. All mice were maintained on a 12hr light/dark cycle and provided food and water *ad libitum*. All experimental procedures were approved by the Institutional Animal Care and Use Committee of Vanderbilt University and were in accordance with the Association for Research in Vision and Ophthalmology Statement for the Use of Animals in Vision and Ophthalmic research.

Ocular blast injury

For our initial experiments, mice were anesthetized with an intraperitoneal injection of ketamine/xylazine (105/8 mg/kg). Due to rising mouse mortality rates (22% and higher (Hines-Beard et al., 2012)), we switched to inhalable isofluorane (4%, Vet Equip, Pleasanton, CA), which caused a decline in the mortality rate. The mice were secured and padded within a housing chamber. The housing chamber was placed inside of a pipe. The left eye of the mouse was positioned against the hole in the pipe, which was aligned with the barrel of a paintball marker. All experiments were performed at a blast pressure of 26psi. Sham mice were anesthetized and placed in the housing chamber within the pipe like the blast mice, but a shield was placed between the marker barrel and the eye hold to prevent blast exposure. Mice were provided gel recovery food (Clear H_2O, Portland, ME) for the first 3 days post-injury. Following initial characterization of the blast injury, we applied lubricating, non-medicated eye drops

(Systane Ultra drops, Alcon, Fort Worth, TX) to the corneas of both eyes immediately post-injury to prevent anterior pathologies, which allowed us to conduct assessments of visual function.

Gross pathology

The eyes of awake mice were assessed prior to blast injury and at 0, 3, 7, 14, 28 and 60 days post-injury using an SZX16 stereomicroscope (Olympus, Center Valley, PA). Representative images were taken using a DP71 camera (Olympus). Eyes were examined for the presence of corneal abrasions, corneal edema, hyphemas, cataracts and corneal neovascularization (CNV).

Ultra high resolution optical coherence tomography

Mice were anesthetized with an intraperitoneal injection of ketamine/xylazine (25/10 mg/kg) or inhalable isofluorane (Vet Equip). A 1% tropicamide solution was used to dilate the eyes. Genteal lubricating eye gel (Alcon, Fort Worth, TX) was used to keep the eyes moist. The mice were wrapped in gauze, placed in a holding chamber and head position was stabilized with a bite bar. A Bioptigen ultra-high resolution spectral domain OCT system with a mouse retinal bore and cornea bore (Bioptigen LLC, Morrisville, NC) was used to image the retina and anterior chamber, respectively.

Visual acuity

Photopic spatial frequency thresholds (i.e. visual acuity) were assessed by optokinetic nystagmus (OKN) (OptoMotry, Canada) in awake mice at baseline and post-

blast or sham. A step-wise, masked paradigm was used. Mice were acclimated to the testing chamber for 5 min prior to the initiation of each test. The speed of sinusoidal grating rotation and contrast were maintained at 0.042 c/d and 100%, respectively.

Electroretinogram (ERG)

Flash ERGs were performed at baseline and 28 days post-blast in mice dark-adapted overnight, anesthetized with ketamine/xylazine, dilated with 1% tropicamide, and placed on a heated mouse platform within the Ganzfeld dome of a Diagnosys LLC Espion Electrophysiology system (Lowell, MA). Mice were exposed to flashes of light ranging from -2 to 2.88 log cd*s/m^2 with a flash frequency of 2000Hz. For flashes below -1 log cd*s/m^2, the inter sweep delay was 10 sec, for the -1 log cd*s/m^2 flash it was 15sec, and for all remaining flashes, the delay was 20 sec. Oscillatory potentials (OPs) were measured at 3 log cd*s/m^2 sampled at 2000Hz with an inter sweep delay of 15sec. Amplitudes were measured from trough to peak.

Tissue collection

Mice were euthanized by an overdose of avertin delivered via intraperitoneal injection and transcardially perfused with 4% paraformaldehyde (PFA, Electron Microscopy Sciences, Hatfield, PA) and phosphate buffered saline (PBS). The tissues were collected and stored in either 4% PFA (for immunohistochemistry) or 4% PFA with 0.5% glutaraldehyde (Electron Microscopy Sciences, for resin).

Retina histology

For histological analysis, eyecups were bisected to allow infiltration of Spurr's resin (Electron Microscopy Sciences), sectioned at 1 micron-thickness on a Reichardt-Jung Ultracut E microtome (Leica Microsystems, Vienna, Austria) and stained with toluidine blue. Representative images were collected on an Olympus Provis AX70 with a 60x oil objective lens. To quantify RPE damage, a grading scale was developed to classify the vacuoles: 1 (normal, very infrequent and small); 2 (small and infrequent); 3 (small and frequent); 4 (large and infrequent); and 5 (large and frequent). The number of pyknotic nuclei in the outer nuclear layer (ONL) or inner nuclear layer (INL) was quantified within a single section of retina through the middle of each eye. A masked experimenter performed the imaging.

Optic nerve histology

Optic nerves were placed in 1% osmium tetroxide in 0.1 M cacodylate buffer, dehydrated in a graded ethanol series and embedded in Spurr's resin (Electron Microscopy Sciences). Starting from the proximal (near the eye) end of the optic nerve, 1 μm-thick sections were collected from a Reichert-Jung Ultracute E microtome and stained with 1% p-phenylenediamine in 50% methanol (Sigma-Aldrich). Sections were imaged on an Olympus Provis AX70 microscope using a 100x oil immersion objective lens. Imaging was performed in a masked fashion.

Retina immunohistochemistry

For immunohistochemistry, eyes were cryo-protected in 30% sucrose overnight at 4^{o}C, embedded in Tissue Freezing Medium (Triangle Biomedical, Durham, NC) and then sectioned on a cryostat (Fisher, Pittsburgh, PA). Ten μm-thick sections were collected on 12 slides, with each slide containing representative sections from the entire eye. The sections were rinsed with PBS and incubated at room temperature in normal donkey serum at 1:20 in 0.1 M phosphate buffer with 0.5% bovine serum albumin and 0.1% Triton X 100 (PBT) for 2 hours, followed by an overnight incubation at 4°C in a primary antibody in PBT. The sections were rinsed with PBS and incubated with a secondary antibody at a 1:200 dilution (Life Technologies, Grand Island, NY) for 2 hours at room temperature, rinsed with PBS and mounted in Vectashield Mounting medium with DAPI (Vector Laboratories, Burlingame, CA). Imaging was performed on a Nikon Eclipse epifluorescence microscope (Nikon, Melville, NY). The tissue was assessed in a masked fashion.

TUNEL quantification

Retina sections were labeled with the TUNEL Apoptosis Detection Kit adhering to the manufacturer's protocol (Merck Millipore, Darmstadt, Germany) and mounted with Vectashield Mounting Medium with DAPI. TUNEL positive cells within the ONL, INL and GCL were counted and the lengths of the regions with TUNEL positive cells (affected regions) were measured using NIS Elements Advanced Research software (Nikon, Melville, NY). The total length of each retinal section with TUNEL positive cells (affected section) was also measured. In order to determine the percentage of the retina with cell

death, we measured and summed the lengths of all sections on the slide. Then, we divided the sum of affected region lengths by the total length of all sections and multiplied this value by 100, which yielded the percentage of retina with TUNEL positive cells. Quantification was performed in a masked fashion.

Statistical analysis

The mean and standard error of the mean were calculated and presented for each data set. We performed both one-way and two-way ANOVAs with a Bonferroni's post-hoc test on the visual acuity, ERG, and immunofluorescence quantification data using GraphPad Prism software (GraphPad, La Jolla, CA). We also used GraphPad Prism to calculate a student's *t*-test to compare the means from the TUNEL and immunofluorescence quantification data.

Results

Mild progressive trauma in the C57Bl/6J mouse

Ocular blast trauma causes focal retinal detachments and outer segment disruption

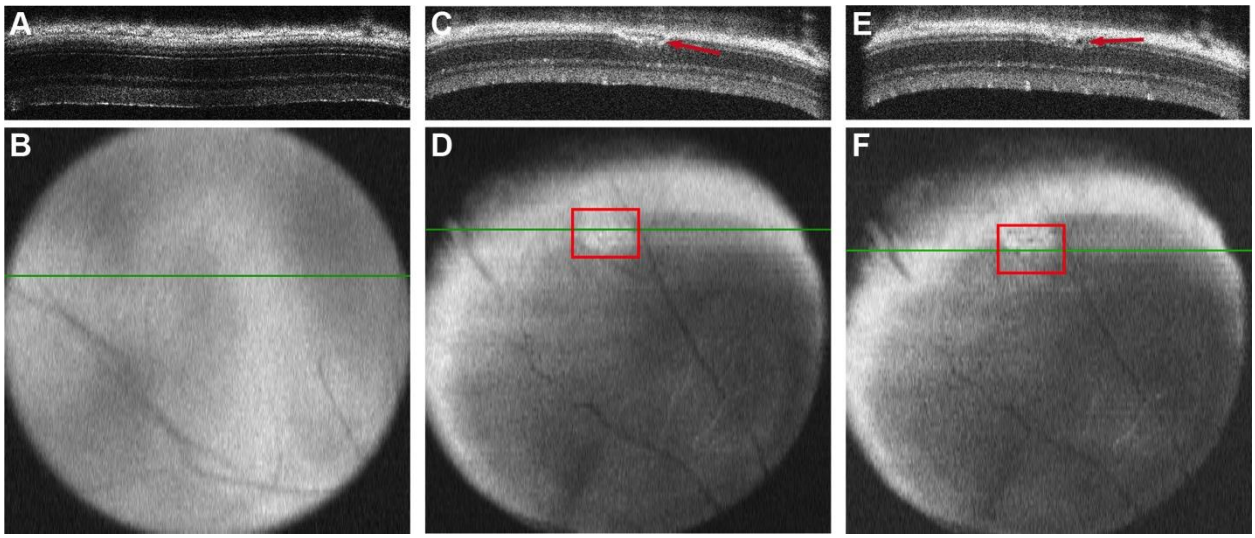

Figure 2.1. Outer segment disruption and retinal detachments occur after blast exposure. B-scan images (A, C, E) show a normal retina (A), outer segment disruption post-blast (C, arrow) and a retinal detachment (E, arrow) post-blast. The green line on the fundus images (B, D, F) denote the location of the b-scan images and the red boxes denote the location of the pathology.

After blast-exposure, the majority of the retina appeared normal (Figure 2.1A-B). However, we detected discrete areas of photoreceptor outer segment disruption (Figure 2.1C-D) in 12% of eyes examined. Outer segment disruption occurred within the mid-peripheral retina and mostly resolved by 1 month post-injury. We also detected retinal detachments (Figure 2.1E-F) in the mid-peripheral retina of 9% of eyes examined. The retinal detachments had a average height of 0.02 mm ± 0.03 and resolved by 1 month post-injury.

Ocular blast trauma damages the retina, RPE and optic nerve

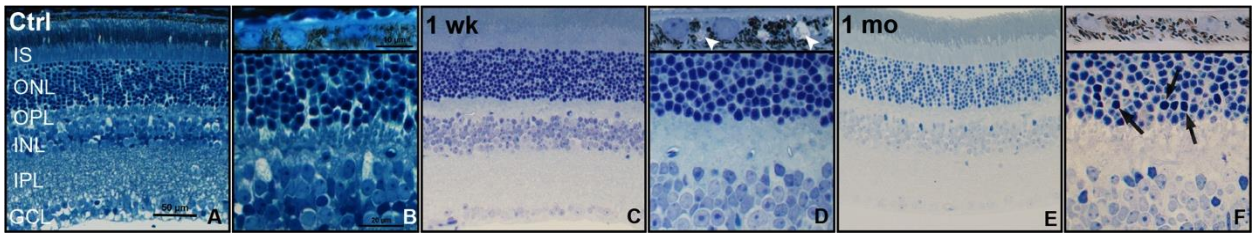

Figure 2.2. Pyknotic nuclei and RPE vacuoles occur after blast exposure. Brightfield micrographs show a control (Ctrl) retina (A-B) and RPE (B, insert), RPE vacuoles at 1 week post-blast (D, arrowheads in insert) and pyknotic nuclei (E-F, arrows) at 1 month post-blast. GCL= ganglion cell layer, IPL= inner plexiform layer, INL= inner nuclear layer, OPL= outer plexiform layer, ONL= outer nuclear layer, IS= inner segments.

Blast exposure induced focal damage in all eyes examined at 1 week and 1 month post-blast. At 1 week post-injury (Figure 2.2C-D), the ONL contained an average of 2 ± 1 pyknotic nuclei and the INL contained an average of 2 ± 2. The number of pyknotic nuclei increased to 15 ± 12 in the ONL and 7 ± 4 in the INL at 1 month post-injury (Figure 2.2E-F). In contrast, small RPE vacuoles occurred in all eyes examined at 1 week post-injury (Figure 2.2C, insert), but rarely occurred at 1 month post-injury (Figure 2.2F, insert).

At 1 and 2 weeks post-injury, the optic nerves appeared similar to controls (Figure 2.3A). However, at 1 month post-injury (Figure 2.3, B, arrowheads), we detected a few degenerating axon profiles in 60% of nerves examined.

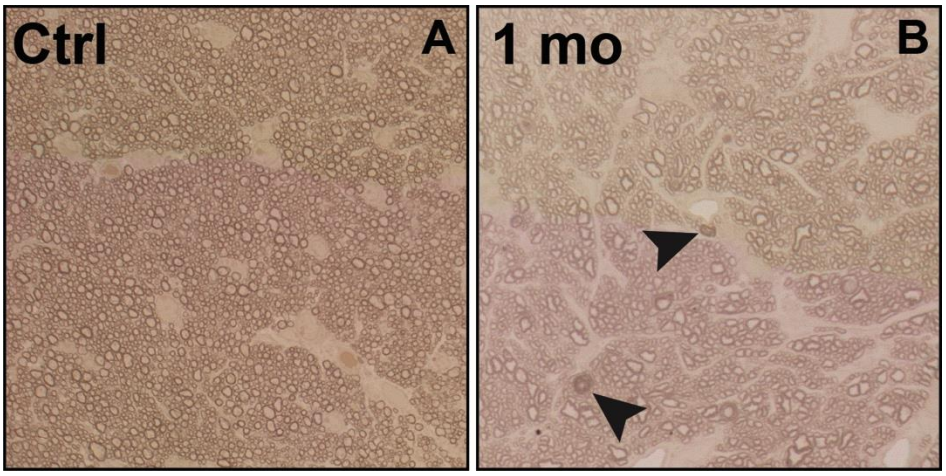

Figure 2.3. Blast causes mild axonal degeneration. Brightfield micrographs show a healthy control optic nerve (A), a 1-month post-injury optic nerve with degenerating axons (B, arrowheads) and a 3 month optic nerve degenerating axons (C, arrowheads).

Ocular blast trauma elicits focal, delayed cell death in a subset of mice

All control, 3 day post-injury and 1-week post-injury retinal sections were TUNEL-negative. At 1 month post-injury, we observed TUNEL-positive nuclei in 3 ± 2 % of the retina in 44% of eyes examined. Clusters of TUNEL-positive cells (defined as 5 or more TUNEL-positive nuclei in an 85 μm^2 area) were primarily located in the mid-peripheral retina and occasionally in the central retina (Figure 2.4A-B,D). The clusters contained 91 ± 49 TUNEL-positive cells, while the average number per mm total retina was 4 ± 3. The majority of TUNEL-positive nuclei were located in the ONL (92%), 8% were present in the INL and none were detected in the GCL. At 3 months post-injury, the percent retina containing TUNEL-positive cells increased to 10 ± 5 % in 83% of eyes examined. Similar to 1-month post-injury, clusters of TUNEL-positive nuclei were restricted to the mid-peripheral retina. The clusters contained 147 ± 38 TUNEL-positive cells, while the average per mm total retina was 53 ± 28. Unlike 1 month post-injury, TUNEL-positive

cells were present in all layers, with 77% in the ONL, 20% in the INL and 2% in the GCL.

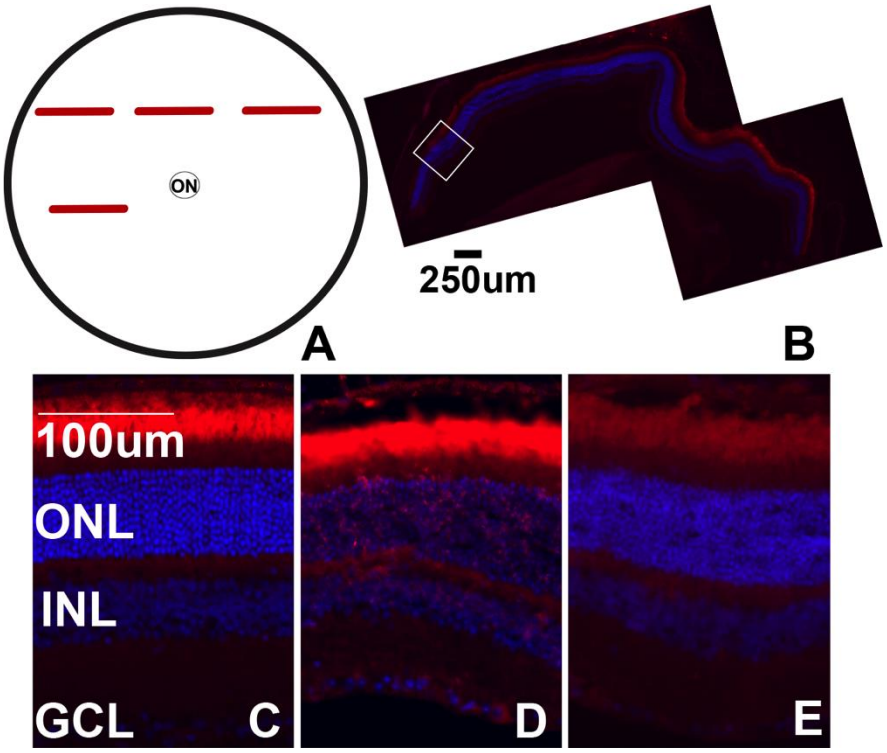

Figure 2.4. Cell death post-blast is focal. Schematic of a flat-mounted retina, red bars indicate regions within retinal cross-sections that are TUNEL-positive (A). Epifluorescence micrograph of a TUNEL-positive mid-peripheral retinal cross-section from a 1-month post-blast eye (B). The white box indicates a cluster of TUNEL-positive cells. Representative epifluoresence micrographs of retinas from control (C) or 1-month post-blast retinas labeled with TUNEL (red) and DAPI (blue). A cluster of TUNEL positive cells (D) and a TUNEL-negative area (E) from the same blast eye are shown. ON= optic nerve.

Blast induces nonapoptotic cell death

At all time points post-blast, changes in RIP1 and RIP3 immunolabeling were restricted to 2-3 sections in the mid-peripheral and sometimes central retina, consistent with the localization and extent of TUNEL labeling. Antibody specificity was confirmed by immunolabeling of retinas from buffer or LPS-injected eyes (Figure 2.5B). At 3 days post-injury, there was a strong increase in RIP1 staining within the Müller glia and IPL

and a reduction in RIP3 labeling, as compared to controls (Figure 2.5A, C). At 1-month after blast, RIP1 labeling was slightly elevated while RIP3 labeling appeared to increase above control levels in the IPL and INL (Figure 2.5D). RIP3 labeling was also present in the ONL at 1 month post-blast (Figure 2.5D).

No caspase-1 labeling was detected in control retinas (Figure 2.5E), but positive cells were detected in inner retinal neurons throughout the retinas of LPS-injected eyes (Figure 2.5F). A few caspase-1 labeled cells were present in the inner portion of the INL in 1 of 4 retinas at 3 days after blast. Positive cells were restricted to small regions, primarily in the mid-peripheral retina (Figure 2.5G). Caspase-1-positive cells were present throughout the ganglion cell layer (GCL) in 2 of 3 retinas at 1-week post-injury (Figure 2.5H). At 1-month post-injury, caspase-1-positive cells were present throughout the retina in the inner portion of the INL and occasionally in the GCL in 4 of 5 eyes (Figure 2.5I). The density of caspase-1-positive cells was much higher at 1 month than at 3 days or 1-week post-blast. However, at 3 months post-blast, caspase-1 positive cells were only occasionally observed in the GCL within the mid-peripheral retina. Double-labeling with choline acetyltransferase (ChAT) revealed colocalization in the majority of cells (Figure 2.5J). There was no colocalization of caspase-1 with tyrosine hydroxylase (TH), a marker of dopaminergic amacrine cells (Figure 2.5K).

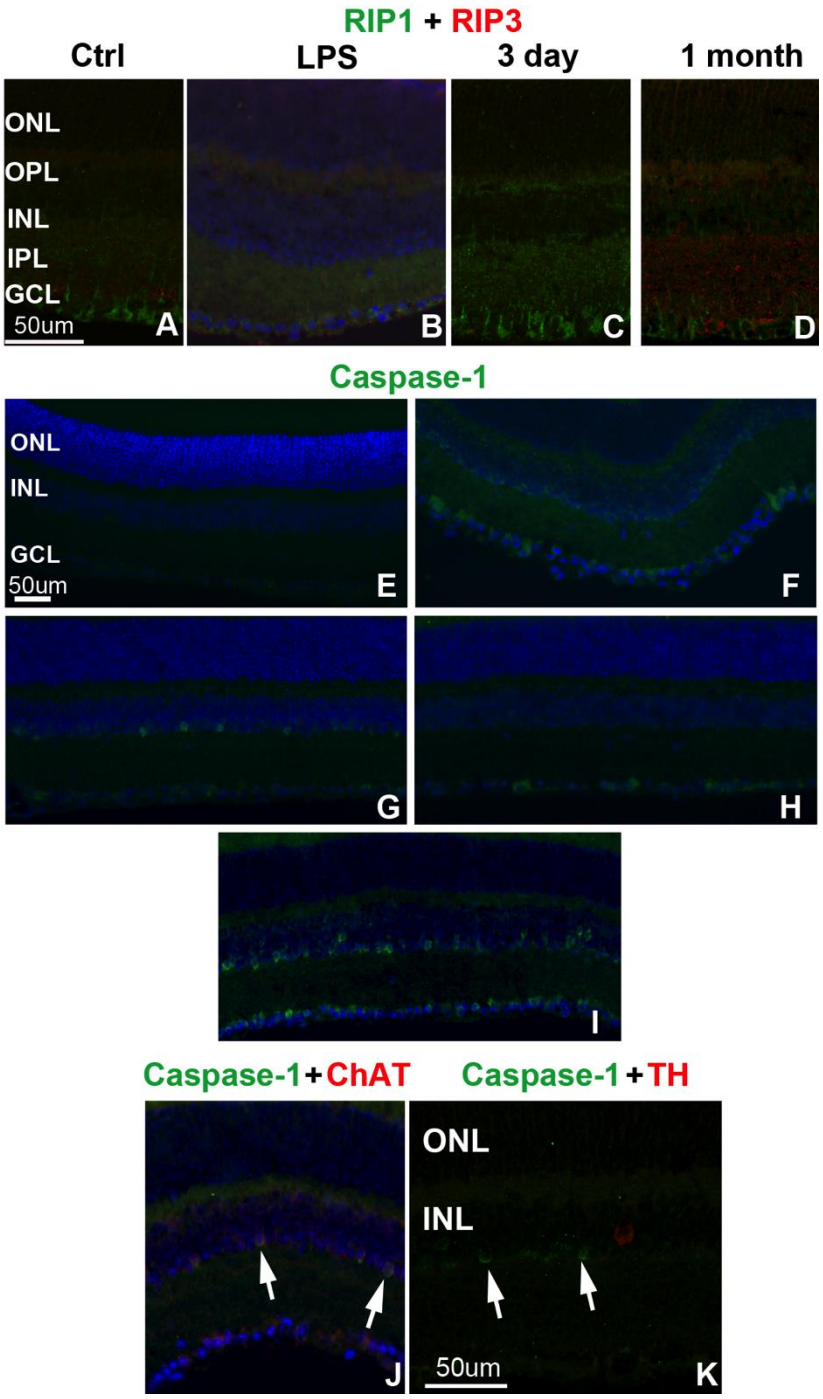

Figure 2.5. Increased cell death pathway marker labeling after blast. Confocal micrographs of RIP1 (green) and RIP3 (red) immunolabeling in control (A), LPS-injected (B) and affected areas (mid-periphery) of 3 day (C) and 1 week (D) post-blast retinas. Epifluorescence micrographs of caspase-1 immunolabeling (green) and DAPI (blue) in control (E), LPS-injected (F) and affected areas in 3 day (G) and 1 week (H) post-injury retinas. The entire retina was caspase-1 positive at 1 month post-blast (I). Epifluorescence micrographs of caspase-1 (green) and ChAT (red, J) or TH (red, K) double-labeling, arrows indicate caspase-1 positive nuclei.

Blast induces glial reactivity

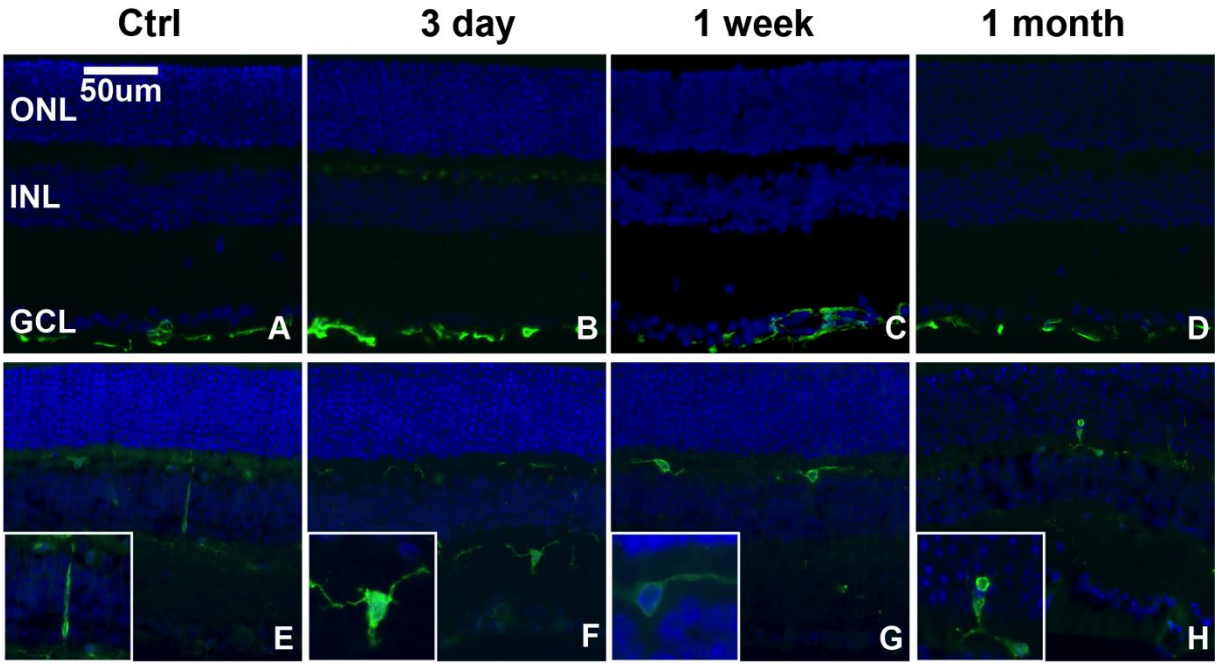

Figure 2.6. Microglia, but not Müller glia, become reactive in response to blast in focal regions of the retina. Epifluorescence micrographs of GFAP immunolabeling (green) in control (A) and in 3 day (B), 1 week (C), and 1-month (D) post-blast retinas. Iba-1 immunolabeling (green) of microglia in control (E), 3 day (F), 1 week (G) and 1-month (H) post-blast retinas. Insets show higher magnification of representative microglia. DAPI labeled nuclei (blue).

Glial fibrillary acidic protein (GFAP) labeling was similar to controls at all time points post-blast (Figure 2.6A-D). In the normal retina and in unaffected regions of the blast retinas, microglia had a typical ramified appearance and small cell body, and their localization was restricted to the inner retina (Figure 2.6E). Within small regions in the mid-peripheral and, occasionally, central retina of 3 day and 1 week post-blast retinas, the microglia exhibited shorter processes and larger cell bodies, indicative of a more reactive state (Figure 2.6F-G). At 1 month after blast, the microglia were amoeboid in appearance and were detected in the ONL (Figure 2.6H).

Blast causes increased nitrotyrosine immunolabeling

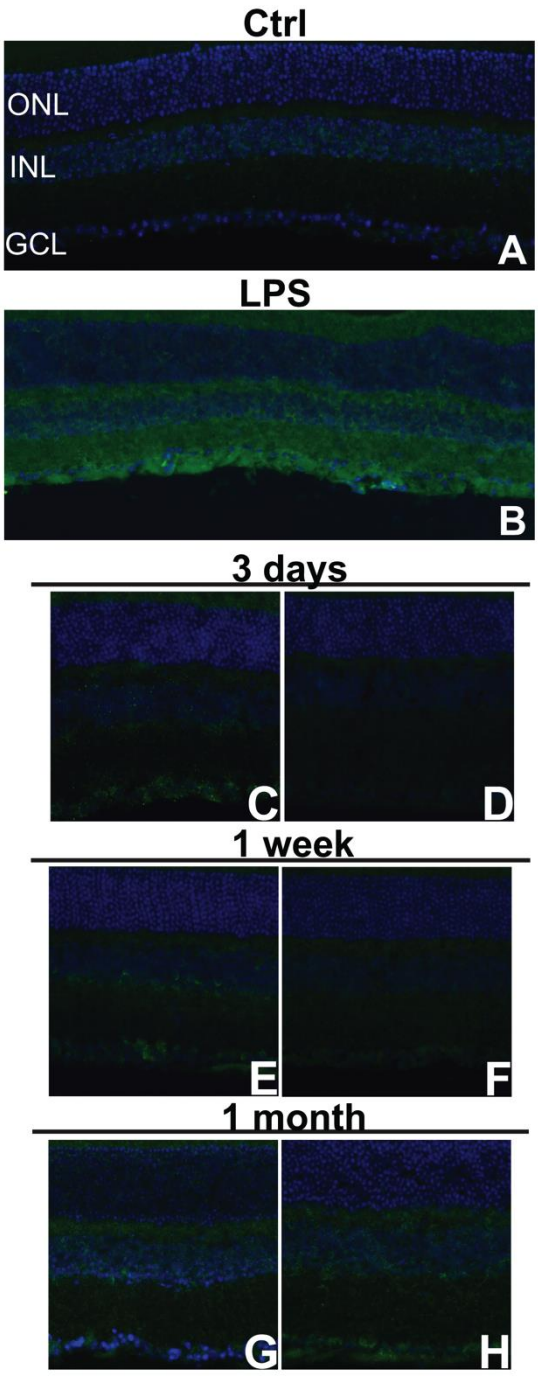

Figure 2.7. Nitrotyrosine immunolabeling increases regionally after blast. Epifluorescence micrographs of control (A), LPS-injected (B) and mid-peripheral (C,E,G) and central (D,F,H) regions of 3 day (C,D), 1 week (E,F) and 1 month (G,H) post-blast retinas labeled with anti-nitrotyrosine (green) and DAPI (blue).

Light nitrotyrosine immunolabeling was present in the normal retina (Figure 2.7A) and labeling was brighter in retinas from LPS injected eyes, as expected (Figure 2.7B). At 3 days and 1 week post-injury, nitrotyrosine was elevated in the inner retina of the mid-peripheral (Figure 2.7C,E), but not central (Figure 2.7D,F), retina. The labeling appeared strongest in the inner portion of the INL (Figure 2.7E). At 1 month post-blast, increased and diffuse immunolabeling was detected in the inner and outer retina and extended throughout the retina (Figure 2.7G-H).

Ocular blast trauma induces transient visual deficits

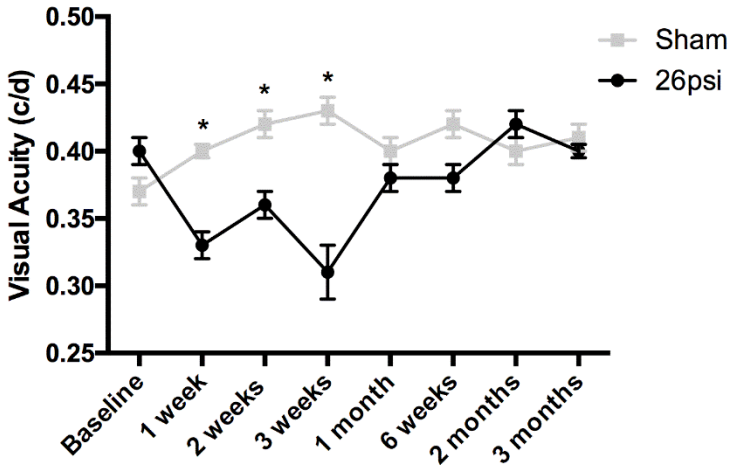

Figure 2.8. Blast induces visual acuity deficits. Visual acuity (mean ± SEM) was significantly reduced in blast-exposed mice at 1 week, 3 weeks and 1 month post-blast when compared to sham mice. *p<0.05

Within the first month post-injury, blast-exposed mice exhibited subtle, but statistically significant deficits in visual acuity when compared with sham mice (Figure 2.8). Visual acuity in blast mice was significantly lower than sham mice at 1 week (0.33 ± 0.01 c/d vs. 0.40 ± 0.005 c/d), 2 weeks (0.36 ± 0.01 vs. 0.42 ± 0.01) and 3 weeks

(0.31 ± 0.02 vs. 0.43 ± 0.01) post-blast. At 1 month post-injury, visual acuity improved in blast-exposed mice and was not significantly different from sham mice. In contrast, ERG a wave amplitudes (Figure 2.9A, C, E, G, I), b wave amplitudes (Figure 2.9B, D, F, H, J) and oscillatory potential amplitudes (Figure 2.10A-C) were not significantly different among blast and sham mice at any time point.

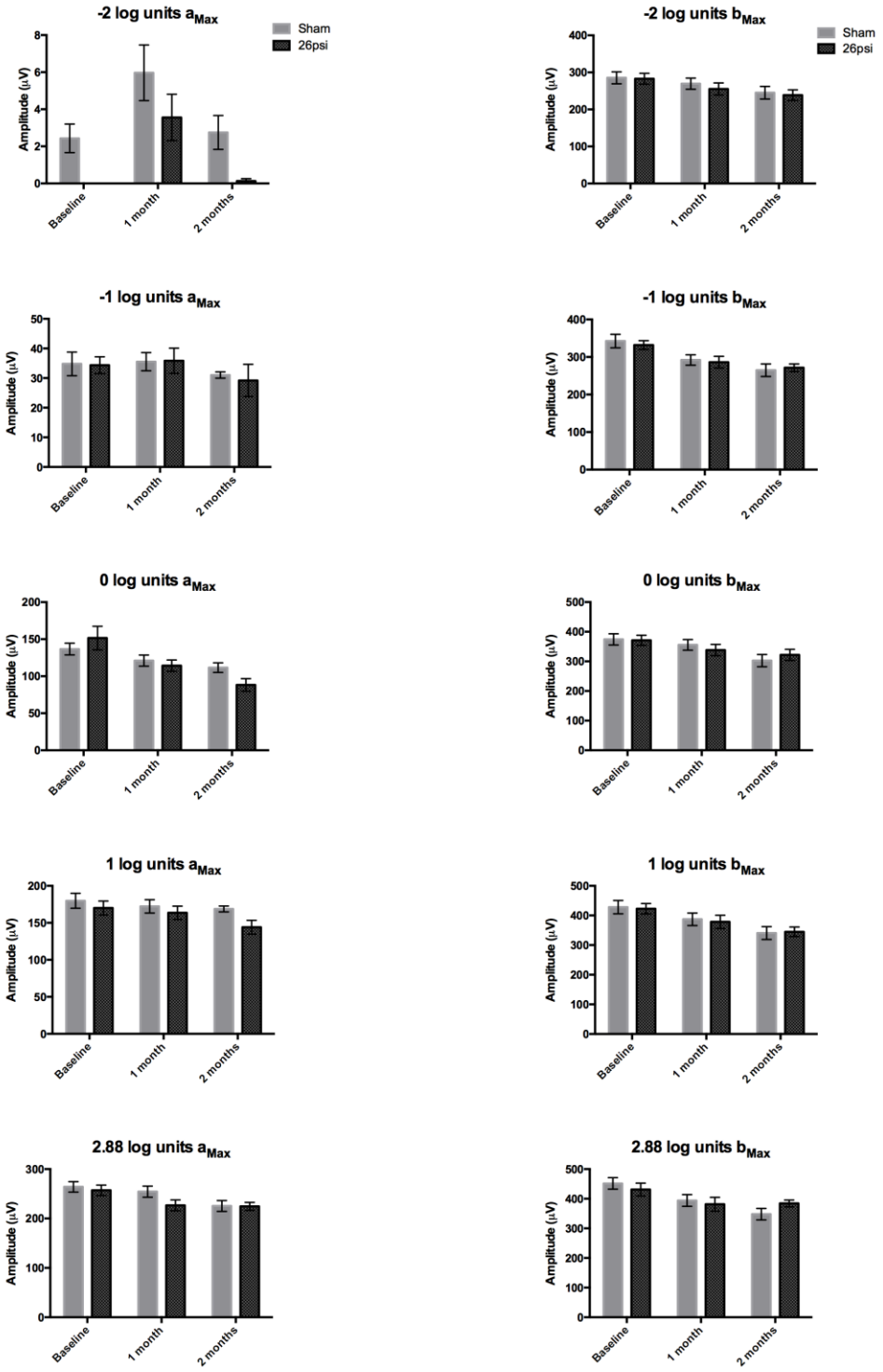

Figure 2.9. Ocular blast trauma does not affect ERG amplitudes. Both ERG a_{max} values (A, C, E, G, I) and b_{max} values (B, D, F, H, J) were not significantly different between blast and sham animals. All values represent the mean ± SEM.

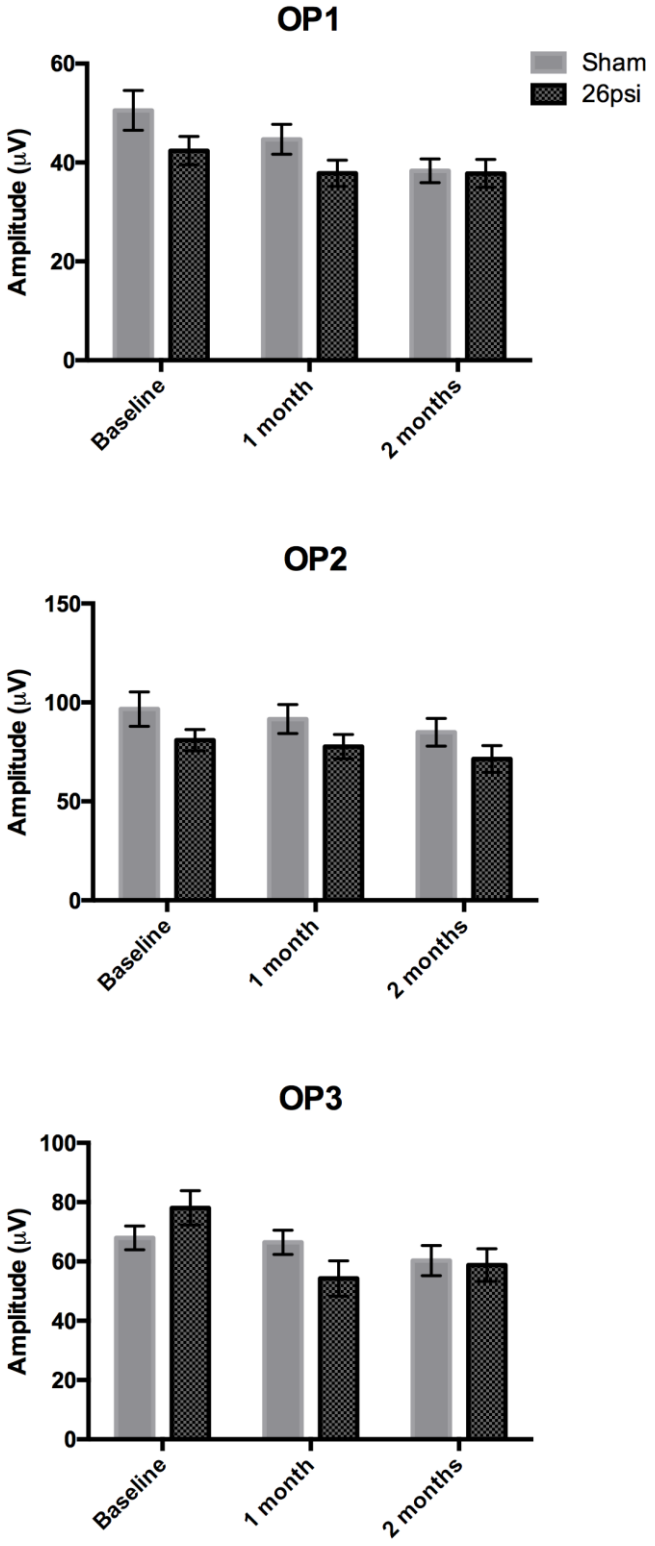

Figure 2.10. Blast exposure does not change oscillatory potential amplitudes. There were no differences between blast and sham mice in OP1 (A), OP2 (B) or OP3 (C). All values represent the mean ± SEM.

Severe trauma in the DBA/2J mouse

Blast exposure damages the anterior pole

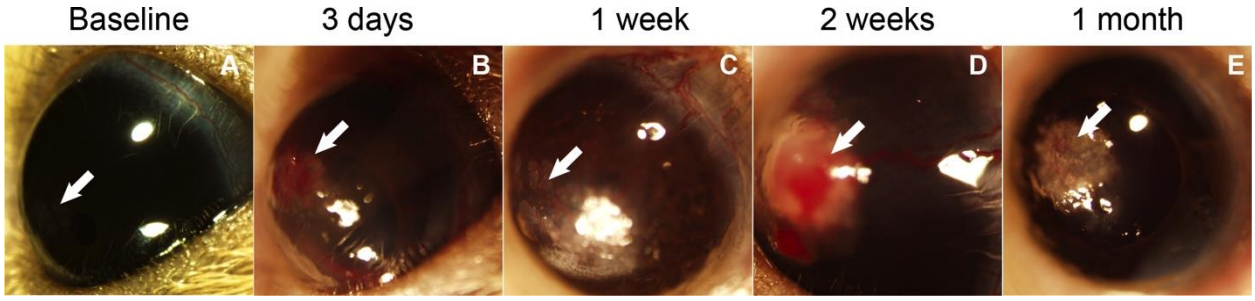

Figure 2.11. Blast trauma injures the ocular surface. The majority of mice had calcium deposits in the cornea at baseline (A). Corneal edema and hyphema at 3 days post-blast (B). Corneal edema and neovascularization at 1 week post-blast (C). A corneal growth with neovascularization and hyphema at 2 weeks post-blast (D). Corneal scarring and neovascularization at 1 month post-blast. Arrows indicate pathologies (E).

Blast caused numerous anterior injuries that varied depending on time after blast (Table 1). Representative images of these pathologies after exposure to a 26psi blast are shown in Figure 1. The eyes appeared normal immediately after blast, but at 3 days (Figure 2.11B) significant pathologies were present including corneal edema (CE), hyphema, cataracts, and a few cases of corneal neovascularization (CNV). The incidence of CE after a 26psi blast remained high (86% of eye examined) out to 1 month post-injury (Figure 2.11E). The incidence of hyphema peaked at 3 days after blast and was completely absent at 1 month post-blast. The incidence of hyphema at 3 days after blast was 26%. In contrast, the number of eyes with CNV increased over time post-blast. At 3 days post-blast 17% of blast eyes exhibited signs of CNV. At 1 month, 29% of blast eyes had CNV.

Table 1. DBA/2J gross pathology post-blast					
	0 day	3 days	1 week	2 weeks	1 month
Type of Injury	(24)[a]	23	14	9	7
Corneal abrasion	4 (17)[b]	1 (4)	0	0	0
CE	0	16 (70)	5 (36)	5 (56)	6 (86)
CNV	1 (4)	4 (17)	2 (14)	4 (44)	2 (29)
Corneal scarring	0	2 (9)	1 (7)	4 (44)	5 (71)
Hyphema	0	6 (26)	1 (7)	0	0
Corneal growth	0	0	0	1 (11)	1 (14)
Torn iris	0	0	0	1 (11)	2 (29)
Traumatic cataract	0	8 (35)	1 (7)	1 (11)	1 (14)

[a] Total number of eyes examined

[b] Number of eyes with pathology (percentage)

Ocular blast trauma causes retinal detachments

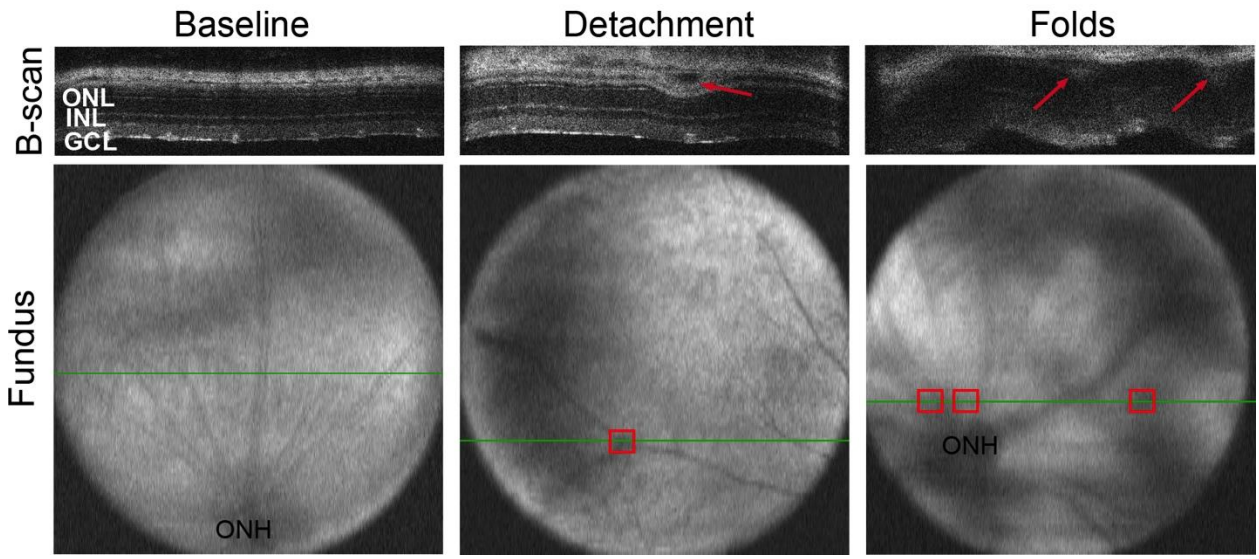

Figure 2.12. Blast exposure damages the retina. At baseline, each layer of the retina appears normal in the b-scan image and the corresponding fundus image shows no signs of pathology (ONH: optic nerve head). The green lines in the fundus images denote the location of the b-line scan images. An example of a retinal detachment after blast is shown. It appears as a dark area between the RPE and photoreceptors (arrow) and as a dark shadow in the mid-peripheral region of the retina fundus image (box). An example of retinal folds with corresponding retinal detachments (arrows; boxes) is shown.

The majority of post-blast retinas appeared normal at all time-points by OCT imaging, despite repositioning the eye multiple times during imaging to examine all retinal quadrants (Figure 2.12). When retinal detachments were detected they were primarily in the mid-peripheral retina and less frequently near the optic nerve head (ONH). At 3 days post-blast, 40% of eyes had a single retinal detachment that had an average height of 0.03mm ± 0.005 (Figure 2.12). At 1 week post-blast, only one eye had retinal detachments. The average height and number of the detachments at 1 week was 0.05mm ± 0.03 and 6 per eye, respectively. One retina had a wavy appearance suggestive of epiretinal membranes and multiple retinal detachments (Figure 2.12). No detachments were observed at 2 weeks post-injury, but it is possible that detachments were missed during imaging. At 1 month, only the retina that appeared wavy at the 1 week time point had retinal detachments, a total of 2, averaging 0.03mm ± 0.00 in height.

Blast damages the retina, RPE and optic nerve

In the normal RPE, there were no vacuoles or debris accumulation present (Figure 2.13A). In contrast, the RPE contained grade 5 vacuoles at 3 days post-blast in the majority of eyes (67%, Figure 2.13B). At 1 month after blast, the RPE vacuoles decreased in size to grade 2 (Figure 2.13C). At both time-points the RPE vacuoles were present throughout the retina. Subretinal debris, consisting of red blood cells and photoreceptor inner and outer segments, were detected in areas of retinal detachments at 3 days post-blast (Figure 2.13B), but appeared to resolve at 1 month post-blast (Figure 2.13C).

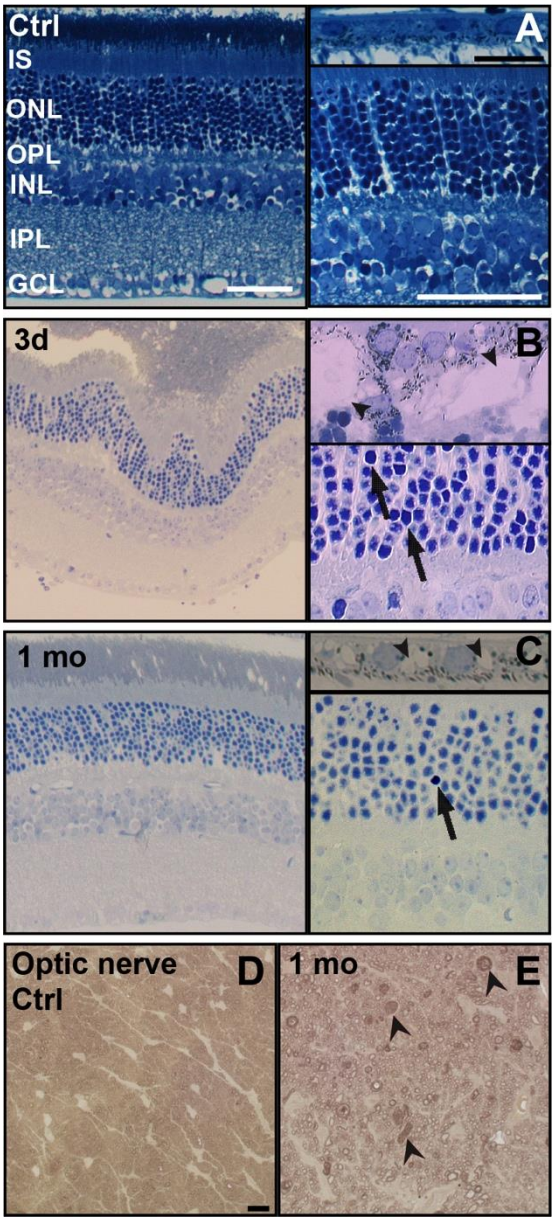

Figure 2.13. Neuronal death, RPE vacuoles and optic nerve degeneration occur after blast. Representative brightfield micrographs of the retina and RPE (A-C). Representative brightfield micrographs of the optic nerve (D-E). Control retina and RPE shows normal histology (A). A retinal detachment with subretinal debris is present in conjunction with pyknotic nuclei (arrows) in the ONL (B). The RPE contains grade 5 vacuoles (arrowheads), and phagocytosed debris. There are fewer pyknotic nuclei (arrow) in the retina and the RPE vacuoles (arrowheads) are smaller in size at 1 month (1 mo) post-blast (C). The control optic nerve appears normal (D). At 1 month post-blast, the optic nerve contains degenerating axons with collapsed myelin (arrowheads) (E). The scale bars in the low and high magnification retina images are 50μm and the scale bar in the RPE images is 20μm. The scale bar for the optic nerve images is 5μm.

While much of the post-blast retina looked normal, clusters of pyknotic nuclei were observed at 3 days and 1 month (Figure 2.13B, C). The average number of pyknotic nuclei at 3 days post-blast was 14±10 in the ONL and 31±21 in the INL. At 1 month post-blast, the average number of pyknotic nuclei decreased to 3±2 and 0±0 in the ONL and INL, respectively. Optic nerves from the first week post-injury (data not shown) looked the same as those from controls (Figure 2.13D). In contrast, degenerating axons with collapsed myelin were prevalent at 28 days post-injury (Figure 2.13E).

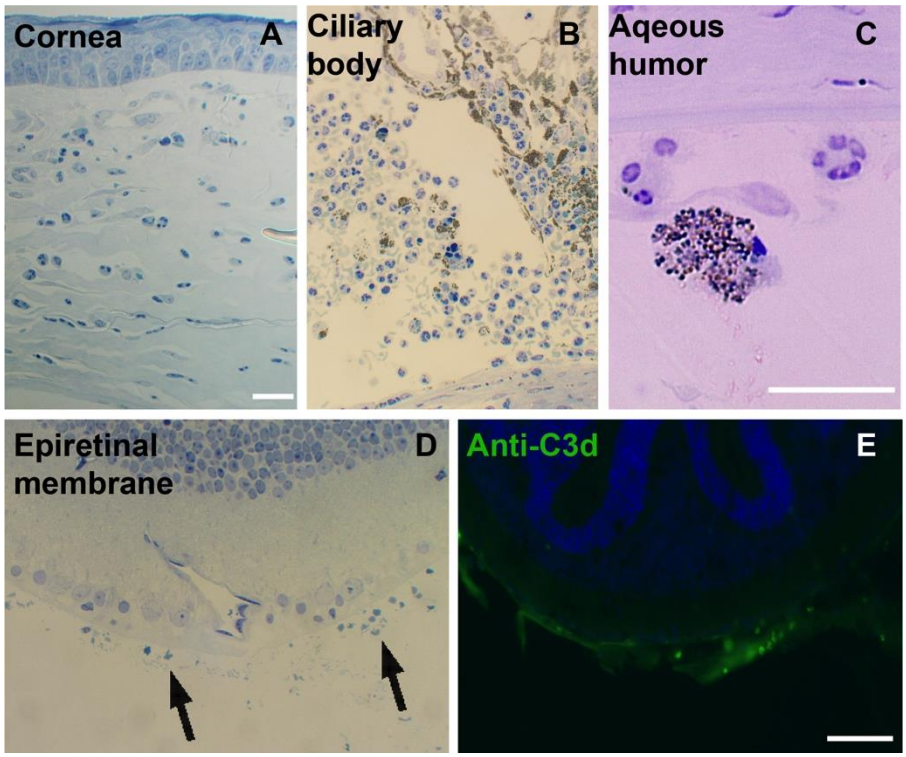

Figure 2.14. Immune infiltrate appear after blast exposure. Immune infiltrate is present in the anterior chamber, including the cornea (A) and the aqueous humor near the ciliary body (B) and the aqueous humor near the cornea (C). An epiretinal membrane after blast (D, arrows). The epiretinal membranes are positive for C3d indicating that they are immune-mediated (E). The scale bar in (A) is 50μm and also applies to (B) and (D); the scale bar in (C) is 5μm; the scale bar in (E) is 25μm.

Immune infiltrate was present in a subset of eyes (33%) at both 3 days and 1 month post-blast. Infiltrate was detected in both the anterior and posterior portions of the eye, including the cornea, aqueous humor, vitreous humor and surface of the retina (Figure 2.14A-C). Immune-mediated (C3d-positive) epiretinal membranes were occasionally detected in areas of retinal detachment (Figure 2.14D-E).

Regional cell death occurs at multiple time points post-blast

After blast, all retinas had areas with TUNEL-positive cells (i.e. affected areas) at 3 days and 1 week post-injury, while 82% of retinas were TUNEL-positive at 1 month post-injury. Cell death was typically present in patches and not evenly distributed across the retina (Figure 2.15). These affected areas were primarily in the mid-peripheral retina, but occasionally were also detected in central retina (Figure 2.15A).

The percentage of total retina containing TUNEL-positive cells, density of TUNEL-positive cells and retinal layer affected were quantified (Figure 2.16A). The majority of TUNEL-positive nuclei, 82%, 70% and 83%, were located in the ONL at 3 days, 1 week and 1 month after injury, respectively (Figure 2.16A). A smaller percentage of TUNEL-positive cells, 12%, 27% and 16% were detected in the INL at 3 days, 1 week and 1 month post-blast, respectively. Finally, 6%, 3% and 1% of all TUNEL-positive cells were in the GCL at 3 days, 1 week and 1 month post-injury, respectively. TUNEL positive nuclei were present in 13±8% of the retina at 3 days post-injury, 2±0.2% at 1 week post-blast, and 5±1% of the retina at 1 month post-injury (Figure 2.16B). When calculated in terms of total retina length, the density of TUNEL was very low, but retained the same trend of higher levels at 3 days as compared to 1

month. The number of TUNEL-positive nuclei per mm total retina was 15±9, 0.1±0.1, and 11±4 at 3 days, 1 week and 1 month post-blast (Figure 2.16C). Within the affected regions, the density of TUNEL-positive cells was 87±44, 10±3, and 215±57 nuclei per mm retina at 3 days, 1 week and 1 month after blast, respectively (Figure 2.16D). These results demonstrate that the area occupied by TUNEL-positive cells decreases over time, but the density of TUNEL-positive cells within affected areas increases.

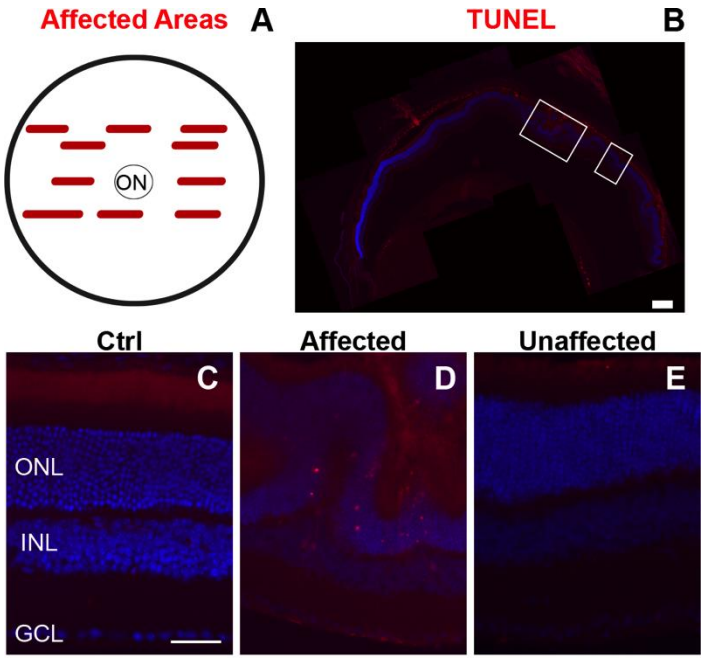

Figure 2.15. Cell death occurs in small, focal areas after blast. A schematic representing an enface view of the retina showing the average number and distribution of affected (i.e. TUNEL positive) areas (red bars) detected in retinal cross-sections collected in serial through the 3 day post-blast eye (A). Montage of low magnification epifluorescence micrographs of a 3 day post-blast retina (B). White boxes indicate affected areas (scale bar is 250μm). Higher magnification epifluorescence micrographs of TUNEL (red) and DAPI (blue) in a control retina (C), and affected (D) and unaffected (E) regions of the retina shown in (B). The scale bar in (C) represents 50μm and also applies to (D) and (E).

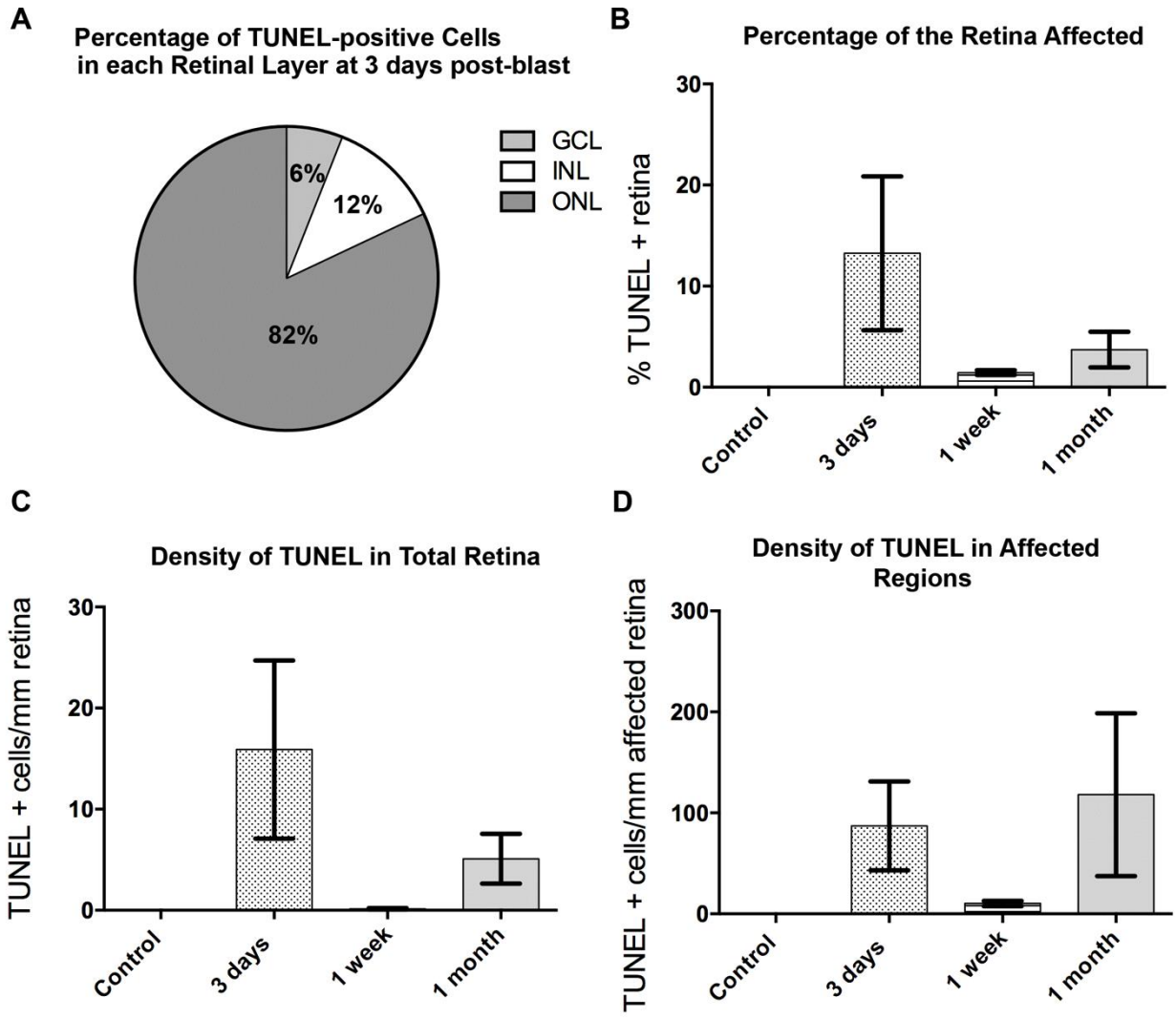

Figure 2.16. Cell death occurs in two waves after blast. Pie chart showing the distribution of TUNEL positive cells through the retinal layers after blast (A). The percentage of total retina containing TUNEL-positive cells at each time point (B). The average number of TUNEL positive cells per mm total retina after blast (C). The average number of TUNEL positive cells per mm within the affected areas after blast (D). Error bars represent SEM for each time point.

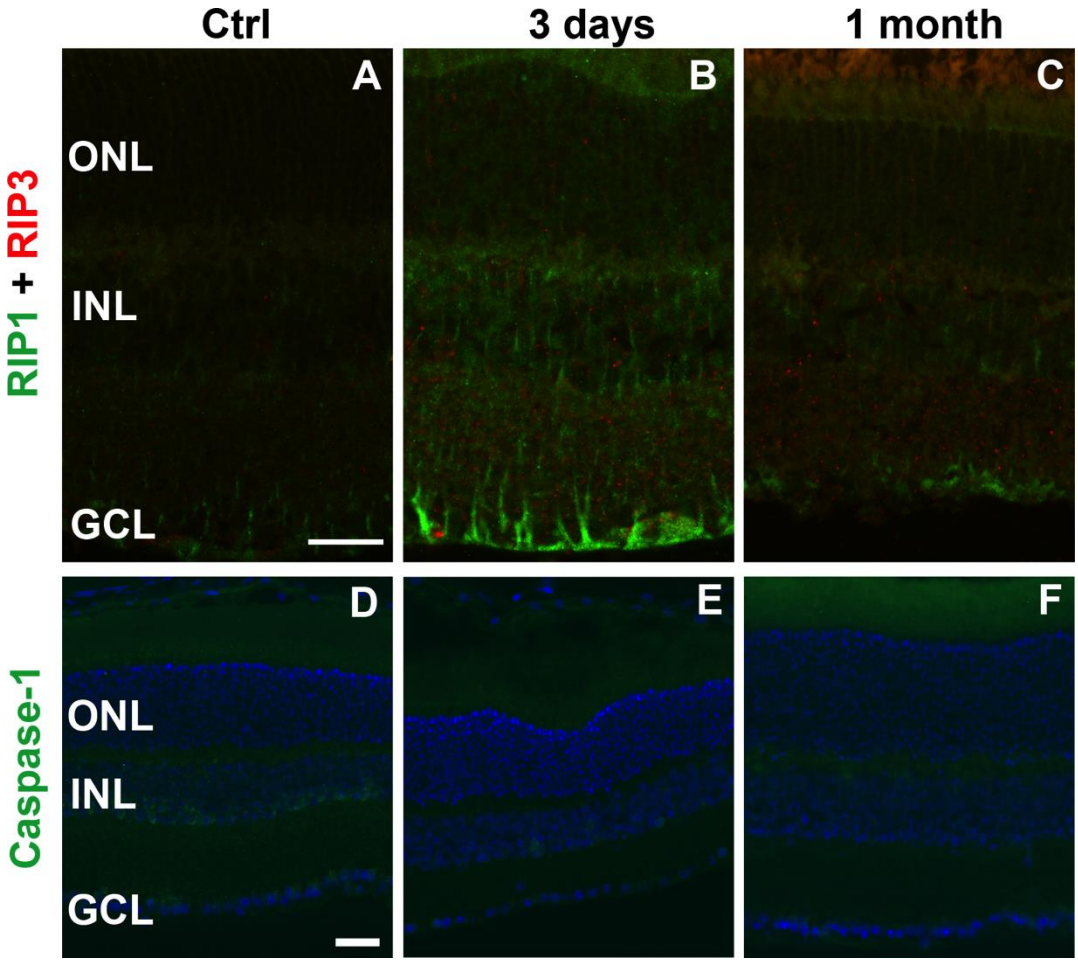

Figure 2.17. Changes in cell death markers after blast suggest a non-apoptotic mode of cell death. Confocal micrographs of retinas immunolabeled for RIP1 (green) and RIP3 (red; scale bar in A-C is 30μm). Epifluorescence micrographs of Caspase-1 (green) immunolabeling and DAPI (blue; scale in D-F is bar is 25μm).

Blast induces changes in cell death pathway markers

Labeling for markers for necroptosis (programmed necrosis; RIP1 and RIP3) was increased after blast. In the normal retina, RIP1 localized to the Müller glia, the IPL and the INL, with some light staining in the OPL (Figure 2.17A). Light RIP3 staining in the normal retina was restricted to the GCL, IPL and INL (Figure 2.17A). At 3 days post-injury, RIP1 increased in the ONL, INL, and Müller glia, while RIP3 increased in the

ONL, INL, IPL, and GCL (Figure 2.17B). As cell death progressed at 1 month post-blast, RIP1 remained elevated in the ONL and INL, while RIP3 remained elevated in the IPL and maintained some light labeling in the ONL (Figure 2.17C).

Caspase-1 was present within the INL and GCL throughout the control retinas (Figure 2.17D). At 3 days post-injury, only one third of retinas exhibited caspase-1 positive cells in the INL and GCL (Figure 2.17E). At 1 month after blast, all retinas were caspase-1 negative (Figure 2.17F). Immunolabeling with anti-ChAT in the DBA/2J showed that starburst amacrine cells were still present at 1 month post-blast (data not shown).

Protein nitration increases in the retina after blast

In the normal retina, nitrotyrosine immunolabeling was light and restricted to the inner retina (Figure 2.18A). Three days after blast, immunolabeling was greatly increased throughout both the inner and outer retina (Figure 2.18B). The immunolabeling seemed less increased, but still elevated in both the inner and outer retina at 1 month post-blast (Figure 2.18C).

Glial reactivity increases in the retina after blast

In the normal retina, GFAP immunolabeling was restricted to the Müller glia endfeet and astrocytes (Figure 2.19A). At both 3 days and 1 month post-injury, GFAP immunolabeling was increased in the Müller cell processes (Figure 2.19B-C). In age-matched control retinas, IBA-1 immunolabeling showed that microglia were

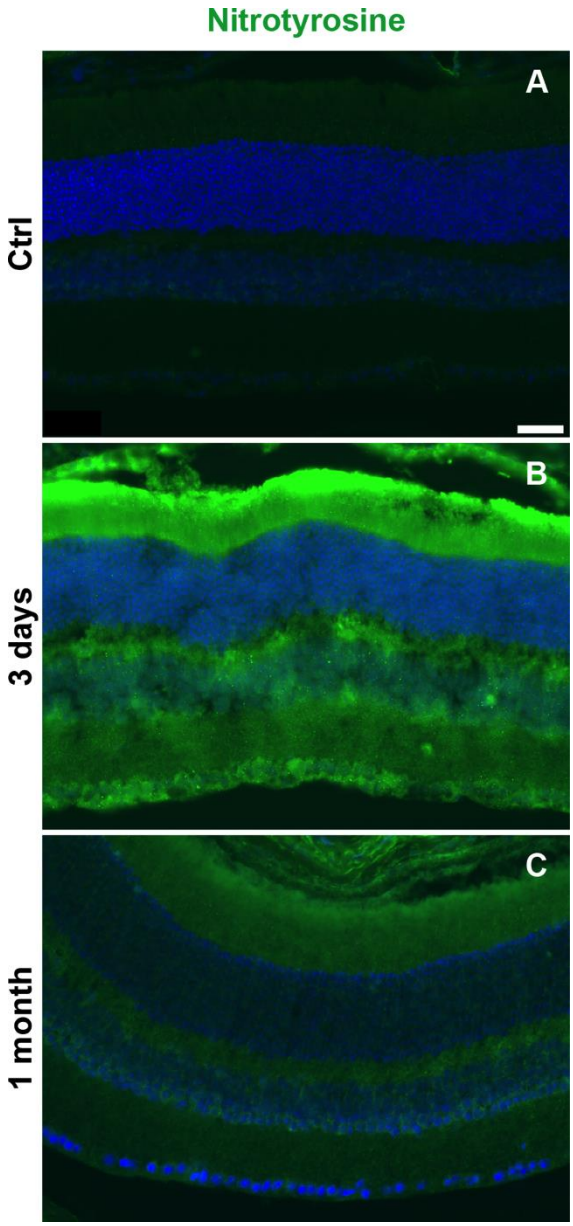

Figure 2.18. Nitrotyrosine increases following blast. Representative epifluorescence micrographs of control (A), 3 days (B) and 1 month (C) post-blast retinas immunolabeled for nitrotyrosine (green) and labeled with DAPI (blue). Scale bar is 25μm and applies to all images.

restricted to the inner retina and were fairly low in density (Figure 2.19D). Microglia were more prevalent after blast when compared to controls beginning at 3 days and 1 month post-blast (Figure 2.19E-F). Reactive microglia, which are amoeboid in appearance, were detected (Figure 2.19E-F, inserts).

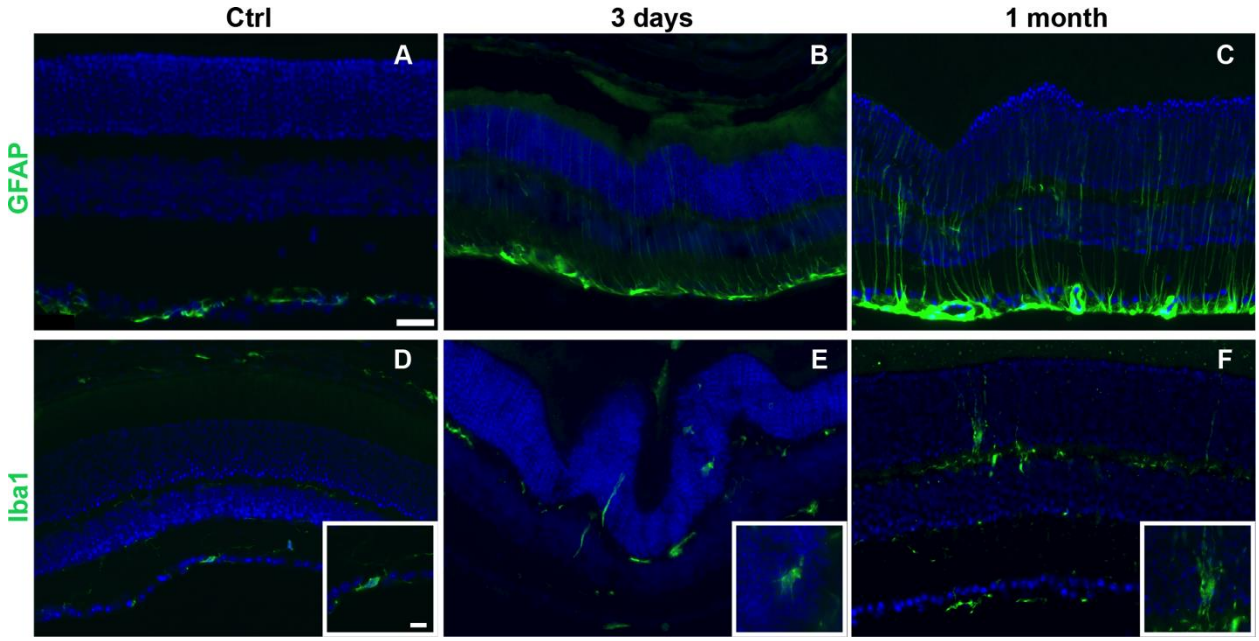

Figure 2.19. Both Müller glia and microglia are reactive after injury. Representative epifluorescence micrographs of control (A), 3 days (B) and 1 month (C) post-blast retinas immunolabeled for GFAP (green). Representative epifluorescence micrographs of control (D), 3 days (E) and 1 month (F) post-blast retinas immunolabeled for Iba1 (green). Higher magnification images of representative microglia are present in inserts. Scale bar is 25μm and applies to all images; DAPI is shown in blue.

Ocular blast trauma causes visual deficits

The ERG a wave amplitude was diminished to approximately 40% of baseline at 1 week post-blast based on an average of the responses at each light intensity (Figure 2.20A). At 2 weeks post-blast, a statistically significant decrease was still present, but the level of decrease was less substantial at an average of 55% of baseline. At 1 month

post-blast, the a wave amplitude was similar to baseline at the brightest flash, but was still reduced at the other flash intensities (Figure 2.20A). The average deficit from baseline at the lower light intensities was 63% at 1 month post-blast.

The ERG b wave amplitude was similar to baseline at the brightest light intensity at all time points post-blast (Figure 2.20B). However, at all other light intensities, there was a deficit averaging 52% below baseline at 1 week post-blast, 74% of baseline at 2 weeks post-blast, and 48% of baseline at 1 month post-blast. The decrease in the b wave amplitude at 1 week post-blast seems to correspond to the decrease in the a wave amplitude at this time point (Figure 2.20B). In contrast, the decrease in the b wave amplitude, particularly at 0 and 1 log cd*s/m^2 ($p<0.01$) at 1 month post-blast was greater than at earlier time-points despite a recovery of a wave.

The OPs were also affected after blast (Figure 2.20C). OP1 was diminished at all time-points after blast ($p<0.01$). OP2 was significantly lower than baseline at both 1 week and 1 month ($p<0.01$). OP3 appeared lower than baseline, but only reached statistical significance at 1 week post-blast ($p<0.01$). A significant decline in visual acuity was observed at 3 days (0.34 ± 0.07, $p<0.05$) and 1 month (0.09 ± 0.02, $p<0.01$) post-blast (Figure 2.20D).

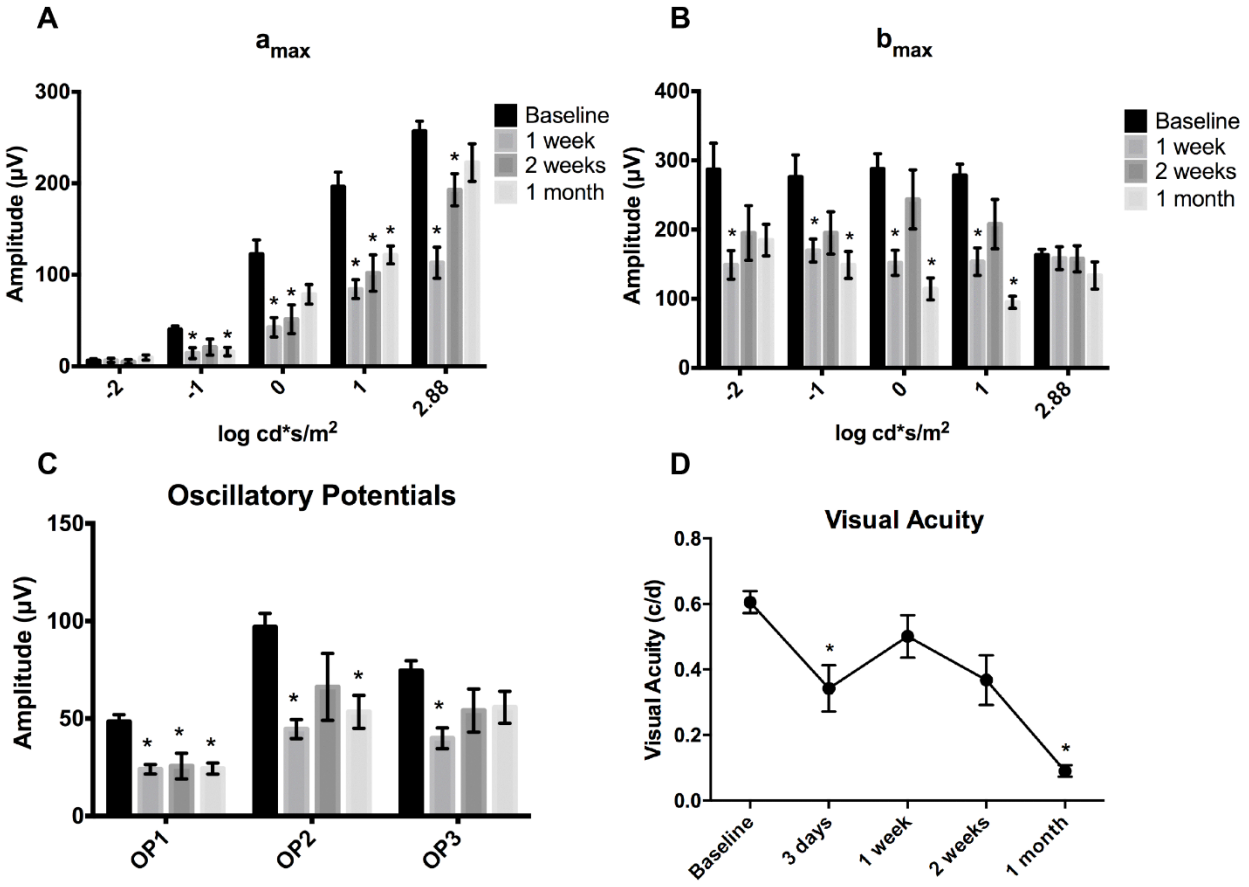

Figure 2.20. Blast causes early and late visual deficits. Bar graph of the ERG a_{max} over light intensity (A). Bar graph of ERG b_{max} over light intensity (B). Bar graph of the oscillatory potential (OP) peak amplitude at each time point (C). Photopic spatial threshold (i.e. visual acuity) is significantly decreased at 3 days and 1 month post-blast (D). *p<0.05. Error bars represent SEM for each graph.

Moderate trauma in the Balb/cJ mouse

Blast induces anterior pathologies

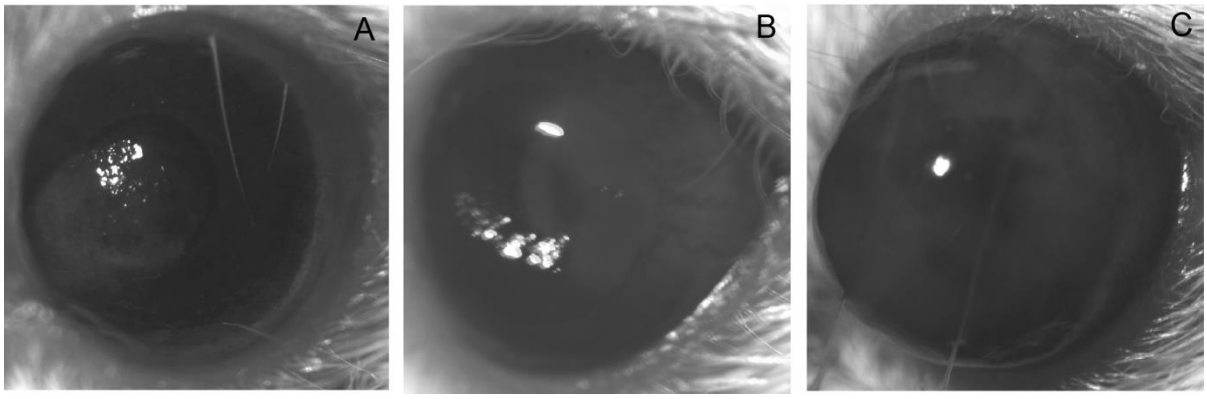

Figure 2.21. Blast causes anterior pathologies. Representative images of common pathologies detected after blast: corneal edema (A), cataract and corneal neovascularization (B), cataract, corneal edema, and hyphema (B).

Immediately post-blast, we observed corneal edema, corneal neovascularization (CNV) and traumatic cataracts in 15% of the mice (Table 2, Figure 2.20 A-C). The incidence of pathology increased over time post-blast. At 1 month post-blast, the hyphemas and corneal abrasions resolved, but corneal edema, CNV, corneal scarring and traumatic cataract remained in 42%, 37%, 42% and 10% of eyes, respectively. At 2 months post-blast, only corneal edema and CNV remained, which were present in 100% and 60% of eyes, respectively. Due to the prevalence of anterior pathologies, we did not assess visual function.

Type of Injury	0d (72)[a]	3d (67)	1 wk (46)	2 wk (9)	1 mo (19)	2 mo (5)
Corneal abrasions	0	6 (8)	2 (4)	5 (55)	0	0
Corneal edema	9 (10)[b]	32 (42)	36 (78)	4 (44)	8 (42)	5 (100)
CNV	2 (2)	11 (14)	11 (24)	5 (55)	7 (37)	3 (60)
Hyphema	0	0	3 (6)	3 (33)	0	0
Corneal scarring	0	0	5 (11)	0	8 (42)	0
Traumatic Cataract	3 (3)	9 (12)	10 (22)	2 (22)	2 (10)	0

[a]Total number of eyes examined
[b]Number of eyes with pathology (percentage); d=days, wk=week, mo=month

Table 2. The incidence of gross pathology in the Balb/cJ

Blast exposure causes retinal detachments

Most retinas appeared similar to non-blast controls (Figure 2.22A). Large retinal detachments were detected in 37% of blast-exposed eyes (Figure 2.22B-C). The appearance of the retinal detachments with high and low areas is suggestive of a fusion of many small retinal detachments (Figure 2.22B-C). The retinal detachments were present in the mid-peripheral retina, which appeared as mottled and/or darkened areas in the fundus images (Figure 2.22D-E, arrows).

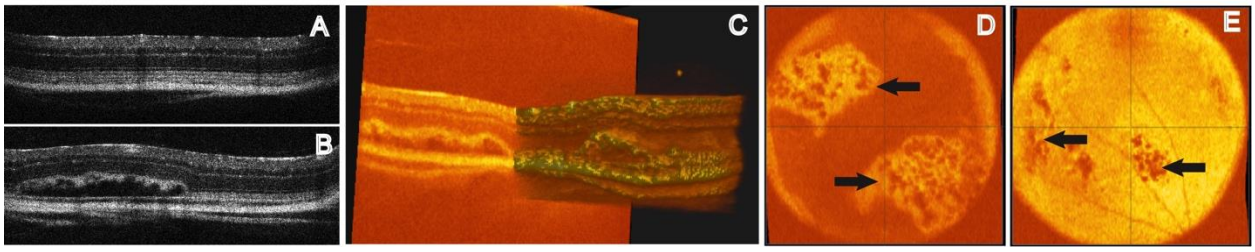

Figure 2.22. Blast induces large retinal detachments. OCT B-line scans of retinas from an uninjured eye (A) and a 3d post-blast eye (B). Three-dimensional reconstruction of a stack of OCT B-line scans from a post-blast eye showing multiple retinal detachments (C). En face OCT images of post-blast retinas showing the peripheral localization and grouping of the retinal detachments (D-E).

Ocular blast trauma damages the retina and RPE

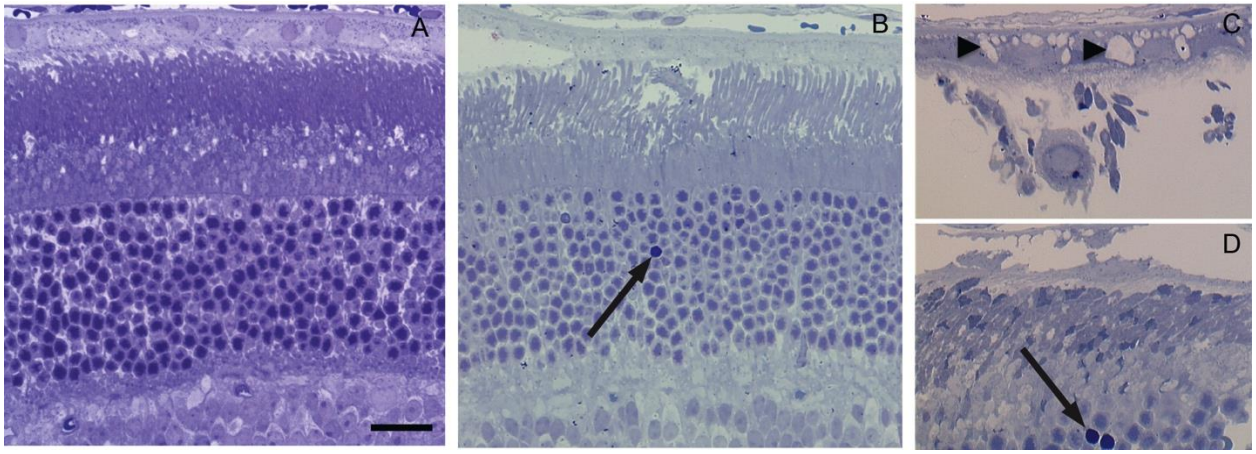

Figure 2.23. Blast injures the retina and RPE. Representative brightfield micrographs of retina (A-B) and RPE (C-D) from uninjured (A), 1 week post-blast (B) and 2 months post-blast (C-D) mice. Arrows indicate pyknotic nuclei. Arrowheads in C indicate RPE vacuoles. Scale bar in A represents 25μm and applies to all images.

Naïve control eyes had healthy retinas and RPE (Figure 2.23A). At 1 week post-blast, small, infrequent vacuoles (grade 2 ± 0.4) were present in the RPE and the retina contained an average of 11 ± 2 pyknotic nuclei in the ONL and 1±0.6 pyknotic nuclei in the INL (Figure 2.23B). At 1 month post-blast, the average grade for RPE vacuoles was 3 ± 0.7, indicative of small, frequent vacuolization. The ONL and INL at this time-point contained 14 ± 9 and 14 ± 13 pyknotic nuclei, respectively. At 60 days post-blast, RPE vacuolization remained high (grade 3 ± 0.6; Figure 2.23C). Pyknotic nuclei were also still detected in the ONL (3 ± 0.4), and INL (2 ± 0.4) even at 60 days post-blast (Figure 2.23D).

Optic nerve degeneration occurs after blast

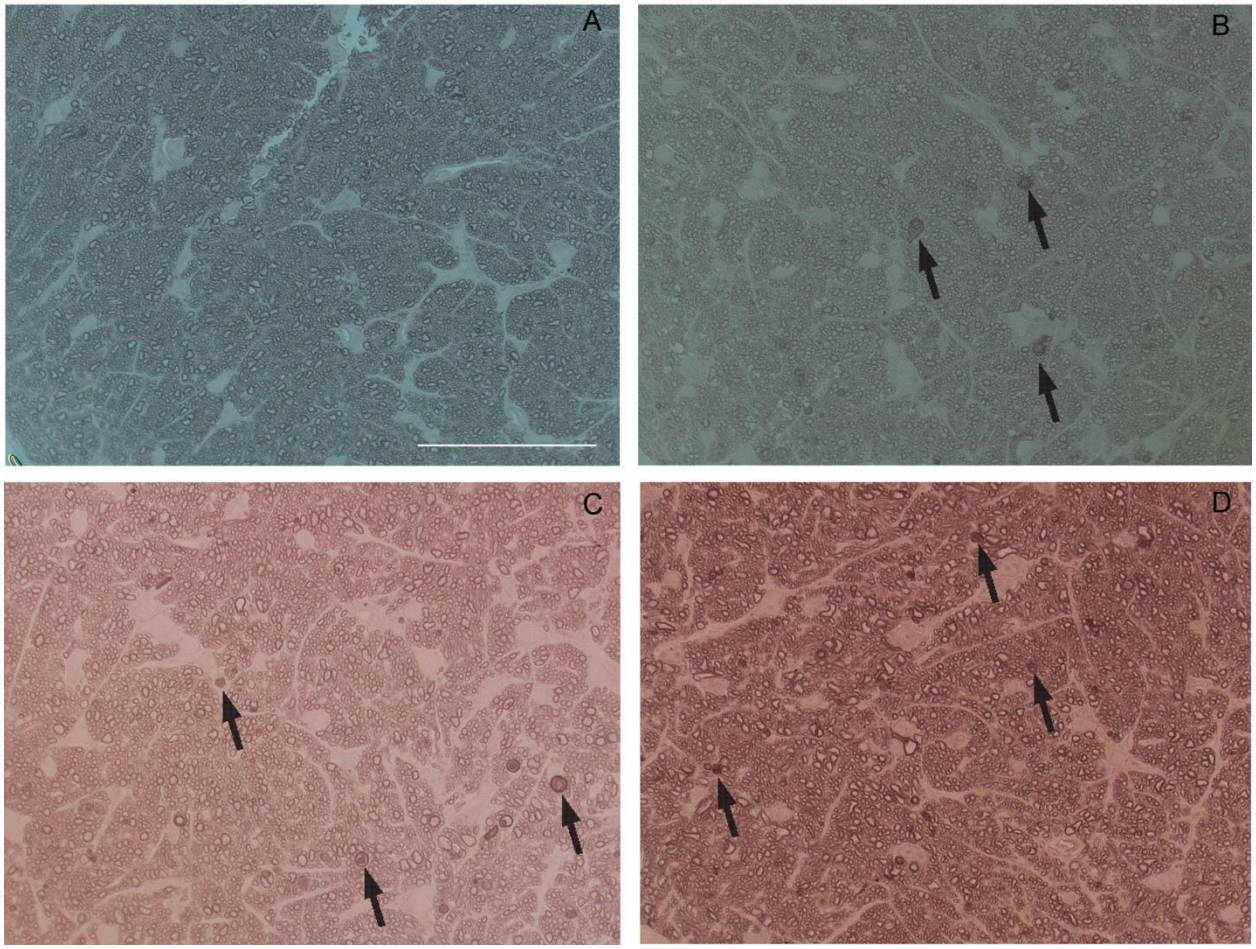

Figure 2.24. Blast trauma causes optic nerve degeneration. Representative brightfield micrographs of optic nerves from uninjured (A), 1 week post-blast (B), 1 month post-blast (C) and 2 months post-blast (D) mice. Arrows indicate degenerating axons. Scale bar represents 50μm and applies to all images.

In the optic nerves from non-blast mice, the axons were tightly ensheathed by myelin and the axoplasm was clear (Figure 2.24A). In contrast at 1 week, 1 month and 2 months post-blast, the optic nerves contained degenerating axon profiles, marked by collapsed and thickened myelin (Figure 2.24B-D, arrows).

Blast exposure causes retinal cell death

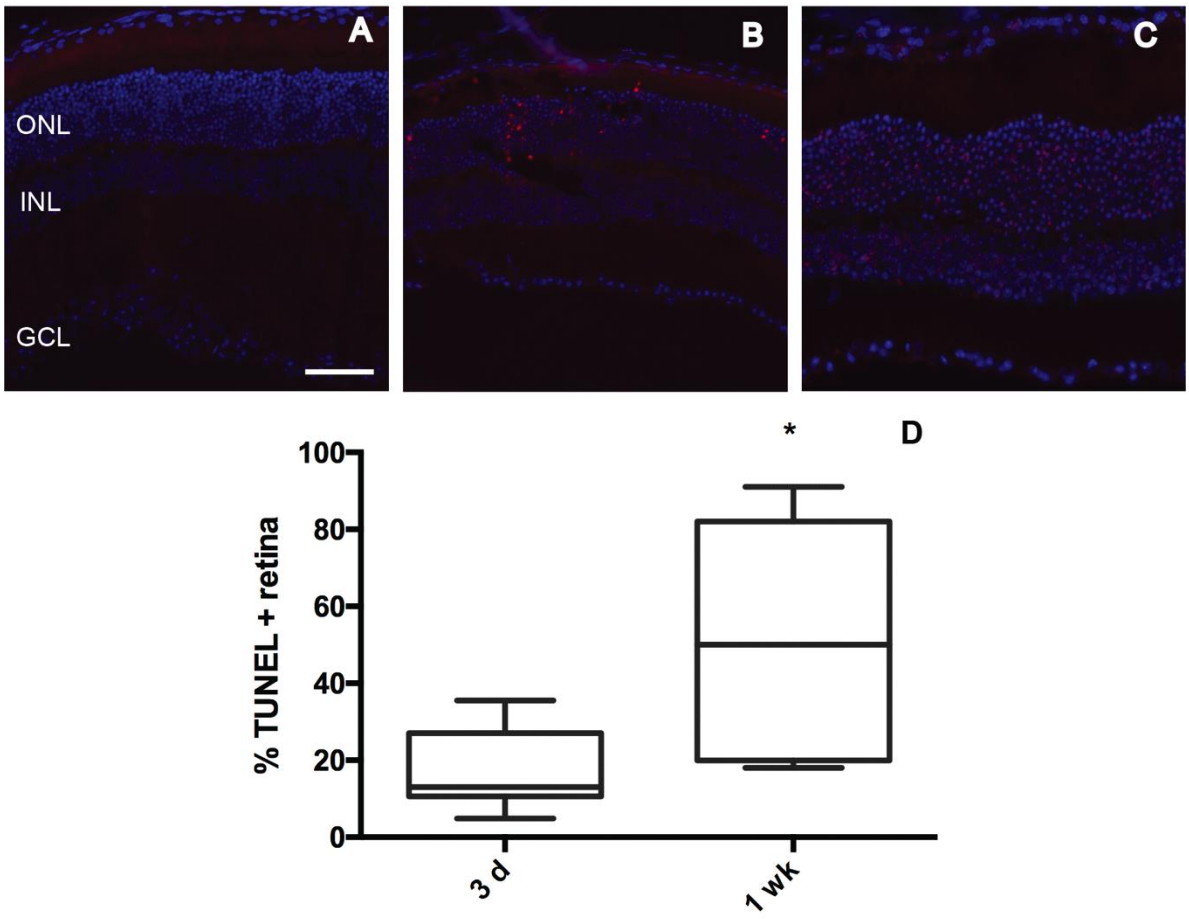

Figure 2.25. Ocular blast trauma induces cell death in the retina. Representative fluorescence micrographs of TUNEL in retina (A-C) from uninjured (A), 1 week post-blast (B) and 1 month post-blast (C) mice. TUNEL (red), DAPI (blue). Scale bar represents 50μm. Box and whisker plot of retinal TUNEL quantification at 3 days and 1 week post-blast, *p<0.05.

All non-blast retinas were TUNEL-negative (Figure 2.25A). In contrast, at 3 days post-blast, 16 ± 4% of the retina was TUNEL-positive (data not shown). At 1week post-blast, 51 ± 12% of the retina contained TUNEL-positive cells (Figure 2.25B), which was significantly higher than the amount of cell death observed at 3 days post-blast (Figure 2.25D). Cell death persisted at 1 month post-blast, with 14 ± 4% of the retina containing

TUNEL-positive nuclei (Figure 2.25C). At all time points, the majority of the TUNEL-positive nuclei were located in the ONL.

Neuroinflammation occurs in first week post-trauma

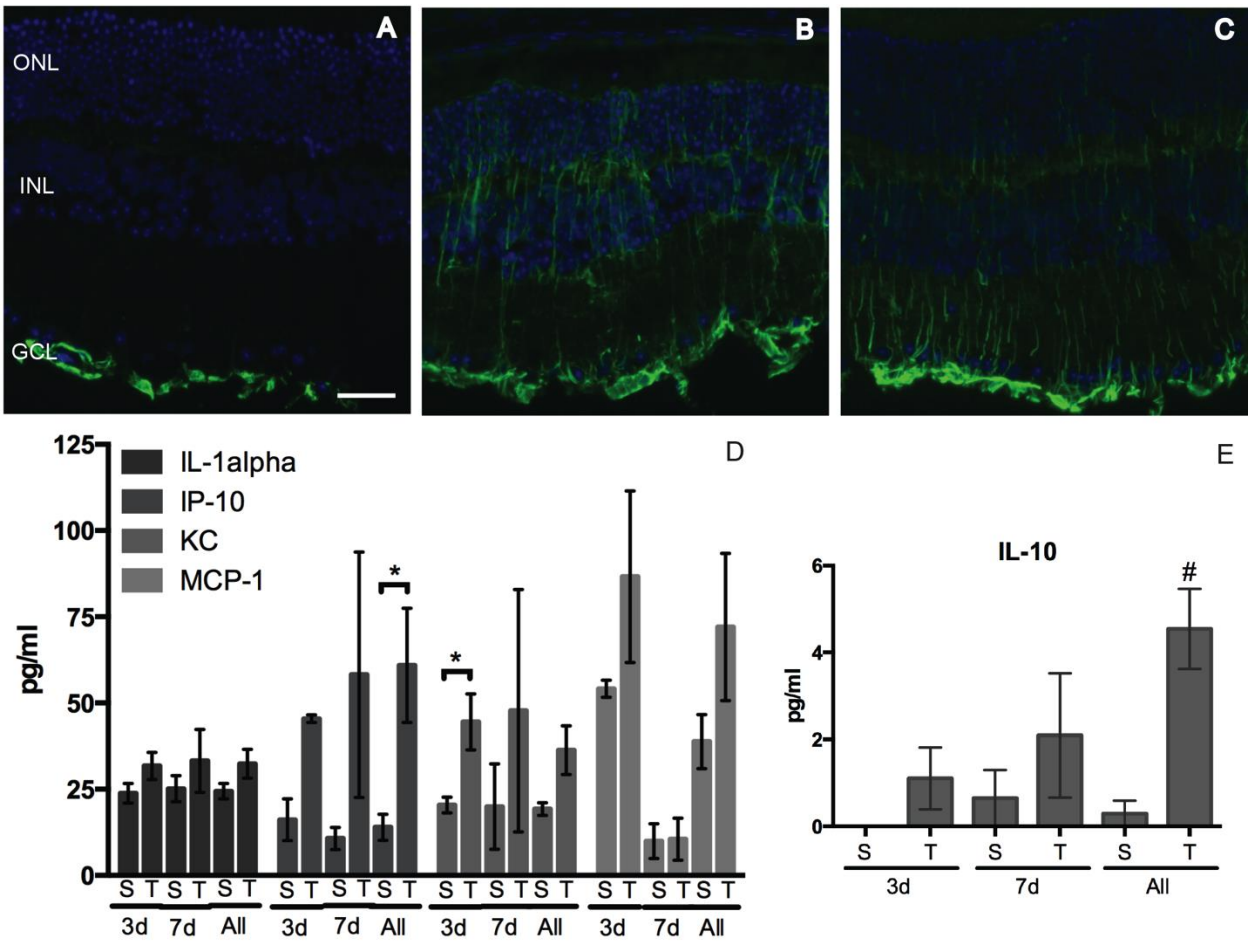

Figure 2.26. Blast induces mild neuroinflammation. Representative fluorescence micrographs of GFAP immunolabeling in retinas from uninjured (A), 1 week post-blast (B) and 1 month post-blast retinas (C). Anti-GFAP (green), DAPI (blue). Scale bar represents 50μm and applies to all images. Bar graphs of cytokines altered or trending towards an increase after injury (D-E). *p<0.05, #p<0.0001; S=sham, T=trauma

In the retinas from non-blast mice, GFAP immunolabeling was present in the Müller glia endfeet and astrocytes (Figure 2.26A). In contrast, GFAP immunolabeling extended into the Müller glial process at 3d (data not shown), 1 week (Figure 2.26B) and 1 month post-blast (Figure 2.26C). These changes were uniform throughout the retina at all time points post-injury. We then assessed if the glial cell hypertrophy also correlated with increased levels of pro-inflammatory cytokines and chemokines (Figure 2.26D-E). A statistically significant increase was detected for KC (i.e. chemokine C-X-C motif ligand-1) at 3 days post-blast as compared to the 3 days post-sham ($p<0.05$; Figure 2.26D). Levels of interleukin 1 alpha (IL-1α), interferon-gamma-inducible protein 10 (IP-10 or chemokine C-X-C motif ligand-10), interleukin 10 (IL-10) appeared equally increased at both 3 days and 1 week after trauma, but were not significantly different from matched sham controls. Due to high variability and small sample size, we combined the 3 days and 1 week groups together to create the all trauma and all sham groups. A statistically significant increase was detected in both IP-10 (Figure 2.26D, $p<0.0001$) and IL-10 (Figure 2.26E, $p<0.05$) in the all trauma group as compared to all sham. Monocyte chemoattractant protein-1 (MCP-1 or chemokine C-C motif ligand-2) trended higher at 3 days, but not 1 week after trauma (Figure 2.26D).

Reactive oxygen species (ROS) are increased after trauma

Using the *in vivo* fluorescent markers CM-H_2DCFDA and DHE, an increase in ROS was detected at 1 week post-blast as compared to shams (Figure 2.27A-D). No fluorescence was detected in sham eyes after injection of either probe (Figure 2.27A,C). In contrast, fluorescence for both markers was present after trauma (Figure 2.27B,D).

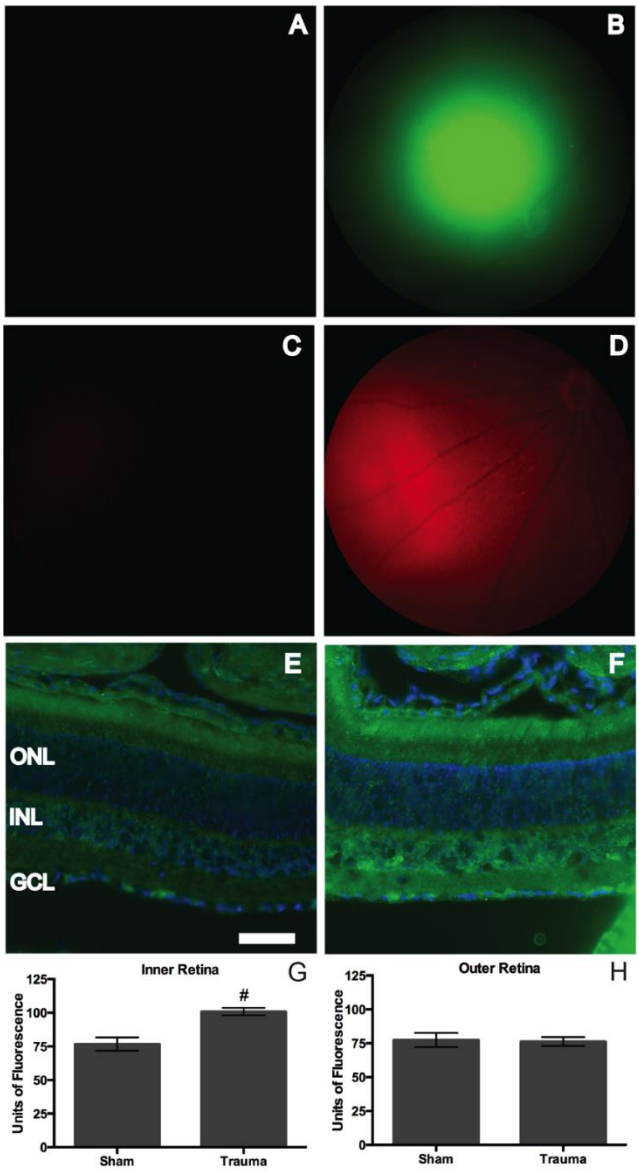

Figure 2.27. Blast induces oxidative stress. *In vivo* images of CM-H_2DCFDA fluorescence, a general indicator of reactive oxygen species, in sham (A) and 1 week post-blast eyes (B). *In vivo* images of DHE fluorescence, an indicator of superoxide, in sham (C) and 1 week post-blast eyes (D). Representative epifluorescence micrographs of nitrotyrosine immunolabeling (green) of sham (E) and 7d post-trauma (F) retinas double labeled with DAPI (blue). Bar graph of nitrotyrosine immunofluorescence quantification in the inner (G) and outer (H) retina. **p<0.01.

The eyes with the greatest amount of fluorescence are shown. In particular, levels of superoxide (as measured by DHE) and ROS (as measured by CM-H_2DCFDA) appear to be elevated at 1 week post-blast (Figure 2.27B,D). Nitrotyrosine immunolabeling was also significantly increased in the inner, but not outer, retina at 1 week post-trauma.

Mild blunt trauma in the contralateral eye after blast

Blunt trauma causes anterior injuries in the D2 mouse

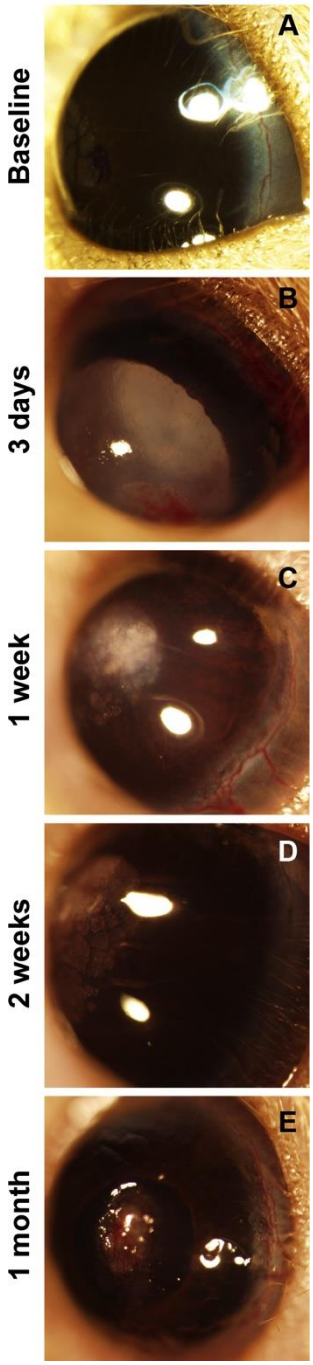

Figure 2.28. The ocular surface is injured in the D2 contralateral eye. Calcium deposits are common in the D2 eye prior to injury (A). Hyphema, CE and cataracts occur at 3 days post-injury (B). CE and calcium deposits occur at 1 week post-injury (C). CE, CNV and calcium deposits at 2 weeks post-injury (D). A corneal scar and CNV at 1 month post-injury (E).

As in the blast-exposed eye, no anterior pathology was detected in the contralateral Bl/6 eye (Bricker-Anthony et al., 2014b). In the contralateral D2 eye, corneal edema (CE) occurred in 52% of eyes at 3 days post-injury (Figure 2.28B) and remained in 43% of mice at 1 month (Figure 2.28E). Cataracts were observed in 30% of D2 contralateral eyes at both 3 days and 1 month post-injury (Figure 2.28B,E). Corneal neovascularization (CNV) and corneal calcifications became more prevalent over time. CNV was detected in 44% and 29% of eyes at 2 weeks and 1 month post-injury, respectively (Figure 2.28D-E). Corneal scarring was detected in 33% and 43% of eyes at 2 weeks and 1 month post-injury, respectively (Figure 2.28D-E).

Ocular trauma causes retinal detachments

In the Bl/6 mouse, disruption of the outer segments (as determined by a bright area on the fundus, (Figure 2.29C) was observed in 25% of contralateral retinae within the mid-periphery at 1 week and in 8% of contralateral retinae at 2 weeks and 1 month post-injury. Retinal detachments were detected in 13% and 15% of Bl/6 contralateral retinae at 1 week and 2 weeks post-injury, respectively (Figure 2.29C). This decreased to 8% of retinas at 1 month post-injury. Up to eight retinal detachments per eye were detected and the average height of the retinal detachments was 0.02±0.003mm at all time points.

In the D2 mice at 2 weeks post-injury, an average of 13 retinal detachments per eye were detected in 17% of contralateral eyes (Figure 2.29D). The average height of the retinal detachments was 0.04±0.07mm. No retinal detachments were detected at 1 week or 1 month post-injury.

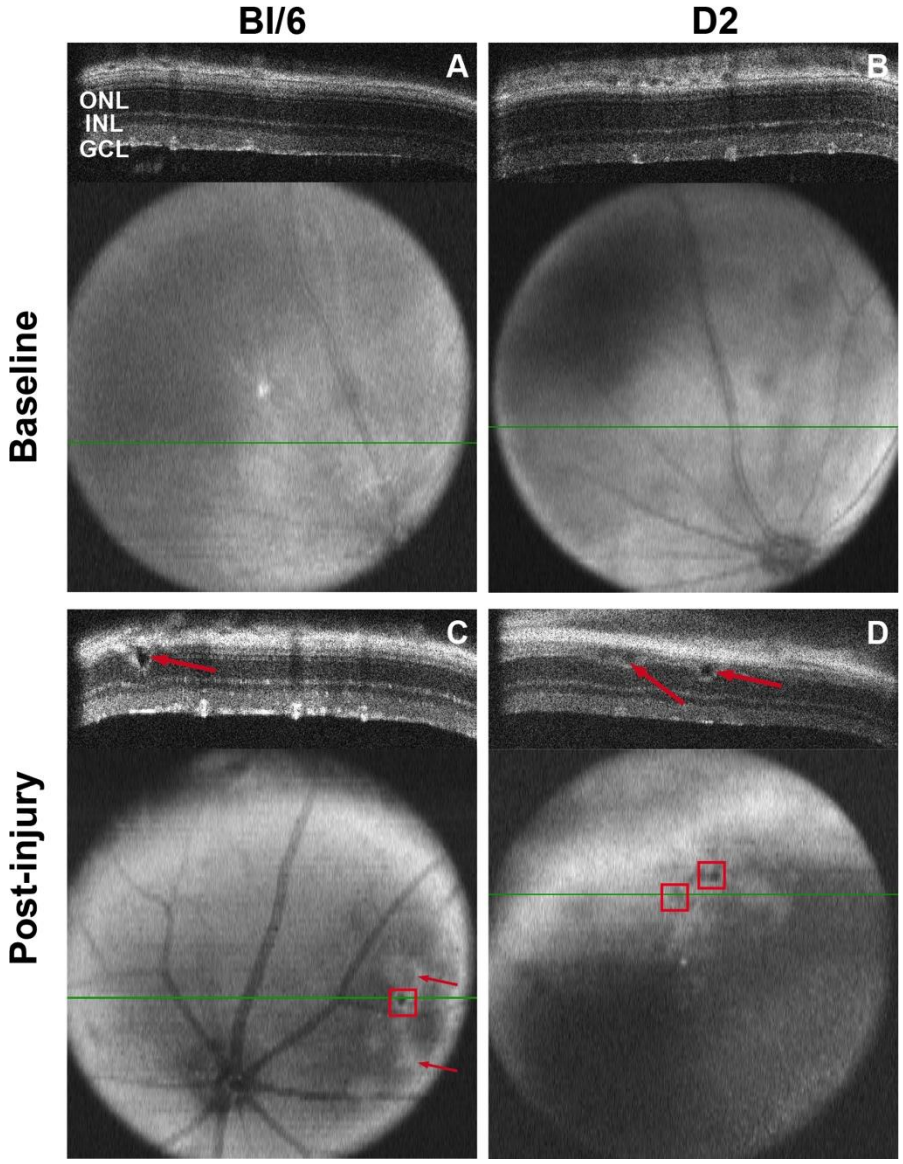

Figure 2.29. Blast induces retinal detachments in both Bl/6 and D2 contralateral eyes. Both Bl/6 (A) and D2 (B) retinas appear normal at baseline in both the b-scan and fundus images. The green line in the fundus image denotes the location of the b-scan. A retinal detachment (arrow) is present at 1 week post-injury in the Bl/6 retina and is visible on the fundus image as a small, round dark area (C, red box). Areas of outer segment disruption appear as white, patchy areas on the fundus image (C, arrows). Retinal detachments in a D2 retina at 2 weeks post-injury (D, arrows, red boxes).

Ocular trauma doesn't displace the lens

In order to detect lens displacement, we imaged and measured the depth of the anterior chamber in a subset of mice (n=16; D2) at baseline and several hours post-injury. There was no statistically significant difference between baseline chamber depth (0.37mm±0.00) and post-injury chamber depth (0.38±0.01mm) in the contralateral eyes.

Trauma damages both the retina and RPE

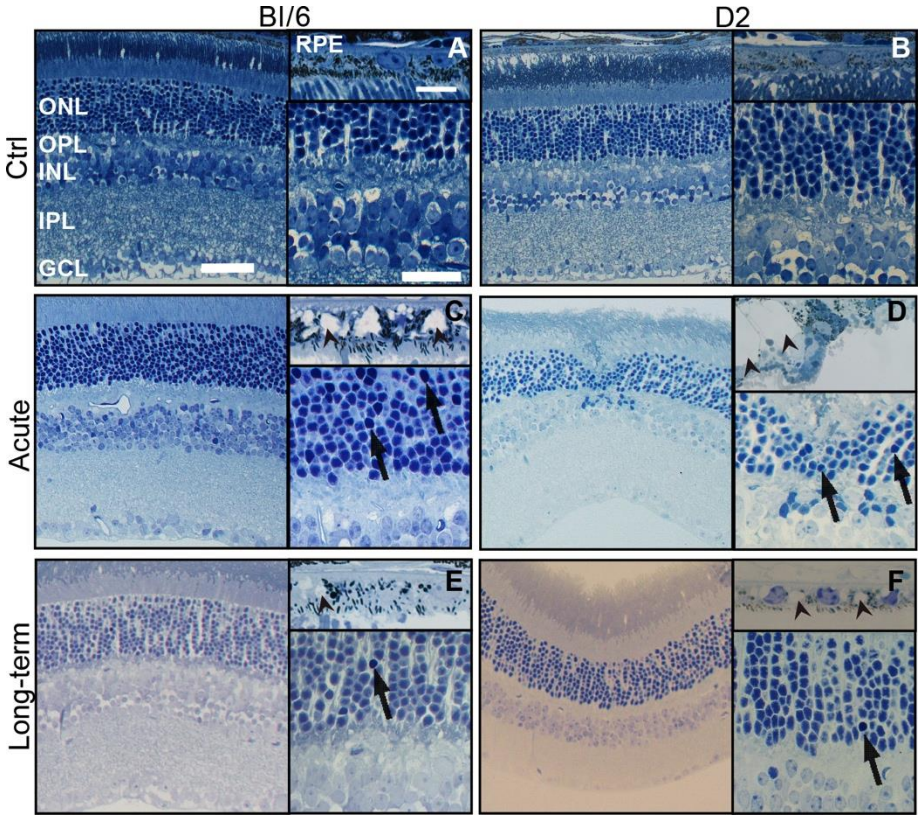

Figure 2.30. Focal retinal and RPE damage occurs in the contralateral eyes of both strains post-blast. Both Bl/6 (A) and D2 (B) control retina and RPE have no pyknotic nuclei and no RPE vacuoles. Both pyknotic nuclei (arrows) and RPE vacuoles (arrowheads) occur at 1 week post-injury in the Bl/6 (C) and at 3 days post-injury the D2 (D). At 1 month post-injury, pyknotic nuclei (arrow) and RPE vacuoles (arrowhead) are rare in the Bl/6 (E), while the D2 eyes contains pyknotic nuclei and smaller RPE vacuoles (F). The scale bars are: 50µm in the low magnification retina image; 25µm in the high magnification retina image; and 5µm in the RPE image.

Controls for both strains had healthy RPE with no vacuoles and retinas lacked pyknotic nuclei or other pathology (Figure 2.30A-B). Due to the lack of pathology at 3 days post-injury, Bl/6 retinas were examined at 1 week and 1 month post-injury. D2 retinas were examined at 3 days and 1 month post-injury. While much of the retina looked normal, focal damage was detected in both strains.

Pyknotic nuclei were present in Bl/6 contralateral eyes post-blast (Figure 2.30C, E). The average number of pyknotic nuclei at 1 week post-injury was 16±6 in the ONL and 21±7 in the INL. At 1 month post-injury, the average number of pyknotic nuclei within contralateral retinae decreased to 3±2 in the ONL and 1±1 in the INL. Grade 3 vacuoles were observed in all contralateral eyes at 1 week post-injury (Figure 2.30C). By 1 month post-injury, the RPE was normal (grade 1) in all of the eyes examined (Figure 2.30E).

In the D2 mice, pyknotic nuclei were also observed in contralateral retinae post-injury (Figure 2.30D, F). At 3 days post-injury, the average number of pyknotic nuclei was 10±3 and 13±1 in the ONL and INL, respectively. At 1 month post-injury, the average number of pyknotic nuclei in the contralateral retinae was 12±1 in the ONL and 4±2 in the INL. The RPE of contralateral D2 eyes contained grade 5 RPE vacuoles at 3 days post-injury in 67% of eyes (Figure 2.30D). At 1 month post-injury, 60% of contralateral eyes contained RPE vacuoles, ranging from grade 2-4 (Figure 2.30F).

Delayed cell death occurs after trauma in both strains

In the Bl/6 contralateral eyes, cell death was not detected until 1 week post-injury and was limited to small patches in the mid-peripheral and occasionally central retina

(Figure 2.30C, E). The majority of the TUNEL-positive nuclei were located in the ONL (Figure 2.30G). TUNEL-positive cells were present in only 4±2% and 3±1% of the retina, at 1 week and 1 month post-injury, respectively (Figure 2.32A). The density of cell death throughout the entire retina was also low at 1 week and 1 month post-injury with 18±11 cells/mm retina and 11±4 cells/mm retina, respectively (Figure 2.32B). Within areas of cell death (affected regions, Figure 2.31E, 2.32A), the density of TUNEL-positive nuclei was 383±179 cells/mm retina at 1 week and 373±77 cells/mm retina at 1 month post-injury (Figure 2.32C). The comparable density and percent retina affected at both time points suggests ongoing cell death in the Bl/6 from 1 week to 1 month post-trauma.

The onset of cell death also occurred at 1 week post-injury in the D2 and was limited to small patches in the mid-peripheral and central retina (Figure 2.31D, F). Like the Bl/6, many TUNEL-positive nuclei were present in the ONL (Figure 2.31H). At 1 week post-injury, 19±8% of the retina contained TUNEL-positive cells (Figure 2.32A). At 1 month post-injury, the percentage of TUNEL-positive contralateral retina decreased to 3±2% (Figure 2.32A). The density of TUNEL-positive nuclei throughout the entire retina of the D2 was low; 49±30 cells/mm retina at 1 week post-injury, decreasing to 12±8 cells/mm retina at 28 dpi (Figure 2.32B). The density of TUNEL-positive nuclei within the affected regions of the D2 retina was 475±81 cells/mm retina at 1 week post-injury and 212±135 cells/mm retina at 1 month (Figure 2.32C). The decrease in both the percent retina affected and the density of cell death in those areas at 1 month post-injury suggests that in the D2 there is a peak of cell death at 1 week that decreases at 1 month post-injury.

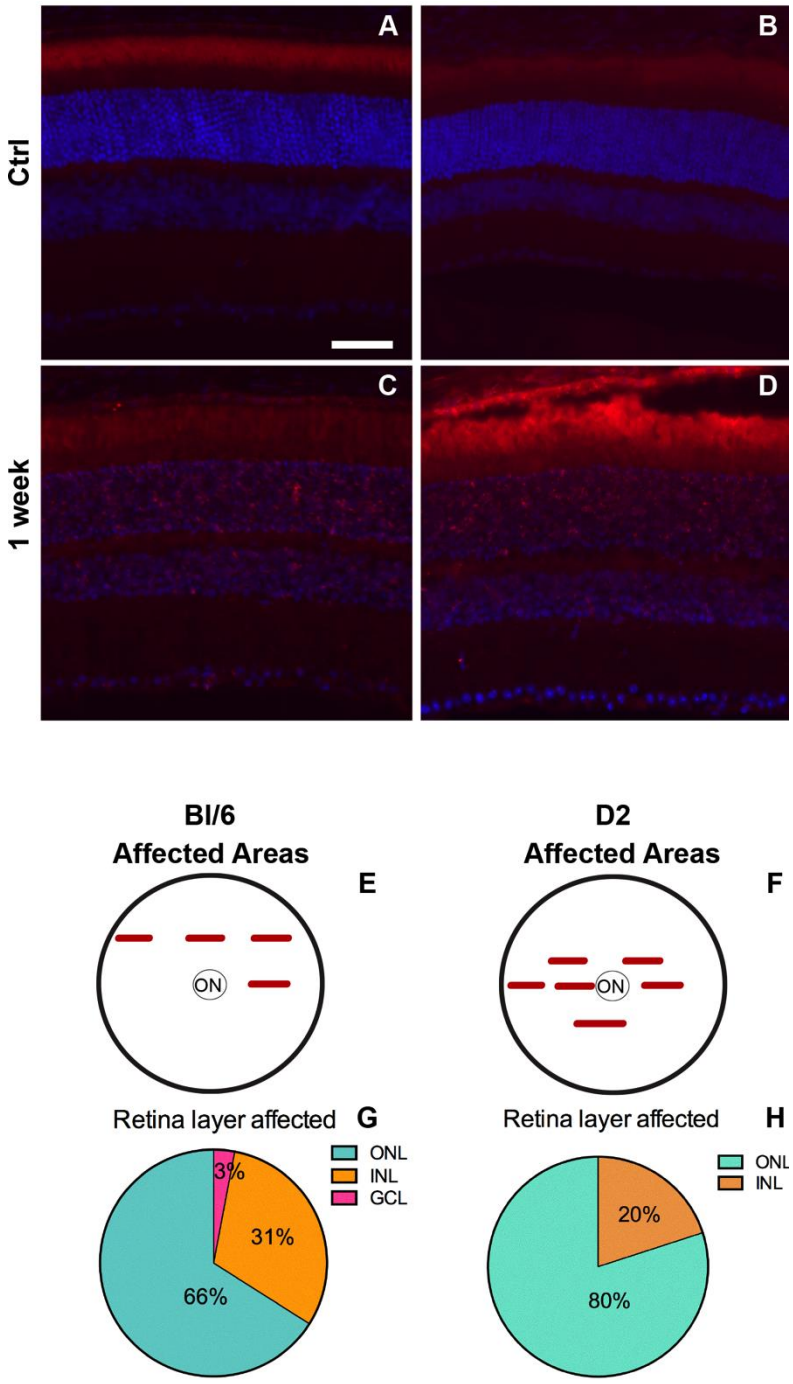

Figure 2.31. Cell death occurs in focal regions after blast in both strains. Epifluorescence micrographs of retinal cross-sections from control Bl/6 (A), 1 week post-injury Bl/6 (C), control D2 (B) and 1 week post-injury D2 (D). TUNEL (red), DAPI (blue). The scale bar in (E) is 50µm and applies to all micrographs. Schematics illustrating the locations of TUNEL-positive retinal cross-sections in relation to the optic nerve (ON) in the Bl/6 (E) and the D2 (F). Pie charts showing the percentage of TUNEL-positive cells in each retinal layer in the Bl/6 (G) and D2 (G).

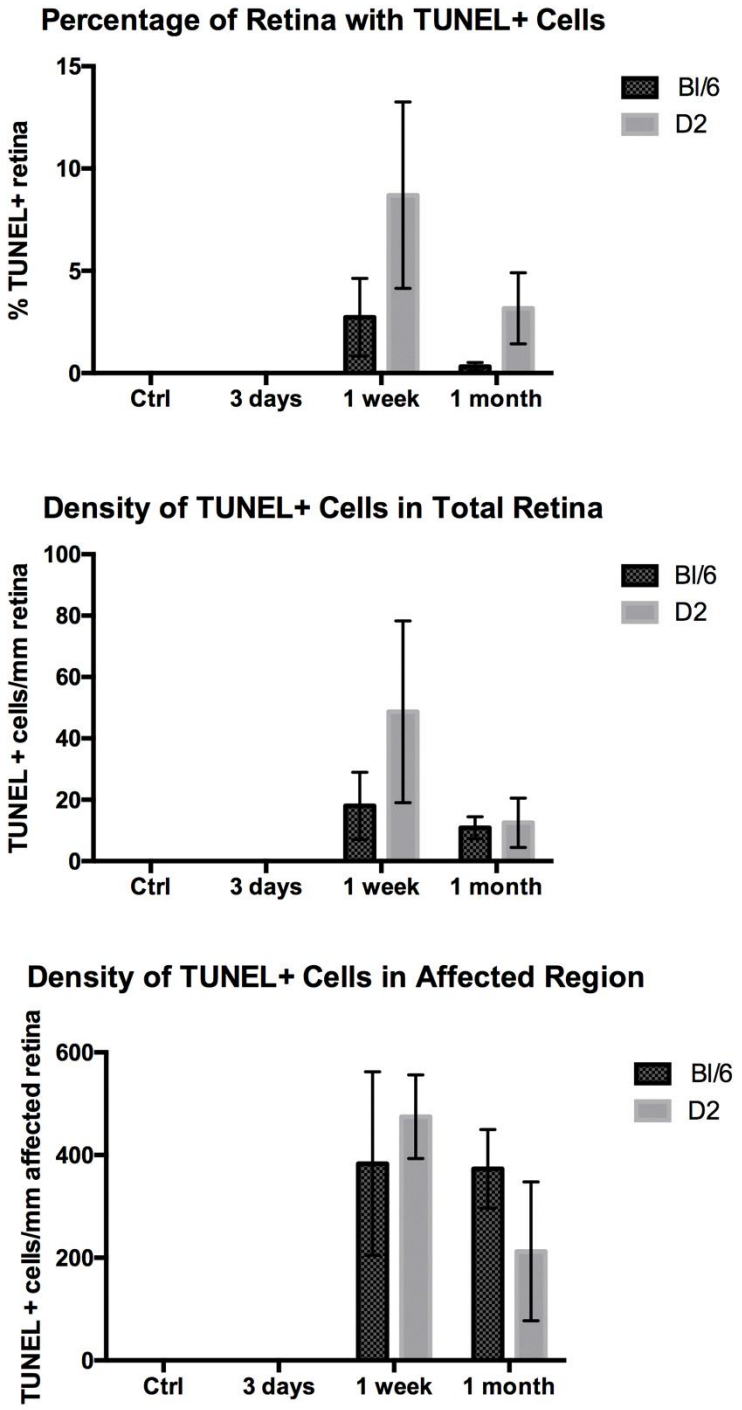

Figure 2.32. Cell death occurs at 1 week and 1 month post-injury in both strains. Bar graphs show the percentage of retina containing TUNEL-positive cells (A), the density of TUNEL-positive cells in the retina (B), and the density of TUNEL-positive cells within the affected region (C). The bar graphs represent the average ± SEM for each time point and strain.

Necroptotic and pyroptotic pathways are activated following injury in both strains

In both Bl/6 and D2 control retinae, RIP1 localized to the Müller glia, the INL and the IPL, with some light staining in the OPL (Figure 2.33A-B). RIP3 immunolabeling was present in the IPL and INL in control retinas from both Bl/6 and D2 mice (Figure 2.33A-B). At 3 days post-injury, RIP1 staining increased within the Müller glia and IPL, but there were no changes in RIP3 labeling (Figure 2.33C). The increased labeling was limited to 3-4 sections from each eye, indicative of focal damage. At 1 month post-injury, no increased RIP1 labeling was present, but RIP3 labeling was increased in the ONL, IPL and GCL (Figure 2.33E). Again, these changes were limited to 3-4 sections in each eye.

In the D2 retina, both RIP1 and RIP3 labeling was similar to controls throughout the eye at 3 days post-injury (Figure 2.33D). At 28 dpi, RIP1 staining was brighter in the ONL and INL, while RIP3 staining was brighter in the ONL, INL, IPL, and GCL (Figure 2.33F). Similar to the Bl/6, these changes were limited to 3-4 sections in each eye.

Caspase-1 immunolabeling was absent in control and 3 day post-injury Bl/6 retinas (Figure 2.34A, B). At 1 month post-injury, 75% of contralateral C57Bl/6J retinae contained caspase-1 positive cells at the inner edge of the INL and in the GCL (Figure 2.34C). The caspase-1 positive cells were present throughout the retina and the labeling did not appear different between central (Figure 2.34D) and mid-peripheral retina (Figure 2.34E). In contrast, caspase-1 positive nuclei were present within the INL and GCL of control D2 retinas (Figure 2.35A). However, at both 3 days and 1 month post-injury in the D2 retinae, no caspase-1 positive nuclei were detected (Figure 2.35B-C).

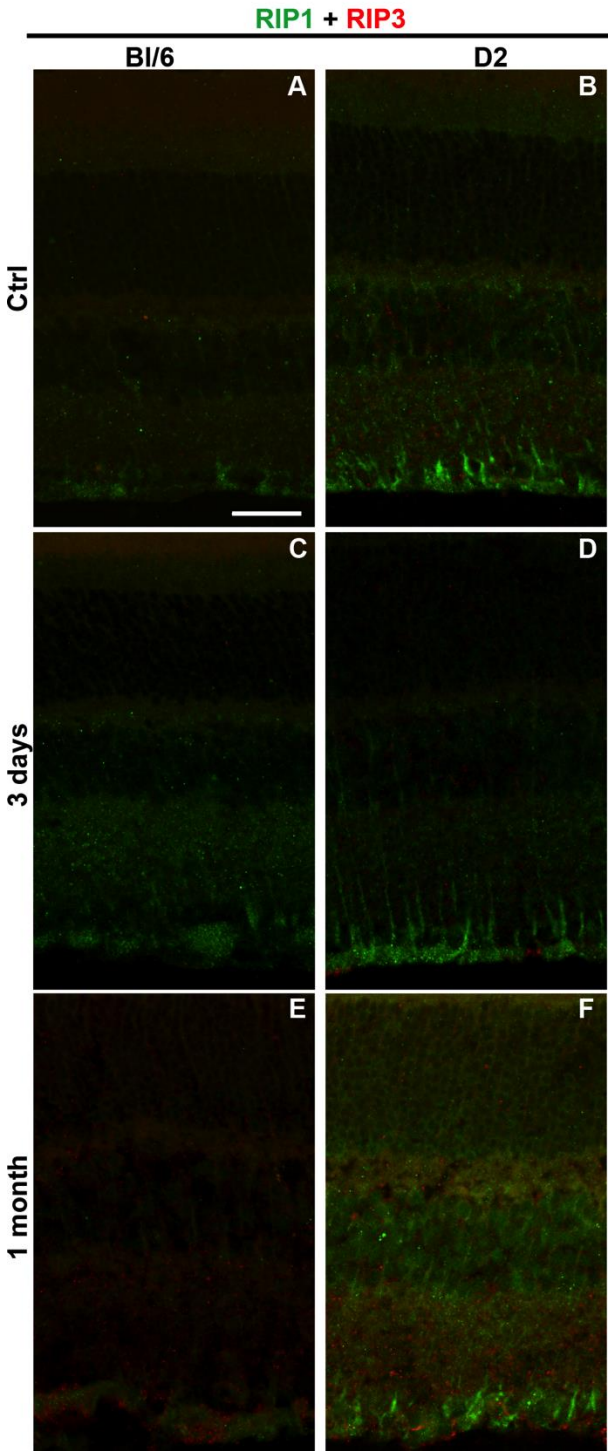

Figure 2.33. RIP1 and RIP3 immunolabeling increases after blast in both the Bl/6 and D2. Confocal micrographs of retinas from control Bl/6 (A), control D2 (B), 3 day post-injury Bl/6 (C), 3 day post-injury D2 (D), 1 month post-injury Bl/6 (E) and 1 month post-injury D2 (F). RIP1 is pictured in green and RIP3 is in red. The scale bar in (A) is 50µm.

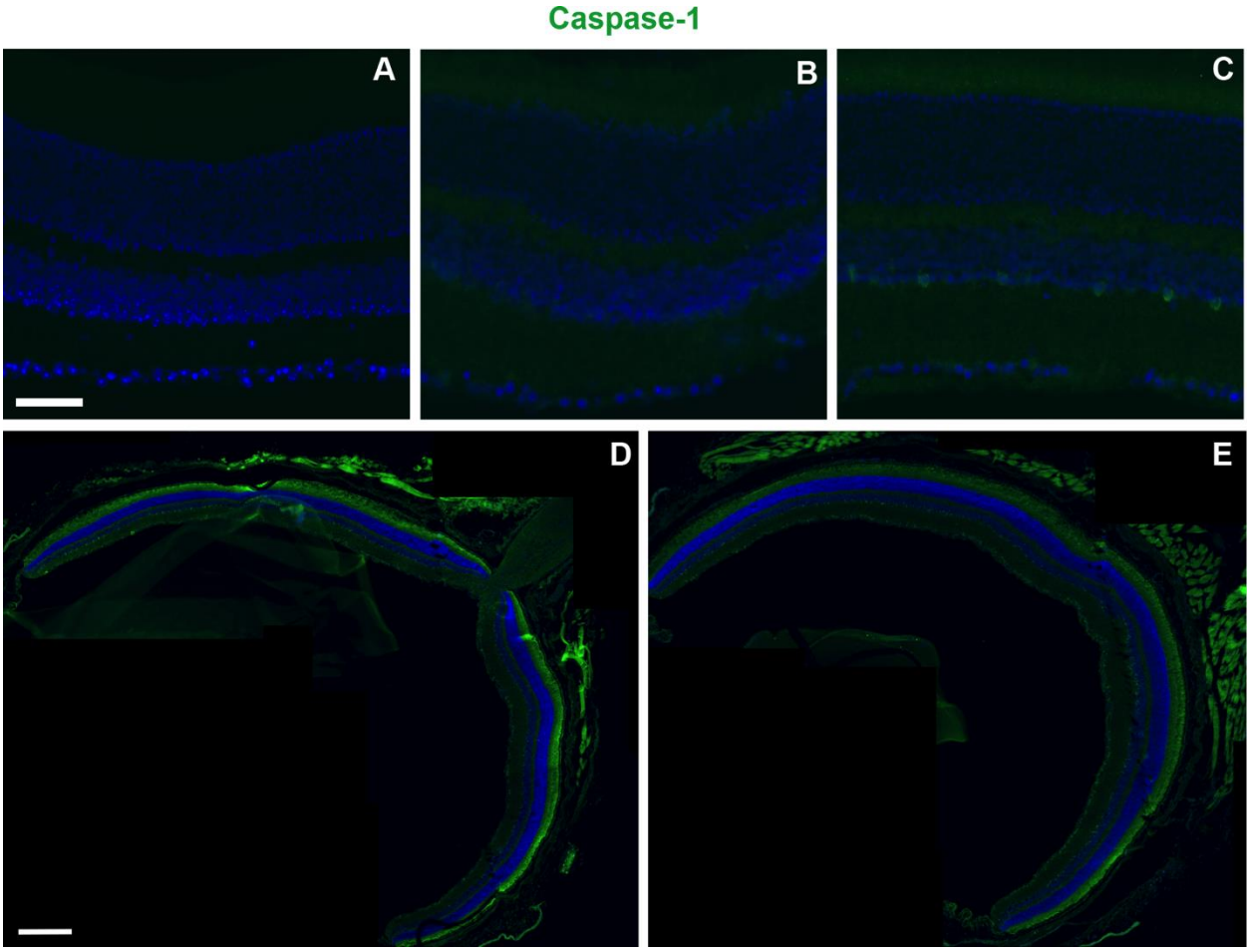

Figure 2.34. Caspase-1 immunolabeling increases at 1 month post-injury in the Bl/6 retina. Epifluorescence micrographs of retinas from control (A), 3 days post-injury (B) and 1 month post-injury (C) eyes labeled with anti-caspase-1 (green) and DAPI (blue). Caspase-1 immunolabeling at 1 month post-injury is the same in both central (D) and mid-peripheral (E) retina. The scale bar is 50µm in (A-C) and 250µm in (D-E).

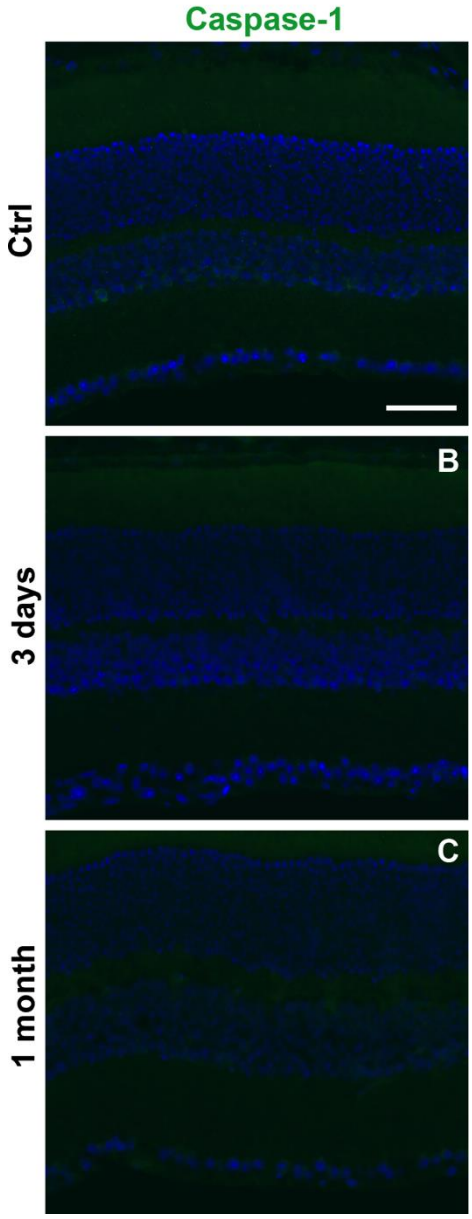

Figure 2.35. Caspase-1 immunolabeling is reduced after trauma in the D2. Representative epifluorescence micrographs of control (A), 3 days post-injury (B) and 1 month post-injury (C) retinas immunolabeled for caspase-1. The scale bar in (A) is 50µm and applies to all micrographs.

Glial reactivity occurs after trauma

Similar to the blast-exposed Bl/6 retina, GFAP immunolabeling was restricted to the astrocytes and Müller glia endfeet at all time points post-injury (Figure 2.36A-D). In contrast, GFAP immunolabeling extended up the Müller cell processes in the D2 retinas (Figure 2.37B-C). At 3 days post-injury, the GFAP positive processes were detected uniformly across the retina (Figure 2.37B). At 1 week post-injury, GFAP positive processes were only detected in small patches in the mid-peripheral and central retina (Figure 2.37C). Increased GFAP immunolabeling was not detected in any region of the retina at 1 month post-injury (Figure 2.37D).

In the normal Bl/6 and D2 retina, microglia had small somas with dendritic ramifications and were present only in the inner retina (Figure 2.38A-B). In the Bl/6 retina, all changes in microglial morphology after injury were limited to focal areas (e.g. 1-2 sections from each eye). At 3 days post-injury, reactive microglia (enlarged somas with fewer shorter processes) were observed in the ONL and INL and microglial processes extended into the ONL (Figure 2.38C). At 1 week and 1 month post-injury, there were no reactive microglial somas in the ONL, but a few reactive microglia were present in the INL and occasional processes were detected in the ONL (Figure 2.38E, G).

Reactive microglia were commonly observed throughout the D2 retina at 3 days post-injury (Figure 2.38D). Macrophages were also occasionally observed in the outer segment layer of the photoreceptors in areas of retinal detachment (Figure 2.38D). At 1 week and 1 month post-injury, microglial reactivity was limited to focal areas of the inner retina in the mid-periphery and occasionally the central retina (Figure 2.38F, H).

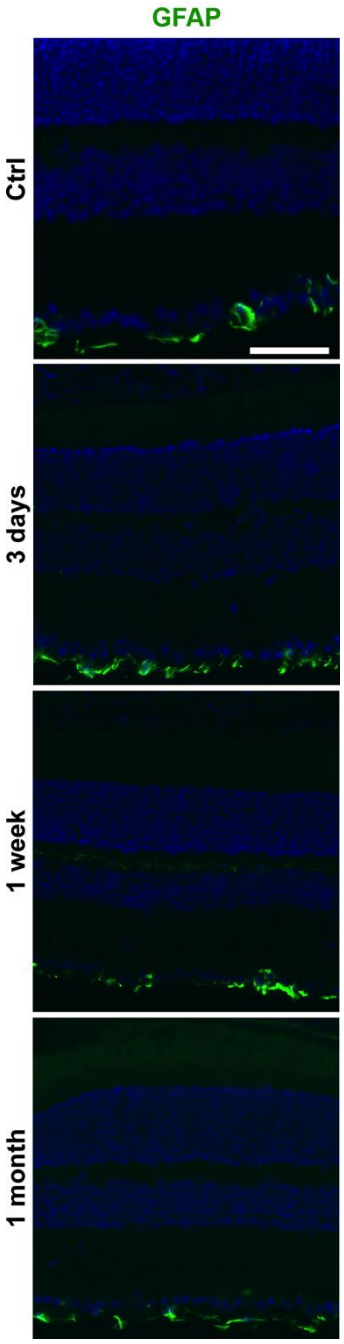

Figure 2.36. GFAP immunolabeling remains restricted to the astrocytes and Müller glia endfeet in the Bl/6 after injury. Representative epifluorescence micrographs of control (A), 3 days post-injury (B), 1 week post-injury (C) and 1 month post-injury (D) retinas immunolabeled for GFAP. The scale bar in (A) is 50µm and applies to all micrographs.

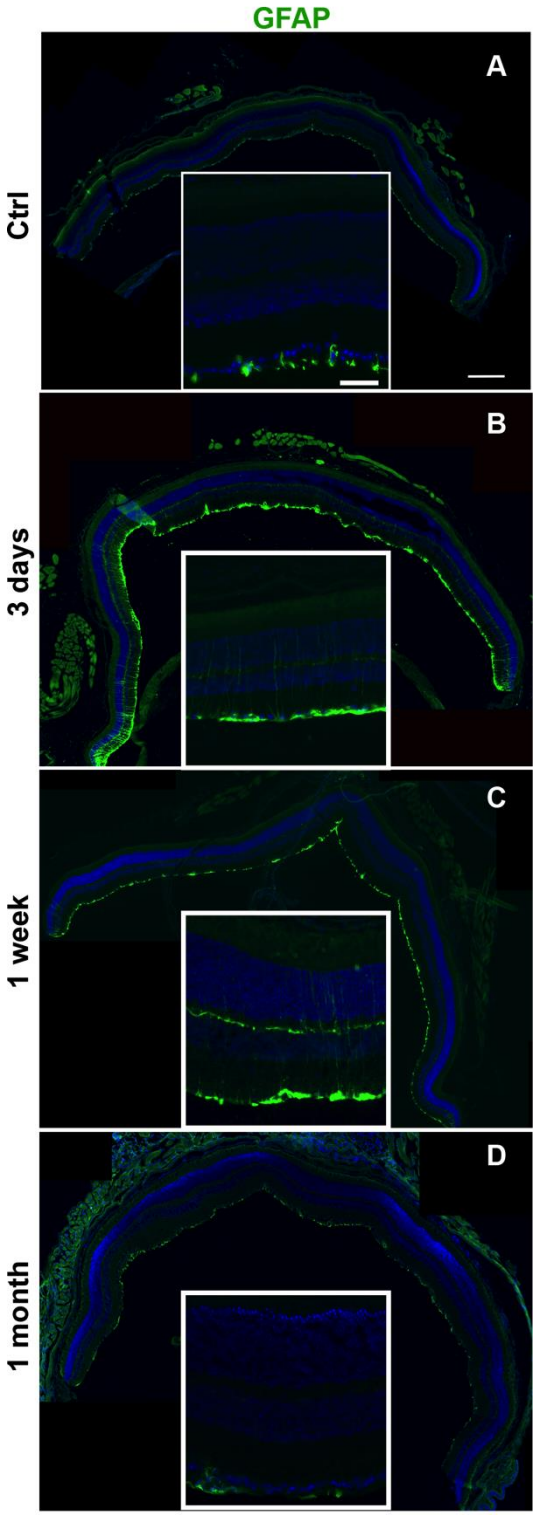

Figure 2.37. GFAP labeling is increased in the Müller glia of D2 eyes at 3 days and 1 week post-injury. Low and high magnification epifluorescence micrographs of control (A), 3 days post-injury (B), 1 week post-injury and 1 month post-injury (D) retinas labeled with GFAP (green) and DAPI (blue). The scale bar for the high magnification micrographs is 50µm. The scale bar for the low magnification micrographs is 250µm.

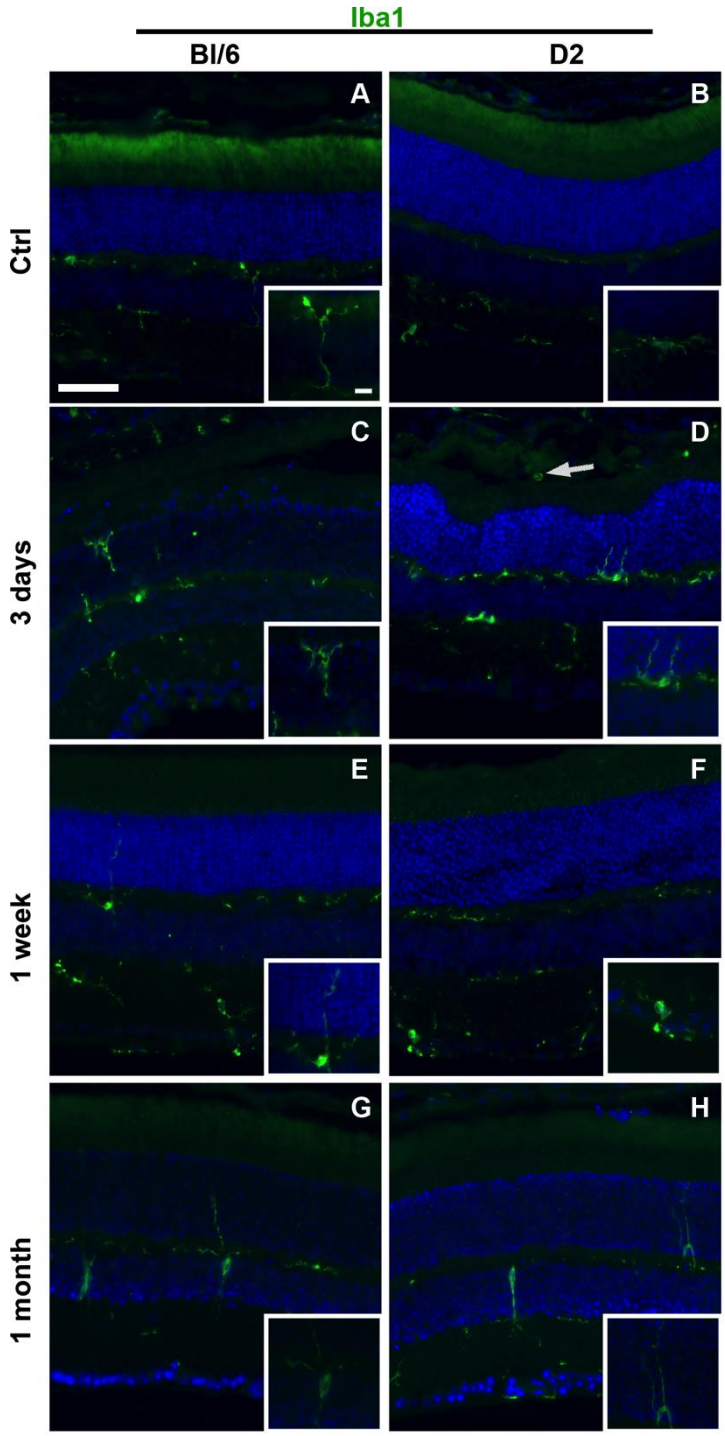

Figure 2.38. Reactive microglia are present in Bl/6 and D2 retinas after injury. Low magnification epifluorescence micrographs and high magnification micrographs (insets) of control (A-B), 3 days post-injury (C-D), 1 week post-injury (E-F) and 1 month post-injury (G-H) retinas immunolabeled with Iba1 (green) and DAPI (blue). The scale bar for the low magnification micrographs is 50µm. The scale bar for the inserts is 10µm.

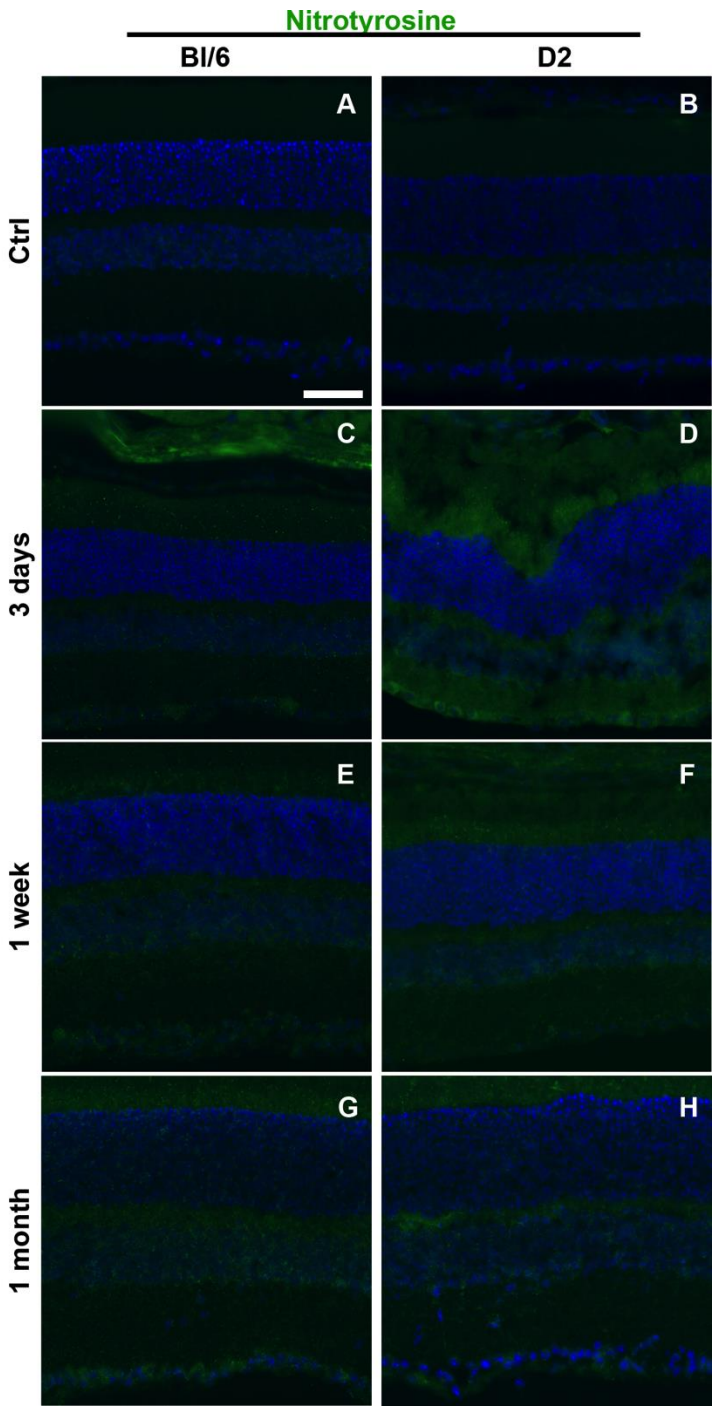

Figure 2.39. Nitrotyrosine immunolabeling increases after blast in the retina of both strains. Epifluorescence micrographs of control (A-B), 3 days (C-D), 1 week (E-F) and 1 month post-injury (G-H) retinal cross-sections labeled for nitrotyrosine (green) and DAPI (blue). The scale bar is 50µm and applies to all micrographs.

Protein nitration increases in the retina after blast

In the Bl/6 mouse, all eyes exhibited a slight increase in nitrotyrosine immunolabeling in the inner retina at 3 days and 1 week post-injury when compared to controls (Figure 2.39C, E). Changes in nitrotyrosine immunolabeling were limited to focal areas within both the mid-peripheral and central retina. At 1 month post-injury, there was nitrotyrosine immunolabeling in the outer retina (absent in the normal retina), in addition to more labeling in the inner retina (Figure 2.39G). The changes in labeling were uniform across the retina.

At 3 days post-injury in the D2 mouse, nitrotyrosine immunolabeling was greatly increased in the inner retina of all eyes with no apparent regional differences when compared to controls (Figure 2.39D). Labeling remained elevated throughout the inner retina of all eyes 1 week and 1 month post-injury, with no apparent regional differences (Figure 2.39F, H).

Ocular trauma causes visual deficits

Both strains showed decreased OKN scores (i.e. visual acuity) in the contralateral eye post-blast (Figure 2.40A-B). In the Bl/6 mouse, OKN scores were only significantly different from baseline (0.41±0.01 c/d) at 1 week post-injury (0.30±0.04 c/d, $p<0.01$, Figure 2.40A). In the D2 mice, OKN scores first declined significantly at 3 days post-injury (0.40±0.06 c/d, $p<0.01$) when compared to baseline values (0.60±0.03 c/d, Figure 2.40B). OKN scores were also significantly different from baseline at 2 weeks and 1 month post-injury (0.25±0.06 and 0.07±0.03 c/d, $p<0.01$, respectively).

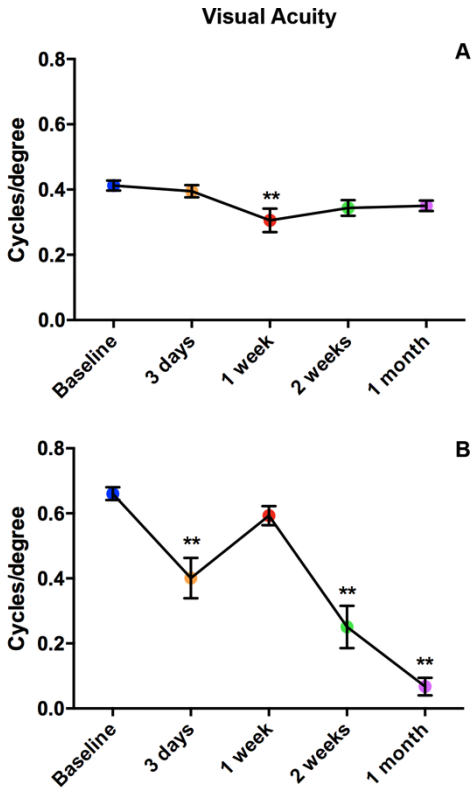

Figure 2.40. Visual acuity declines after blast in both Bl/6 (A) and D2 (B). The average cycles/degree ± SEM are plotted over time. **p<0.01

There were no significant changes in the ERG a_{max}, b_{max} or oscillatory potentials at any time point assessed in the Bl/6 eye after injury (Figure 2.41A, C, E). However, there were significant reductions in both a_{max} and b_{max} in the D2 after blast when compared to baseline values (Figure 2.41B, D). At 1 week post-injury, the a_{max} was significantly lower than baseline at light intensities that correlate with daytime light levels. At 0 log cd*s/m^2 the a_{max} was decreased by 39% from 135.7 ± 9.6 μV at baseline to 82.5 ± 14.2 μV, $p<0.01$ (Figure 2.41B). At 1 log cd*s/m^2 the a_{max} was decreased by 29% from 194.3 ± 12.2 μV to 137.9 ± 20.2 μV, $p<0.05$ (Figure 2.41B). At 1 month post-injury, the a_{max} recovered, but the b_{max} was significantly reduced at several light

intensities. At -1 log cd*s/m^2 the b_{max} was decreased 42% from 335.2 ± 18.2 µV to 193.7 ± 31.4 µV, p<0.01 (Figure 2.41D). At 1 log cd*s/m^2 the b_{max} was decreased 33% from 451.3 ± 25.9 µV at baseline to 301.2 ± 35.7 µV, p<0.01 (Figure 2.41D). The oscillatory potentials did not change after blast in the D2 (Figure 2.41E).

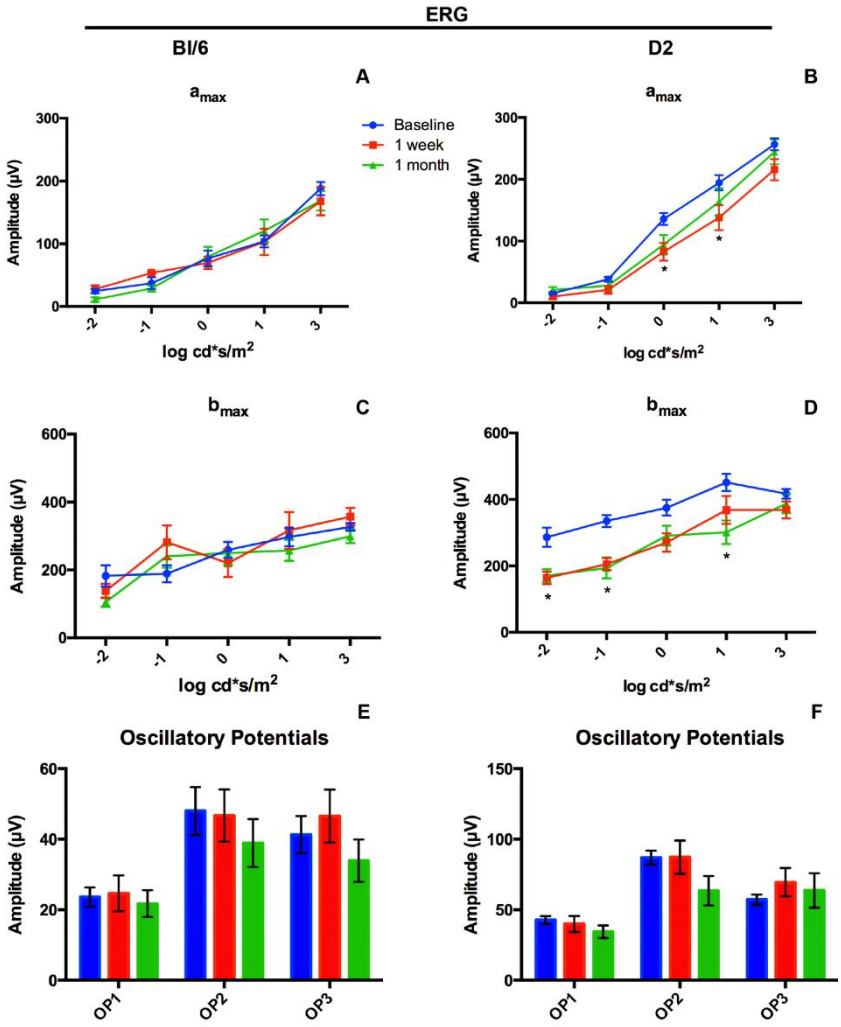

Figure 2.41. Blast causes ERG deficits in the D2, but not the Bl/6. Graphs of the average ± SEM of a_{max} (A-B), b_{max} (C-D) and oscillatory potentials (E-F) for Bl/6 and D2 mice, respectively, at baseline, 1 week and 1 month post-injury. *p<0.05

Ocular trauma did not damage the olfactory epithelium or optic nerves

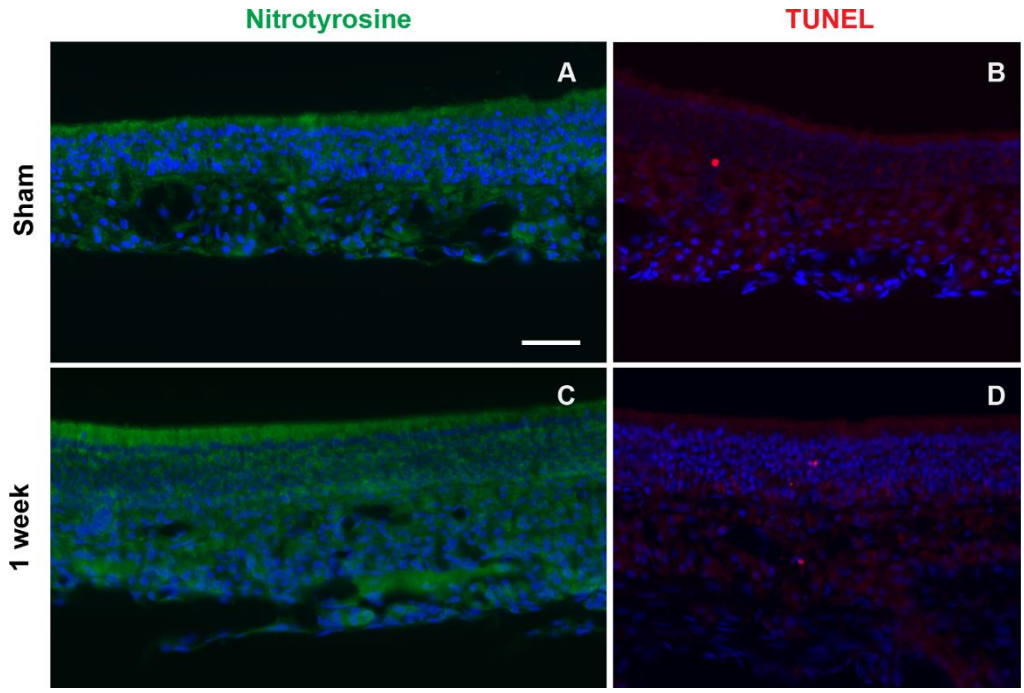

Figure 2.42. Blast has no effect on the Bl/6 olfactory epithelium. Representative epifluorescence micrographs of sham (A-B) and 1 week post-injury (C-D) olfactory epithelium immunolabeled for nitrotyrosine (A,C, green) and TUNEL (B,D, red). The scale bar in (A) is 50µm and applies to all images.

The olfactory epithelium was examined in 1 week post-injury Bl/6 mice for evidence of blast injury to the tissue between the eyes (Figure 2.42A-D). We observed no differences between sham and blast animals with either nitrotyrosine immunolabeling (Figure 2.42A, C) or TUNEL (Figure 2.42B, D).

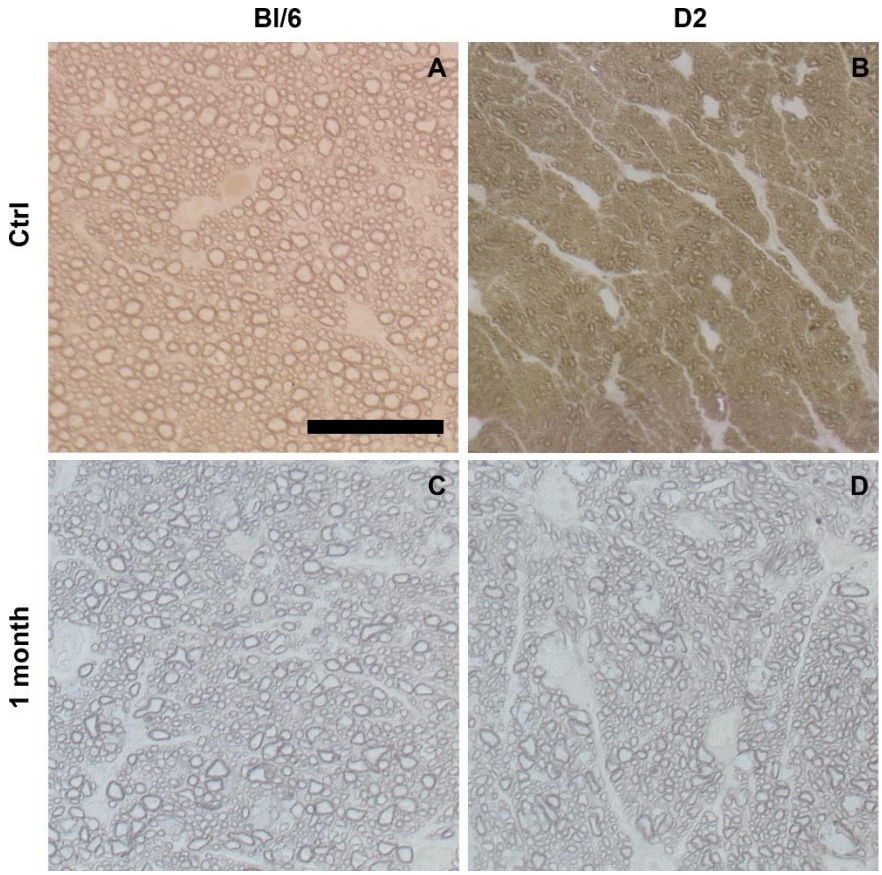

Figure 2.43. The optic nerve is unaffected by trauma. Representative micrographs of control (A-B) and 1 month post-injury (C-D) optic nerve cross-sections. The scale bar in (A) is 20μm and applies to all micrographs.

Since degenerative axons in the blast-exposed optic nerve were most evident at 1 month post-injury, we examined contralateral optic nerves from both strains at 1 month post-injury (Figure 2.43A-D). There were no differences between contralateral optic nerves (Figure 2.43C-D) and control optic nerves (Figure 2.43A-B).

Discussion

Mild, progressive trauma in the Bl/6 mouse

Ocular blast trauma in the Bl/6 mouse induces a delayed injury response similar to what has also been described in models of TBI (Johnson et al., 2013) and in Veterans with blast-induced mild TBI (Cockerham et al., 2009, 2011; Weichel et al., 2009). The injury phenotype is mild when compared to the D2 and Balb/cJ mice (Bricker-Anthony et al., 2014a, 2016b) and is similar to closed-globe injuries reported in blast-exposed veterans (Cockerham et al., 2011). However, certain findings such as delayed cell death and optic nerve degeneration, as well increased oxidative stress and inflammation over time, are suggestive of subtle, ongoing degeneration after blast exposure.

Cell death did not occur in the Bl/6 eye until 1 month post-injury and only covered 3% of the retina, whereas substantial cell death occurred in the D2 and Balb/cJ retinas within days of the injury. Since most cell death occurred in the outer retina, we expected to see deficits in the ERG. However, the small, focal pockets of cell death we observed are likely insufficient to interfere with visual function. Normal ERG amplitudes after blast is also consistent with findings in the shock tube model (Mohan et al., 2013).

RIP3, a marker of necroptosis, was the only cell death marker substantially increased in the outer retina after blast. RIP3 directly interacts with several mitochondrial enzymes and pushes metabolism into overdrive when overexpressed, resulting in excess production of reactive oxygen species and necrosis (Bergsbaken et al., 2009). Both TNF-α and RIP3 have also been reported to increase activation of microglia (Trichonas et al., 2010). Detection of RIP3 in the ONL at 1 month after blast

correlated with detection of reactive microglia and increased nitrotyrosine immunolabeling in the ONL. These findings suggest that RIP3 may also contribute to both microglial activation and oxidative stress in the outer retina, which may result in ongoing retinal degeneration after blast.

TUNEL-positive cells were also detected in the INL in a subset of retinas. In other blast models, the most consistent and robust molecular changes were detected in the inner retina and involved nitrosative stress (Mohan et al., 2013; Zou et al., 2013). Exposure to TNT at the same the same blast pressure used in our study elicited increased iNOS labeling in the inner retina (Zou et al., 2013). Therefore, it is possible that increased peroxynitrite immunolabeling and increased RIP1, RIP3 and caspase-1 immunolabeling in the INL are linked, as oxidative stress both initiates and results from pyroptosis and necroptosis (Bergsbaken et al., 2009; Fink et al., 1999; Jin and Flavell, 2010).

Caspase-1 immunolabeling in the starburst amacrine cells has interesting implications for both functional and pathological outcomes following blast injury. Starburst amacrine cells are critical for signaling directional selectivity onto downstream RGCs and are, therefore, necessary for the OKN response that is used to measure visual acuity (Taylor and Smith, 2012). Damage to the starburst amacrine cells could explain the decrease in visual acuity after blast in our model. Caspase-1 immunolabeling was also present in inner retinal cells negative for ChAT. AII amacrine cells, which belong to a major amacrine cell population (glycinergic amacrine cells) in the retina (Haverkamp and Wässle, 2000), are involved in the transmission of rod photoreceptor signals to the retinal ganglion cells (Helga Kolb, 2016). The spread of

caspase-1 labeling from small retinal regions at 3 days post-blast to amacrine cells throughout the entire retina at 1 month post-blast suggests spread of a molecular signal inducing increased levels of caspase-1 in neighboring cells. AII amacrine cells are connected to each other by connexin-mediated gap junctions (Hampson et al., 1992), through which small signaling molecules can travel to enact neuroprotection or neurodegeneration (Danesh-Meyer et al., 2012; Massey et al., 2003; Paschon et al., 2012; Striedinger et al., 2005; Yoon et al., 2010).

Despite the lack of RGC death in our model at 28 days post-blast, our results suggest that the RGCs may die at later time points, as reported in other blast models (Koliatsos et al., 2011; Mohan et al., 2013). First, we begin to detect axon degeneration at 1 month post-blast, which may precede RGC death as it does in traumatic optic neuropathy (Warner and Eggenberger, 2010). Second, labeling for nitrotyrosine and markers of pyroptosis and necroptosis in the GCL are increased at 1 month post-blast, which is consistent with other studies showing the first evidence of RGC death at 4 months post-blast (Mohan et al., 2013).

In summary, markers of oxidative stress and inflammation increase over time after blast and are primarily localized to the inner retina, suggesting that inner retinal changes may drive visual deficits and that further cell death may be expected at later time points after blast. This study provides molecular insight into the effects of ocular trauma on the neural retina that may underlie the delayed vision loss that occurs in blast-exposed patients despite a normal ophthalmological exam.

Severe trauma in the D2 mouse

A large influx of immune cells into the eye occurred after blast in the D2, but not in the Bl/6 or Balb/cJ, which have a fully intact ACAID. The immune response after trauma elicited formation of epiretinal membranes, increased nitrosative stress, greater cell death, and more severe vision loss than was detected in the Bl/6 or Balb/cJ mice (Bricker-Anthony et al., 2014b, 2016b). The RPE damage in the D2 at 3 days post-injury was severe when compared to the Bl/6 and Balb/cJ at 1 week post-blast. Remarkably, despite the early and dramatic vacuolization and significant amount of subretinal debris present within days after blast, the RPE and subretinal space appeared near normal at 1 month after injury, like the Bl/6. These findings show that the RPE cells are very resilient and are adept at phagocytosing and removing subretinal debris.

The differences in response to blast between the D2 mouse and the Bl/6 and Balb/cJ mouse strains are consistent with comparisons between open globe and closed globe trauma patients (Scott, 2011). Blast injury in the D2 mouse resulted in rapid, severe vision loss that failed to recover by 1 month (Bricker-Anthony et al., 2014a). In contrast, blast injury in the Bl/6 mouse only induced a mild deficit in visual acuity that recovered by 1 month (Bricker-Anthony et al., 2014b). In blast-exposed human patients, open globe injuries initially caused severe visual acuity deficits, ranging from 5/200 to no light perception (Erdurman et al., 2011). After 6 months, 45% of the patients had no light perception, while the remaining 55% of patients had visual acuity ranging from >20/40 to light perception (Erdurman et al., 2011). In contrast, human patients with blast-induced closed injuries had better initial visual acuity (ranging from >20/40 to light perception) and 66% of the patients had visual acuity >20/40 after 6 months (Erdurman

et al., 2011). Blast injury in the D2 mouse also induced peripheral immune cell infiltration, which was absent in both the Bl/6 and Balb/cJ mice after blast. Peripheral immune cell infiltration also occurs in endophthalmitis, an inflammatory intraocular condition (Egan et al., 2016) that can affect human patients with open globe injuries, but typically does not affect patients with closed globe injuries (Cebulla and Flynn, 2009). In endophthalmitis, ocular immune privilege is lost and peripheral immune cells invade the eye and secrete damaging inflammatory cytokines that can lead to retinal cell death and profound vision loss (Callegan et al., 2002).

As in the post-blast Bl/6 retina, the cell death pathway appeared to be non-apoptotic in the D2 retina (Bricker-Anthony et al., 2014b). In both mice, we detected increases in markers for necroptosis (RIP1 and RIP3) after blast, suggesting that necroptosis is the main cell death pathway activated after blast. The peak of cell death was earlier in the D2 – 3 days as compared to 1 month in the Bl/6 or 1 week in the Balb/cJ (Bricker-Anthony et al., 2014b, 2016b). Additionally, we observed more TUNEL-positive nuclei in the D2 retina than in the Bl/6 or Balb/cJ retinas. Like the Bl/6, optic nerve damage occurred at 1 month post-injury, but it was more severe than in the Bl/6 or Balb/cJ at the same time point.

There were also differences between our blast model in the D2 and other models of blast injury. Unlike the whole body/head blast models (Goldstein et al., 2012; Mohan et al., 2013), photoreceptor cell death was present in this model and in a TNT blast study (Zou et al., 2013). The discrepancies may be due to the physics of head movement in their model as compared to our model and the TNT model (Zou et al., 2013). Similar to Mohan et al., we detected RGC death and degeneration in the optic

nerve (Mohan et al., 2013). They reported axon degeneration and RGC loss at 10 months post-blast in the Bl/6 mouse while we showed that it may begin as early as 3 days in the D2 and Balb/cJ mice or 1 month post-blast in the Bl/6 mice.

The pathological changes after blast in the D2 mouse, such as Müller glia reactivity, nitrosative stress and immune infiltrate, were consistent with findings in the high-level blast exposure group at 2 weeks post-injury in the TNT model (Zou et al., 2013). The Bl/6 and Balb/cJ mice exhibited a milder phenotype like the low-level blast group in the TNT study. We suspect these differences are due to the presence of immune infiltrate in the D2 mouse and their high-level blast animals, which was absent from our Bl/6 and Balb/cJ mice and their low-level blast animals.

Compared to Bl/6, the D2 mice had significant visual function deficits post-injury as measured by the ERG. Acutely, the visual acuity and ERG amplitude deficits appear to be driven by damage to the outer retina. Photoreceptor and RPE damage likely drove the early ERG deficits, as the a wave was more affected than the b wave. These deficits in visual function correlated with the presence of retinal detachments and extensive vacuolization in the RPE, indicative of oxidative stress (Fujihara et al., 2008), in the first week after injury. The RPE damage may have temporarily impaired recycling of 11-cis-retinal (Schraermeyer and Heimann, 1999), which could have driven the transient reduction in the ERG a wave. The recovery of the OKN at 1 week post-blast may reflect resolution of the RPE damage in combination with an improvement in the OKN response as a result of repeat testing (Prusky et al., 2008). A similar decrease and subsequent recovery of visual function occurred in our model with the Bl/6 mouse and in Mohan and colleagues' blast model (Bricker-Anthony et al., 2014b; Mohan et al., 2013).

Temporary deficits in visual acuity are also observed in patients following blast injury (Alam et al., 2012; Phillips et al., 2013).

At 1 month post-blast, the ERG amplitudes were affected in a different manner. The ERG b wave and visual acuity continued to decrease at 1 month post-blast as the a wave improved. These findings suggest ongoing dysfunction in the inner retina after blast. These results are supported by the detection of a second wave of TUNEL-positive cells and significant optic nerve degeneration at 1 month post-blast. The detection of TUNEL positive cells prior to any degenerating axons in the optic nerve suggests that the axon degeneration is secondary to RGC death.

In summary, this study demonstrates that an overpressure air-wave directed at the eyes of adult DBA/2J mice could be potentially used as a model for open-globe ocular trauma. This model is attractive because the globe remains intact, avoiding complications from potential bacterial infections. Treatment options for open globe trauma patients are very limited and none have shown a high degree of success. We expect that this model will be useful as a platform for identifying the mechanisms underlying ongoing vision loss and testing potential therapeutics for the treatment of open-globe ocular trauma.

Moderate trauma in the Balb/c mouse

Optic nerve degeneration occurred rapidly in the Balb/c after blast, compared to the Bl/6 and D2. We did not detect any degenerating axon profiles in the Bl/6 and D2 optic nerves until 1 month post-injury (Bricker-Anthony et al., 2014b; a). In contrast, the Balb/c optic nerves contained degenerating axons as early as 1 week post-injury.

Traumatic optic neuropathy, which can occur after blast or blunt trauma in humans (Phillips et al., 2013; Thach et al., 2008; Weichel and Colyer, 2008), is thought to be induced by two different injury mechanisms: primary (shearing of the axons and ischemia) and secondary (initial damage and death of the retinal ganglion cells) (Samardzic et al., 2012). We detected very little cell death in the GCL after blast, so it is possible that the retinal ganglion cells remained alive prior to axon degeneration, supporting a role for primary optic nerve injury. The Balb/cJ is more susceptible to optic nerve crush than the Bl/6 and the D2 (Li et al., 2007), so it is possible that genetic differences are driving the early onset of axonal degeneration in the Balb/cJ post-blast. Further, this model may be more representative of clinical traumatic optic neuropathy than the optic nerve crush or axotomy models.

Vacuolization of the RPE, a symptom of oxidative stress (Fujihara et al., 2008), occurred in all three mouse strains post-injury. RPE damage was also reported in 36% of blast-exposed soldiers (Phillips et al., 2013). In contrast to the Bl/6 and D2 mice, RPE vacuolization did not resolve in the Balb/cJ (Bricker-Anthony et al., 2014b; a). The RPE is an important component of the blood-retina barrier (Peyman and Bok, 1972) and is essential for photoreceptor health and function (Strauss, 2005). Enduring oxidative damage to the RPE could potentially cause loss of ocular immune privilege and ensuing inflammation. Oxidative stress and blood-brain-barrier permeability also occur in models in blast-induced traumatic brain injury, suggesting a similar mechanism in the eye and brain (Abdul-Muneer et al., 2013; Readnower et al., 2010).

Delayed neuronal cell death after blast exposure is a common finding in models of blast-induced traumatic brain injury (Koliatsos et al., 2011; Mohan et al., 2013). The

accelerated cell death in the D2 and Balb/cJ as compared to the Bl/6 in our model might be due to the greater inflammatory response exhibited by these two strains including Müller cell reactivity and peripheral immune cell infiltration (Bricker-Anthony et al., 2014b; a). Reactive Müller cells can cause retinal edema, secrete inflammatory cytokines and promote macrophage infiltration (Tong and Verkman, AS, 2004; Nakazawa et al., 2006). We also detected increases in some pro-inflammatory cytokines and chemokines as early as a few days post-trauma, including IP-10 and KC. IL-1α can induce expression of IP-10, KC, and MCP-1 from neurons (Tsakiri et al., 2008). While we did not detect a statistically significant increase in IL-1α, levels at both time points trended up and might explain the increases in these chemokines. These chemokines are also increased in other models of CNS injury and can act on both glia and neurons to mediate the recruitment and infiltration of peripheral immune cells into the CNS (Barbero et al., 2002; Cho and Miller, 2002). These findings suggest that there may be an increase in microglia in the retina after ocular blast trauma. While acute neuroinflammation is protective, chronic neuroinflammation can contribute to neurodegeneration.

The increase in IL-10 in the combined 3 day and 1 week post-trauma retinas is suggestive of an endogenous protective response. IL-10 is an anti-inflammatory cytokine that inhibits activation of macrophages, microglia and astrocytes and blocks production of pro-inflammatory cytokines and iNOS, resulting in lower levels of peroxynitrite (Bogdan et al., 1992; Cunha et al., 1992; de Waal Malefyt et al., 1991; Ledeboer et al., 2000; Lodge and Sriram, 1996; Pousset et al., 1999; Sawada et al., 1999). Gene delivery of IL-10 decreases nitrotyrosine immunolabeling and preserves

ganglion cells in an optic nerve axotomy model (Koeberle et al., 2004). This strategy may also be effective in the treatment of ocular blast trauma.

In conclusion, the Balb/cJ mouse model of ocular blast trauma provides a good platform for testing cell-based therapies. These therapies are much needed, as there are currently no treatment options for eye trauma patients.

Mild blunt trauma in the contralateral eye after blast

The mechanism of injury to the contralateral eye in this model system appears to be mild blunt trauma based on three main findings. First, absence of cell death and nitrosative stress in the olfactory epithelium argues against blast wave propagation through the head, as this would likely damage the delicate tissue. Second, the lack of damage to the contralateral optic nerve also supports this hypothesis since blast waves contain shearing forces that are particularly damaging to long structures such as axons (Garman et al., 2011). Third, the timing of cell death was the same in the contralateral eyes of both mouse strains, but was different from the respective blast-exposed eyes (Bricker-Anthony et al., 2014b; a). One would expect similar timing of cell death if both eyes were injured by the same injury mechanism (i.e. blast).

Our injury system produced pathology similar to that observed in animal models of blunt ocular trauma and in patients with commotio retinae (Blight and Hart, 1977; Sipperley et al., 1978; Bunt-Milam et al., 1986; Blanch et al., 2012). Commotio retinae is characterized by focal damage to the RPE and photoreceptors that spontaneously resolves in the majority of patients (Blight and Hart, 1977; Sipperley et al., 1978; Bunt-Milam et al., 1986; Blanch et al., 2012). Similar to our findings, focal pyknotic

photoreceptor nuclei were also detected soon after ocular trauma in both primate and rodent models (Sipperley et al., 1978; Blanch et al., 2012). Finally, porcine and feline models of blunt trauma also exhibit RPE vacuolization and focal photoreceptor damage within the first week post-injury, which resolved at one month post-injury (Blight and Hart, 1977; Bunt-Milam et al., 1986). Also consistent with trauma, we detected retinal detachments in both strains. Surprisingly, in the D2 mouse, we detected retinal detachments at 2 weeks, but not 1 week post-trauma. One possible explanation is that we missed the retinal detachments at 1 week due to how the mouse was positioned in the OCT system, or which retinal regions were imaged. However, since we rotate the mouse and probe to visualize as much of the retina as possible, we find this explanation unlikely. Another possible explanation is that the retinal detachments developed over time. A recent study detected delayed retinal detachments in trauma patients (Xia et al., 2015).

In contrast with these other models, we also observed TUNEL-positive nuclei and labeling with necroptotic cell death markers in the inner retina. In a rat model of ocular trauma, the authors stated that the inner retina was mostly spared and did not report TUNEL quantification for the inner retina (Blanch et al., 2012). The pattern of their ERG deficits is also incongruous with our findings. They reported a deficit in both the $a_{\max}$ and $b_{\max}$ with equal timing and extent, while we saw an initial decrease in the a_{max}, followed by a recovery of the $a_{\max}$ and subsequent decline in the $b_{\max}$ in the D2 mice. These findings suggest that the ERG deficits observed in their model were due to photoreceptor cell loss that resulted in loss of downstream signaling to the inner retina. In contrast, our ERG results show an early, transient deficit in the photoreceptor cells

followed by inner retina dysfunction. These incongruent results are likely due to differences between the injury models and the rodent species (Bl/6 and D2 mice were used in our study and Lister hooded rates were used in their study).

The visual acuity in the Bl/6 eyes were consistent with our previous findings in the blast-exposed eyes (Bricker-Anthony et al., 2014b). While OKN scores normally improve with repeat testing in mice, there was no improvement in the Bl/6 eyes after injury (Prusky et al., 2008). The ongoing cell death from 1 week to 1 month post-injury in the Bl/6 eyes may contribute to the decreased OKN response. There were also no changes in the ERG post-injury, like the blast-exposed eye (Bricker-Anthony et al., 2014b). The lack of lens displacement suggests that the discrepancy is not due to altered optics. It is feasible that the blunt trauma injured other, non-retinal, neuronal pathways necessary for the OKN response (Chevallier et al., 2013). In contrast, the OKN scores and ERG results were very similar between D2 blast-exposed and contralateral eyes (Bricker-Anthony et al., 2014a).

In conclusion, our model, which directs a blast of air towards one eye, causes injury to the contralateral eye likely because of pushing the head onto the cushioning within the housing chamber. The lack of ERG deficits, optic nerve damage, anterior pathologies and the spontaneous recovery of the outer retina damage suggest that this is a model of mild blunt trauma. The injury profile in the contralateral retina of the D2 mouse is more severe than that of the Bl/6 mouse, which is consistent with the greater neuroinflammation in the D2. Thus, our model system can be used to explore mechanisms and functional outcomes of both blast and blunt ocular trauma (e.g. damage from both the primary and secondary effects of blast) separately. Future

studies may investigate the effects of combining both blast and blunt injuries in the same eye, as this is relevant for blast-injured U.S. military veterans who often experience a combination of both primary and secondary blast trauma.

CHAPTER 3

DELAYED TREATMENT WITH ERYTHROPOIETIN REDUCES RETINAL CELL DEATH AND NITROSATIVE STRESS AFTER OCULAR BLAST TRAUMA[3]

Introduction

EPO is an endogenous cytokine best known for its role in stimulating hematopoiesis and is clinically approved for the treatment of anemia (Eschbach et al., 1987). Many laboratories became interested in EPO when it was shown to exert neuroprotection *in vitro* (Morishita et al., 1996). Previous studies demonstrated that EPO is neuroprotective and improves cognitive outcomes following traumatic brain injury (Lu et al., 2005; Yatsiv et al., 2005). As such, the efficacy of EPO treatment for traumatic brain injury is currently being evaluated in several clinical trials (www.clinicaltrials.gov). EPO is composed of four α-helices joined together by three crossover loops (Cheetham et al., 1998). There are two binding sites for the EPO receptor homodimer (EPOR) on the surface of EPO, consisting of a high affinity and a low affinity binding site (Cheetham et al., 1998). EPO mRNA is highly expressed in the kidney and liver, but is also present in neuronal tissue (Tan et al., 1992). EPO is a potentially promising treatment for traumatic brain injury and other insults, but systemic

[3] Portions of this chapter were published as Bricker-Anthony C (2014). Ocular blast trauma: models, mechanisms and a potential therapeutic strategy. VRN 6; Bricker-Anthony C, D'Surney L, Lunn B, Hines-Beard J, Jo M, Bernardo-Colon A and Rex TS (2016). Erythropoietin either prevents or exacerbates retinal damage from eye trauma depending on treatment timing. Optom Vis Sci 93.

treatment with EPO can lead to the development of polycythemia, a potentially life-threatening condition.

To reduce the risk of polycythemia when EPO is used for neuroprotection, Leist and colleagues generated several modified forms of EPO (Leist et al., 2004). Carbamylation of EPO (CEPO) resulted in a dearth of binding to the EPOR homodimer, yet it remained neuroprotective both *in vitro* and *in vivo* (Leist et al., 2004). Two separate mutations in the low affinity binding site, S100E and R103E, were also effective at preventing binding to the EPOR homodimer while maintaining neuroprotection (Leist et al., 2004). Our lab also developed a mutant form of EPO, EPO-R76E, which protected RGCs in D2 glaucomatous mice and displayed attenuated erythropoiesis, indicative of poor binding to EPOR homodimer (Sullivan et al., 2011). Brines and colleagues demonstrated that EPO and CEPO bind an EPO R and ILβ-subunit R heterodimer, which provides tissue protection without stimulation of hematopoiesis (Brines et al., 2004).

Though EPO is neuroprotective in multiple models of neuronal stress and disease, its precise mechanisms are still unclear. The addition of neurprotective EPO mutants with attenuated or abolished hematopoietic activity by Leist and colleagues and our lab also complicates the question of EPO's protective mechanisms (Leist et al., 2004; Sullivan et al., 2011). Binding of EPO to its native receptor homodimer initiates erythropoiesis via the Jak/Stat signaling cascade and appears to promote erythrocyte survival via GATA-1-mediated upregulation of anti-apoptotic Bcl-XL (Gregory et al., 1999; Parganas et al., 1998). However, EPO neuroprotective pathways appears to vary

even among different neuronal populations and may have a more widespread impact than just preventing cell death at the level of the individual neuron.

In an *in vitro* model of neuronal hypoxia, administration of EPO induced increased phosphorylation of Stat5, Akt, ERK1 and ERK2 in hippocampal neurons (Sirén et al., 2001b). Addition of inhibitors of the MAPK and PI3K pathways in conjunction with EPO treatment prevented phosphorylation of ERK1, ERK2 and Akt and abolished EPO neuroprotection (Sirén et al., 2001b). Activation of the MAPK pathway provides protection via inhibition of pro-apoptotic BAD and phosphorylation of CREB, which transcribes pro-survival genes (Bonni et al., 1999). Phosphorylation of Akt within the P13K pathway also prevents activation of BAD and leads to downstream activation of Nf-κB, which promotes transcription of pro-survival genes (Brunet et al., 2001).

Another *in vitro* model of excitotoxicity and neuroinflammation in cerebrocortical neurons showed that Jak2-mediated activation of Nf-κB was necessary for EPO neuroprotection (Digicaylioglu and Lipton, 2001). Following phosphorylation of Jak2 by the EPOR, Jak2 phosphorylated IκBα, a potent suppressor of Nf-κB (Digicaylioglu and Lipton, 2001). Together, these findings support a common pathway for EPO neuroprotection, as Jak2 contributes to both MAPK and PI3K signaling cascades (De Vos et al., 2000; Wolf et al., 2013).

However, findings from Weishaupt and colleagues challenged the notion that MAPK signaling was involved in EPO neuroprotection within RGCs (Weishaupt et al., 2004). To test the efficacy of EPO neuroprotection in RGCs, Weishaupt and colleagues used both an *in vitro* (trophic factor deprivation in RGC cultures) and *in vivo* (optic nerve transection, an acute model of glaucoma) approach. The authors documented EPOR

expression, RGC survival, phosphorylated Akt expression and the effects of a PI3K inhibitor, Wortmannin.

The authors detected EPOR on the RGCs of both control and optic nerve transected rats. The authors claimed that the EPOR expression was much weaker in other cell types of the retina. However, this finding disagrees with data from Xie and others, who reported EPOR expression throughout the layers of the retina without strong localization within the RGCs in normal Sprague-Dawley rats, the same rat breed used by Weishaupt and colleagues (Xie et al., 2007). Grimm and colleagues also reported a different EPOR expression pattern within the normal mouse retina (strong staining within photoreceptor inner segments and the outer plexiform layer, weak labeling within the inner retina), but these results could be due to a species difference (Grimm et al., 2002). A current challenge in the field is the lack of specificity of EPOR antibodies (Elliott et al., 2006).

EPOR expression also failed to change significantly in response to optic nerve transection or EPO treatment. The lack of change in EPOR expression is not surprising, given that HIF-1α induces increases in EPO and increases in both EPO and EPOR have been reported in the hypoxic brain (Semenza, 2001; Sirén et al., 2001a). In contrast, optic nerve transection is not a hypoxic injury and is not likely to induce increased expression of HIF-1α.

Surprisingly, EPO treatment elicited phosphorylation of Akt, but not of ERK1/2 in optic nerve transected retinas. Both the MAPK and PI3K pathways are active and involved in EPO neuroprotection in cerebral ischemia and intracerebral hemorrhage (Kilic et al., 2005; Lee et al., 2006b; Sirén et al., 2001b). A possible explanation for the

lack of ERK1/2 phosphorylation in this study is that the neuroprotective cascade initiated by EPO differs in RGCs compared to cerebral neurons. However, a recent study demonstrated that inhibition of MAPK, PI3K, or Stat5 in cultured rat RGCs challenged with trophic factor withdrawal, TNF-α, or NMDA resulted in a significant loss of EPO neuroprotection (Chang et al., 2013). However, the reduction in EPO neuroprotection varied among RGC types and with the type of insult. These findings suggest that different cytotoxic stimuli and cell types may result in alterations in EPO's neuroprotective signaling cascades, which needs to be explored further in future experiments.

In addition to preventing apoptosis at the level of the individual neuron, EPO has also been shown to affect both astrocytes in the brain and Müller glia in the retina (Gunnarson et al., 2009; Hu et al., 2010). EPO treatment significantly reduced water permeability within AQP4 positive astrocytes and decreased abnormal calcium oscillations following induction of edema (Gunnarson et al., 2009). In a model of diabetic retinopathy, EPO treatment also reduced reactive gliosis and promoted expression of neurotrophins in Müller glia (Hu et al., 2010). EPO may also modulate immune responses in neuronal disease and injury, as recently discussed by Brines and Cerami (Brines and Cerami, 2012).

EPO may also provide neuroprotection through reduction of oxidative stress. Previous studies demonstrated that EPO treatment reduces oxidative stress in both diseased and injured states (Wang et al., 2010; Yazihan et al., 2008). EPO may reduce oxidative stress directly by scavenging reactive oxygen species or indirectly by activating the antioxidant response element and increasing antioxidant enzyme levels

(Bond and Rex, 2014). If oxidative stress contributes to neurodegeneration after blast exposure, then EPO may block its effects.

Given its ability to protect neurons in a variety of cytotoxic conditions, EPO is a promising treatment for ocular blast trauma. However, many important questions about EPO neuroprotection remain. Several studies reported dose-response differences with EPO treatment (Chang et al., 2013; Digicaylioglu and Lipton, 2001; Sirén et al., 2001b; Weishaupt et al., 2004). Determining an optimal dosage for EPO neuroprotection will be crucial for moving forward into patient populations.

Two final questions include local versus systemic administration and the timing of treatment. Weishaupt and colleagues obtained neuroprotection with an intravitreal injection of EPO protein (Weishaupt et al., 2004). However, an intravitreal injection may not be suitable for the injured eye. If EPO mutants are utilized, then systemic administration is an option, given that hematopoiesis is attenuated with EPO mutants and EPO can cross the blood-retina barrier. For acute treatment of ocular blast trauma, systemic administration of wild-type EPO is also acceptable, as it would not greatly impact hematocrit as it would in the context of chronic treatment. Another possible treatment method is gene therapy. Rex and colleagues showed significant therapeutic benefit with intramuscular injection of a viral vector (recombinant adeno-associated virus; rAAV) driving expression of EPO protein in a rat model of retinal light damage, a mouse model of retinal degeneration and mouse model of glaucoma (Rex et al., 2004; Sullivan et al., 2011b). A gene therapy approach may be beneficial for ocular blast trauma, as it allows for sustained expression of EPO over time, which could combat any

long-term neurodegeneration, which was observed Mohan and colleagues' model of ocular blast trauma (Mohan et al., 2013).

To evaluate the efficacy of EPO for the treatment of ocular blast trauma, we used D2 and Balb/cJ mice, which exhibited severe and moderate damage, respectively, after blast exposure. We used EPO protein to determine if short-term treatment with EPO soon after blast would be sufficient to protect the D2 retina. We chose a 3 day time point to coincide with the peak of cell death after blast in the D2 mouse and a 7 day time-point to allow sufficient time for changes in gene expression to overcome the elevation in erythropoiesis. Since EPO has a short half-life, frequent re-injection was needed so the shortest duration was optimal to limit the number of re-injections necessary. To provide long-term, sustained delivery, we used an rAAV in the Balb/cJ mice, which exhibited the most retinal damage with 7 days of injury and the most optic nerve damage within 1 month of injury. To avoid the large increase in erythropoiesis that is caused by sustained production of EPO, we instead delivered EpoR76E, a form of EPO with attenuated erythropoietic activity and well-characterized neuroprotective properties in multiple models of retinal disease and injury (Sullivan et al., 2011b; a, 2012). We injected mice with rAAV.EpoR76E either before or one day after blast to compare the efficacy of treatment (elevated EPO-R76E) at blast to treatment initiated at 3 weeks after blast, long after the early rise in oxidative stress.

Materials and Methods

Animals

Three-month old DBA/2J or Balb/cJ mice (The Jackson Laboratory, Bar Harbor, ME) were maintained on a 12h light/dark cycle and provided access to food and water *ad libitum*. All experimental procedures were approved by the Institutional Animal Care and Use Committee of Vanderbilt University, according to AALAC guidelines. Age-matched controls were used throughout the study. For histological analyses mice were perfused with 4% paraformaldehyde (PFA; Electron Microscopy Sciences, Hatfield, PA) and phosphate buffered saline (PBS), enucleated, and the eyes were stored in 4% PFA. For RNA collection mice were euthanized, corneas were bisected, and forceps were used to separate the retina from the posterior globe. The vitreous was removed from the isolated retina, which was then frozen on dry ice and stored at -80^{o}C.

Ocular Blast Injury

Isofluorane anesthetized mice were secured and padded within a housing chamber that was placed within a larger tube, which shielded the body and head of the mouse from blast. The left eye of the mouse was positioned against a hole in the tube and was aligned with the barrel of the blast device. An overpressure air-wave with a peak pressure of 26psi was produced by a modified paintball marker (Empire Paintball, Sewell, NJ).

Erythropoietin Therapy – DBA/2J

Mice were given three intraperitoneal injections of 5,000U/kg EPO (Procrit, Ortho Biotech, Bridgewater, NJ) at 24h intervals. Control mice received Ringer's buffer. There were four treatment groups based on the timing of EPO delivery after blast and timing of tissue collection: 1) EPO delivered at 0, 24, and 48h post-blast, tissue collected at 7-days post-blast; 2) EPO delivered at 6, 30, and 54h post-blast, tissue collected 7-days post-blast; 3) EPO delivered at 24, 48, and 72h post-blast, tissue collected at 7-days post-blast; and 4) EPO delivered at 24, 48, and 72h post-blast, tissue collected at 3-days post-blast.

Gene Therapy – Balb/cJ

Mice were given a single intramuscular injection of recombinant adeno-associated virus (rAAV) carrying either enhanced green fluorescent protein (rAAV2/8.CMV.eGFP) or a mutated form of EPO with attenuated erythropoietic activity (rAAV2/8.CMV.EpoR76E) at $1x10^9$gc into the quadriceps. Vectors were produced, purified, and titred at the University of Pennsylvania Vector Core (Philadelphia, PA). In the pre-blast group mice were injected 1-month prior to blast and collected at 1-month post-blast. In the post-blast group mice were injected 1-day post-blast and collected at 1-month post-blast. The rAAV2/8 serotype reaches peak gene expression levels three weeks after intramuscular injection (Louboutin et al., 2005). The collection time point was chosen based on the amount of time necessary for gene expression from rAAV and our previous data showing persistence of cell death at this time point. This paradigm allowed us to test if delayed delivery of EPO-R76E was therapeutic.

Immunohistochemistry

Eyes were embedded in Tissue Freezing Medium (Electron Microscopy Sciences) and 10μm thick sections were collected in-round on 12 slides such that each slide contained a representation of all areas of the eye/retina. Slides were rinsed with phosphate buffered saline (PBS) and incubated at room temperature in normal donkey serum at 1:20 in 0.1 M phosphate buffer with 0.5% bovine serum albumin and 0.1% Triton X 100 (PBT) for 2 hours. The slides were incubated overnight at 4°C in anti-nitrotyrosine (1:500, Millipore, Billerica, MA), anti-glial fibrillary acidic protein (GFAP, 1:400, DAKO, Carpinteria, CA), or anti-H ferritin (1:100, Abcam, Cambridge, MA) in PBT, rinsed with PBS and incubated with a secondary antibody (Life Technologies, Grand Island, NY) for 2 hours at room temperature. Slides were rinsed with PBS and mounted in Vectashield Mounting medium with 4',6-diamidino-2-phenylindole (DAPI; Vector Laboratories, Burlingame, CA) for imaging on a Nikon Eclipse epifluorescence microscope (Nikon, Melville, NY).

Quantification of Fluorescence Intensity

Non-overlapping, but adjacent images of all areas of all retinal sections were collected using the same gain and exposure settings. Fluorescence was quantified within a rectangle of a set width and a height equivalent to the height of the retinal layer of interest using Image J according to previously published methods (Weitlauf et al., 2014).

Quantification of GFAP-positive processes

Non-overlapping, but adjacent images of all areas of all retinal sections, with the exception of the far periphery, were collected at low magnification and montages were assembled in Photoshop (Adobe). Using Image J, the total length of retina and the length of retina containing GFAP-positive processes were measured. The percent of retina containing GFAP-positive Müller cell processes was calculated by dividing the length of GFAP-positive retina by the total length of retina and multiplying by 100.

Tdt dUTP Nick End Labeling (TUNEL) Quantification

Retina sections were labeled with the TUNEL Apoptosis Detection Kit according to manufacturer's protocol (Millipore, Billerica, MA) and mounted with Vectashield Mounting Medium with DAPI. Each slide contained 24 representative sections from all retinal regions. All sections were imaged and used in the quantification resulting in the analysis of an average of 57mm retina/group. The length of retina assessed in each group was not statistically different from the other groups with the following exceptions. The 3-day EPO and pre-blast therapy groups had less overall length of retina imaged and the 6hr EPO 7d post-blast group had slightly more retina imaged ($p<0.05$). A TUNEL-positive cluster was defined as an $85\mu m^2$ area of retina containing five or more TUNEL-positive cells. Clusters within the inner retina (INL and GCL) and outer retina (ONL) were counted separately. The total number of TUNEL positive cells within each defined cluster was also quantified. Measurements were performed using NIS Elements Advanced Research software (Nikon, Melville, NY). The number of 3-day retinas analyzed was 3 for buffer-injected and 7 for EPO-injected. The number of 7-day post-

blast retinas assessed per group was 17 for Buffer treated, 13 for 0h EPO, 9 for Group 6h EPO, and 9 for 24h EPO. The number of Balb/c mouse retinas quantified was: 9 rAAV.eGFP, 7 pre-blast rAAV.EpoR76E, and 9 post-blast rAAV.EpoR76E.

Optic Nerve Histology

Optic nerves were post-fixed in 4% paraformaldehyde and 1% glutaraldehyde and subsequently placed in 1% osmium tetroxide in 0.1 M cacodylate buffer, dehydrated in a graded ethanol series and embedded in Spurr's resin (Electron Microscopy Sciences). Starting from the proximal end of the optic nerve, 1 μm-thick sections were collected using a Reichert-Jung Ultracute E microtome and stained with 1% p-phenylenediamine in 50% methanol (Sigma-Aldrich). Sections were imaged on an Olympus Provis AX70 microscope using a 100x oil immersion objective lens. Axons were manually counted using ImageJ software by sampling 20% of the total nerve cross-sectional area using a fixed grid overlay to estimate axon density in the nerve (axons/mm^2). Total number of surviving axons was estimated as the product of mean axon density and nerve cross-sectional area. Imaging and quantification were performed in a masked fashion.

Oxidative Stress PCR Array

The Qiagen oxidative stress RT2 profiler mouse oxidative stress kit was used according to manufacturers' protocol. Five retinas were pooled for each plate. Data was normalized to the housekeeping gene, monogalactosyldiacylglycerol.

Statistical Analysis

All statistical analyses were calculated using Graphpad Prism software (San Diego, CA). The 7-day DBA/2J analyses were performed using ANOVA and a Tukey post-hoc test. All other data-sets were pair-wise comparisons and thus the Student's t-test was performed. The means ± SEM were calculated and presented for each data set.

Results

Delayed, not acute, EPO therapy decreases retinal cell death after blast

No TUNEL-positive cells were detected in sham blast retinas (Figure 3.1A). In the buffer-injected DBA/2J mice, 85% contained small clusters of TUNEL positive cells in the retina at 3 days and 1 week post-blast, consistent with our previously published findings (Figure 3.1B, D; (Bricker-Anthony et al., 2014a). We have defined these clusters as an 85μm^2 area of retina containing 5 or more TUNEL-positive cells. Clusters of TUNEL-positive cells were also present in 3 day post-blast retinas from mice that received EPO (Figure 3.1C). Occasional TUNEL-positive cells were detected in the EPO-treated 1 week post-blast retinas, but no clusters were found (Figure 3.1E). There was no quantitative difference in the number of TUNEL-positive clusters between groups at 3 days or 1 week post-blast (Figure 3.1F, G). However, there was an increase in the density of TUNEL-positive cells within the clusters in the 3 day post-blast retinas from EPO-treated mice, $p<0.05$ (Figure 3.1H). In contrast, there were no TUNEL-positive cells detected in the 24h EPO treated, 1 week post-blast retinas as compared to an average of 9.8 ± 3.7 dying cells in the other groups, $p<0.001$ (Figure 3.1I).

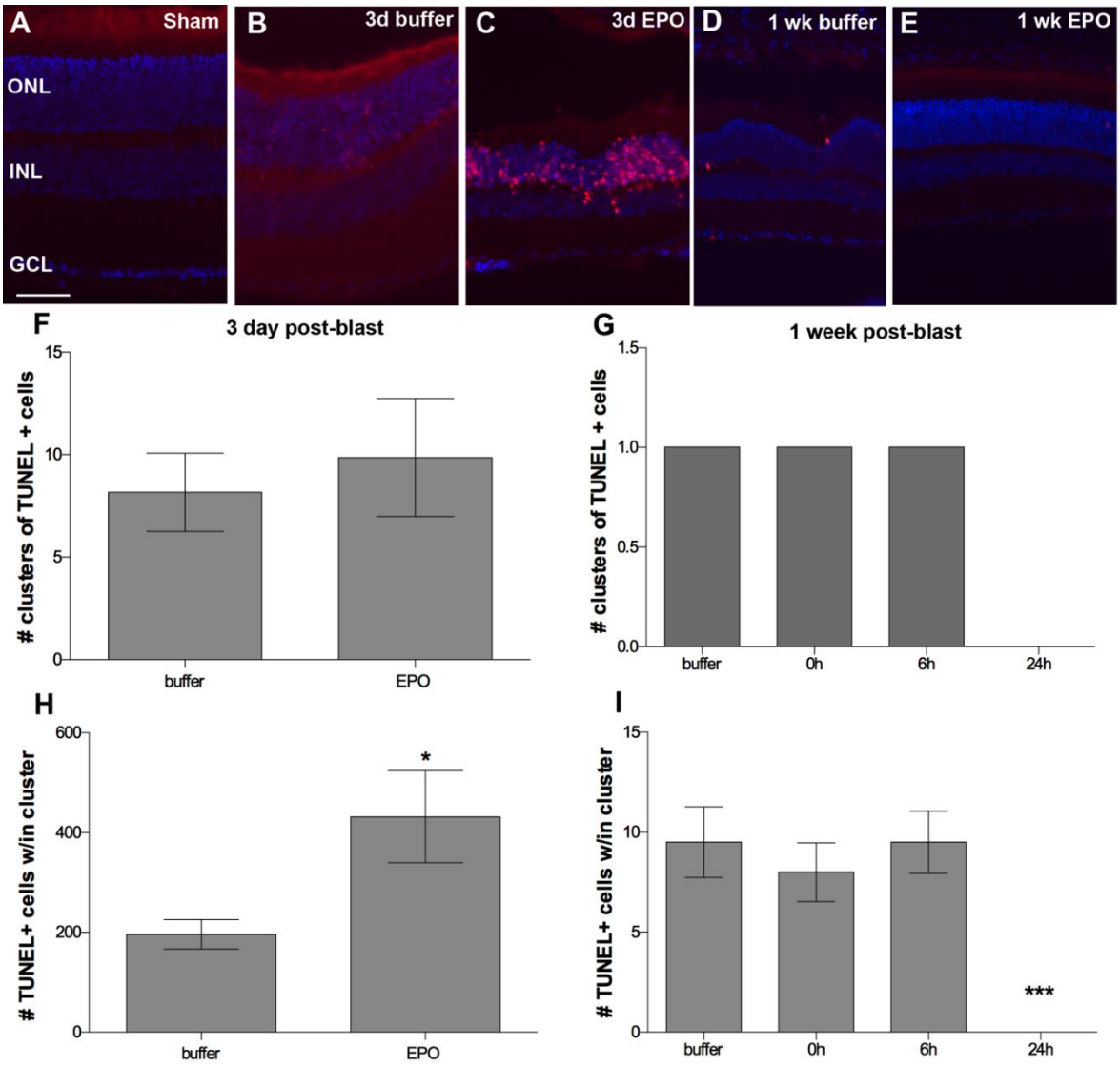

Figure 3.1. Treatment with EPO beginning at 24h post-blast decreases cell death at 1 week, but not 3 days post-blast. Representative fluorescence micrographs of clusters of TUNEL-positive cells in sham blast (A), buffer-injected 3-day post-blast (B), EPO-injected 3-day post-blast (C), buffer-injected 1 week post-blast (D) and EPO-injected 1 week post-blast (E) DBA/2J retinas. Scale bar represents 50μm. Bar graphs of clusters of TUNEL-positive cells at 3-days (F) and 1 week post-blast (G). Bar graphs of the density of TUNEL-positive cells within each cluster at 3 days (H) and 1 week post-blast (I). ***p<0.001.

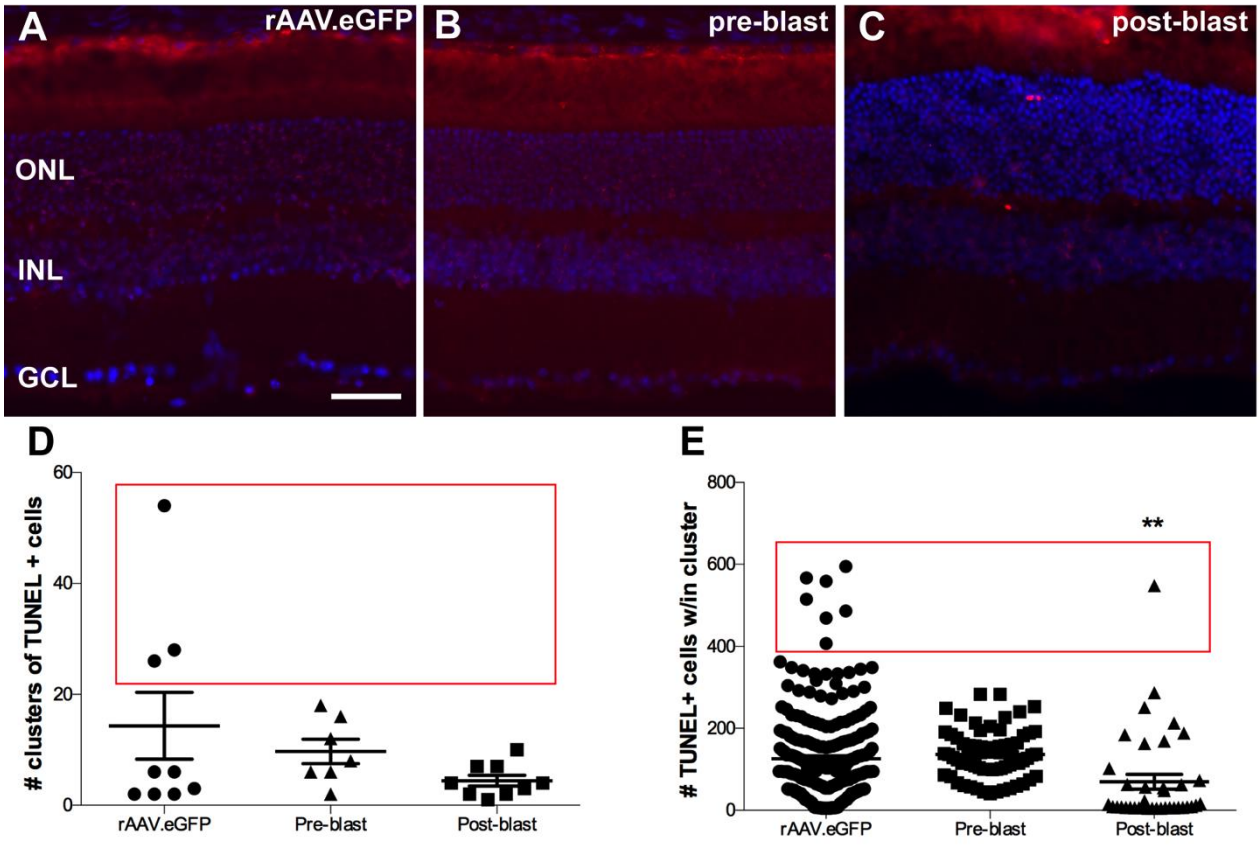

Figure 3.2. Treatment with rAAV.EpoR76E after blast decreases the number of TUNEL-positive cells at 1 month post-blast in Balb/c mice. Representative fluorescence micrographs of clusters of TUNEL-positive cells in retinas from mice injected with rAAV.eGFP (A), rAAV.EpoR76E 1-month prior to blast (B, pre-blast), or rAAV.EpoR76E 1-day after blast (C, post-blast). TUNEL (red), DAPI (blue). Scale bar represents 50μm. Scatter plots of the number of clusters of TUNEL-positive cells (D) and the density of TUNEL-positive cells within each cluster (E). **p<0.01. Red boxes indicate statistically significant difference in variance between rAAV.eGFP and both rAAV.EpoR76E treatment groups.

Clusters of TUNEL-positive cells were present in retinas from 1-month post-blast Balb/c mice treated with rAAV.eGFP (Figure 3.2A) or rAAV.EpoR76E (Figure 3.2B,C) regardless of treatment timing. The average number of clusters of TUNEL positive cells was similar across groups (Figure 3.2D). However, a subset of retinas from rAAV.eGFP treated mice had as many as 25-55 clusters, whereas the rAAV.EpoR76E treated mice never had more than 20 clusters of TUNEL-positive cells per retina (Figure 3.2D, red

box; Bartlett's test of variance, $p<0.0001$). The density of TUNEL-positive cells within each cluster was comparable between the rAAV.eGFP and pre-blast rAAV.EpoR76E mice (Figure 3.2E). In contrast, there were fewer TUNEL-positive cells per cluster in the retinas of Balb/c mice treated with rAAV.EpoR76E post-blast, $p<0.01$ (Figure 3.2E). In addition, there was a statistically significant difference in density variance between these groups, $p<0.0001$ (Figure 3.2E, red box). With the exception of one cluster in the post-blast treatment group, the TUNEL-positive cell densities within the clusters were less than 300 cells in the rAAV.EpoR76E groups (Figure 3.2E) while the rAAV.eGFP group had several clusters with densities between 400-600 cells.

Timing of EPO therapy affects optic nerve axons after blast

A small number of degenerated axons were present at 1 month post-blast in the Balb/c mouse injected with rAAV.eGFP as determined by dark profiles from collapsed myelin, or loose myelin (Figure 3.3A, C). Rare degenerating axons were also detected in the optic nerves of mice treated with rAAV.EpoR76E (Figure 3.3B,D). Upon quantification, a decrease in degenerating axons was detected in the mice injected with rAAV.EpoR76E after, but not in those injected prior, to blast (Figure 3.3E). The total number of axons was similar in all groups, likely due to the small number of degenerating axons (Figure 3.3F).

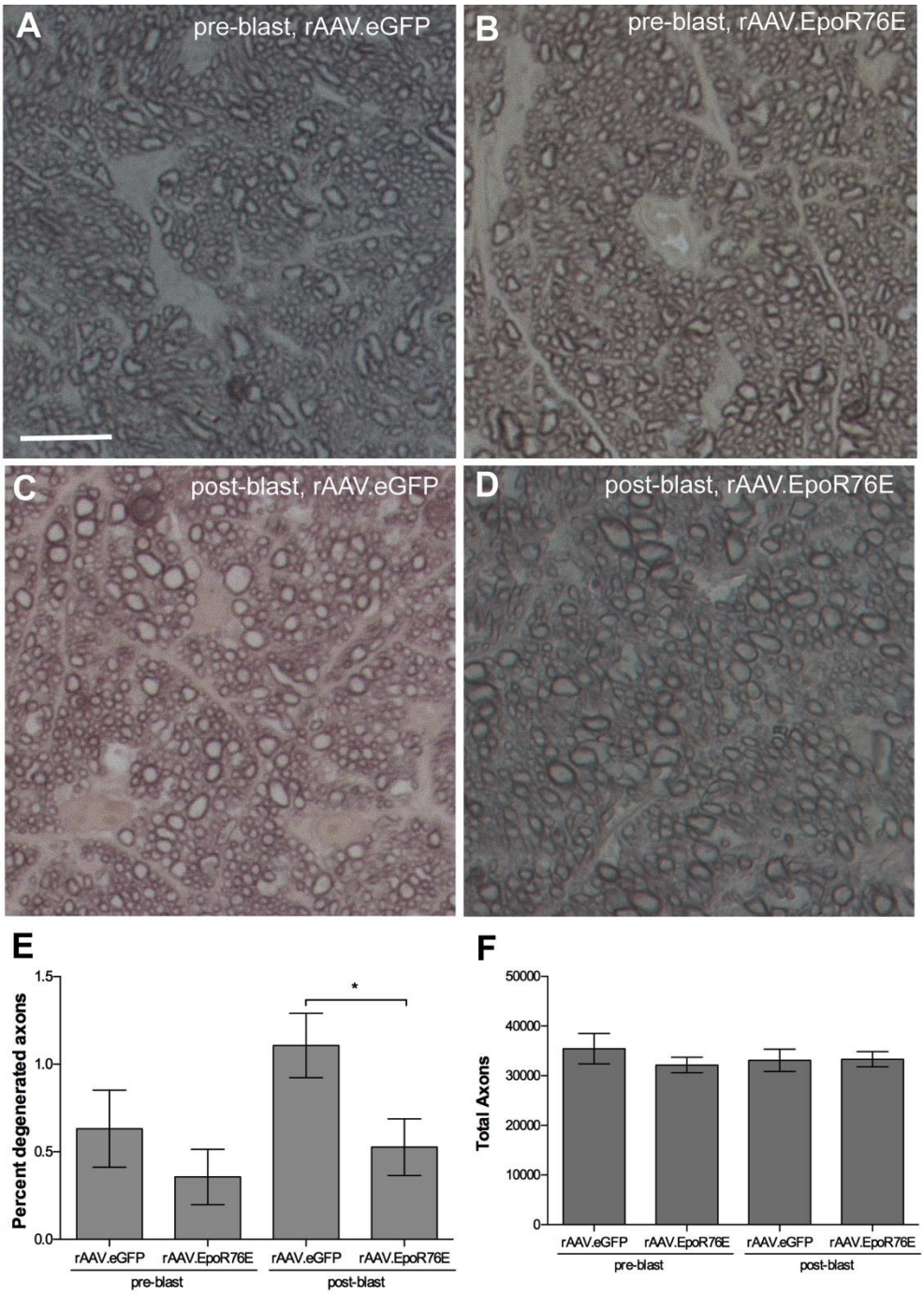

Figure 3.3. Treatment with rAAV.EpoR76E decreases axon degeneration in the Balb/c optic nerve at 1 month post-blast. Representative brightfield micrographs of optic nerve cross-sections from mice given: rAAV.eGFP pre-blast (A), rAAV.EpoR76E pre-blast (B), rAAV.eGFP post-blast (C), or rAAV.EpoR76E post-blast (D). Scale bar represents 10μm and applies to all images. Bar graphs of the percent degenerating axons (E) and the total number of axons (F). *$p<0.05$.

Timing of EPO therapy affects glial reactivity after blast

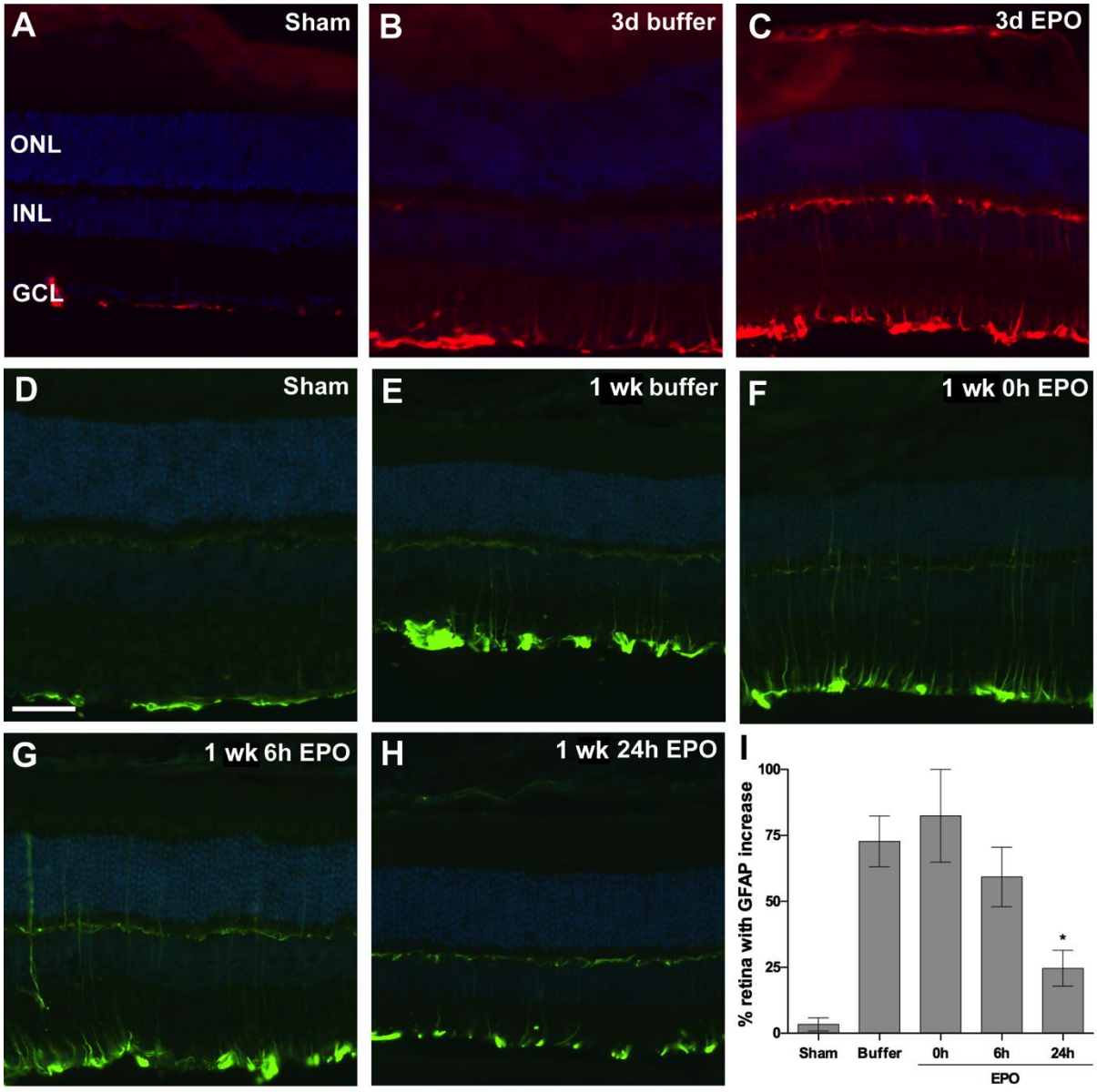

Figure 3.4. Treatment with EPO beginning at 24h post-blast decreases glial reactivity at 1 week, but not 3 days post-blast. Representative fluorescence micrographs of GFAP immunolabeling in retinas from sham blast mice (A), or 3 day post-blast mice injected with buffer (B) or EPO (C). GFAP (red), DAPI (blue). Representative fluorescence micrographs of GFAP immunolabeling in retinas from sham blast mice (D), or 1 week post-blast mice injected with: buffer (E) or EPO beginning at 0hr (F), 6h (G), or 24h (H) after blast. GFAP (green), DAPI (blue). Scale bar in D represents 50μm and applies to all images. I) Bar graph of the percent of retina containing GFAP-positive Müller cell processes. *p<0.05.

In retinas from sham blast mice, GFAP immunolabeling was restricted to astrocytes and Müller cell endfeet (Figure 3.4A, D). Focal increases in GFAP immunolabeling occurred in the Müller cells of DBA/2J mice at both 3 and 7-days post-blast (Figure 3.4B, E). GFAP-positive Müller cell processes were typically located within the mid-peripheral retina. GFAP-positive Müller cell processes were also present in EPO-treated post-blast retinas, although to a lesser extent in the 7-day post-blast group that received EPO beginning at 24h after blast (Figure 3.4C, F-H). The decrease in GFAP labeling in the latter group was statistically significant when compared to the buffer treated group, $p<0.05$ (Figure 3.4I). The extent of GFAP immunolabeling in the 3-day post-blast mice was not quantified since the labeling appeared equivalent between the buffer and EPO-treated mice.

In sham blast Balb/c mice, GFAP immunolabeling was also restricted to astrocytes and Müller cell endfeet (data not shown). After blast, GFAP immunolabeling extends into the Müller cell processes regardless of treatment (data not shown). Quantification confirmed no difference in the extent of retina containing GFAP-positive Müller cell processes between groups.

Nitrosative stress post-blast is affected by EPO therapy

We detected low levels of immunolabeling in sham blast DBA/2J mouse retinas (Figure 3.5A) and bright immunolabeling for nitrotyrosine in focal areas of the retina primarily localized to the inner retina after blast (Figure 3.5C,E). Immunolabeling was also present, primarily within the inner retina, in all EPO-treated retinas regardless of blast exposure (Figure 3.5B,D,F-H). In the 3-day post-blast DBA/2J retinas there was a

large increase in nitrotyrosine immunofluorescence in retinas from EPO-treated mice as compared to buffer-treated mice, $p<0.0001$ (Figure 3.5I). In the 7-day post-blast cohort nitrotyrosine levels were also increased as compared to sham controls, $p<0.001$ (Figure 3.5J). This increase was blunted by treatment with EPO, $p<0.001$.

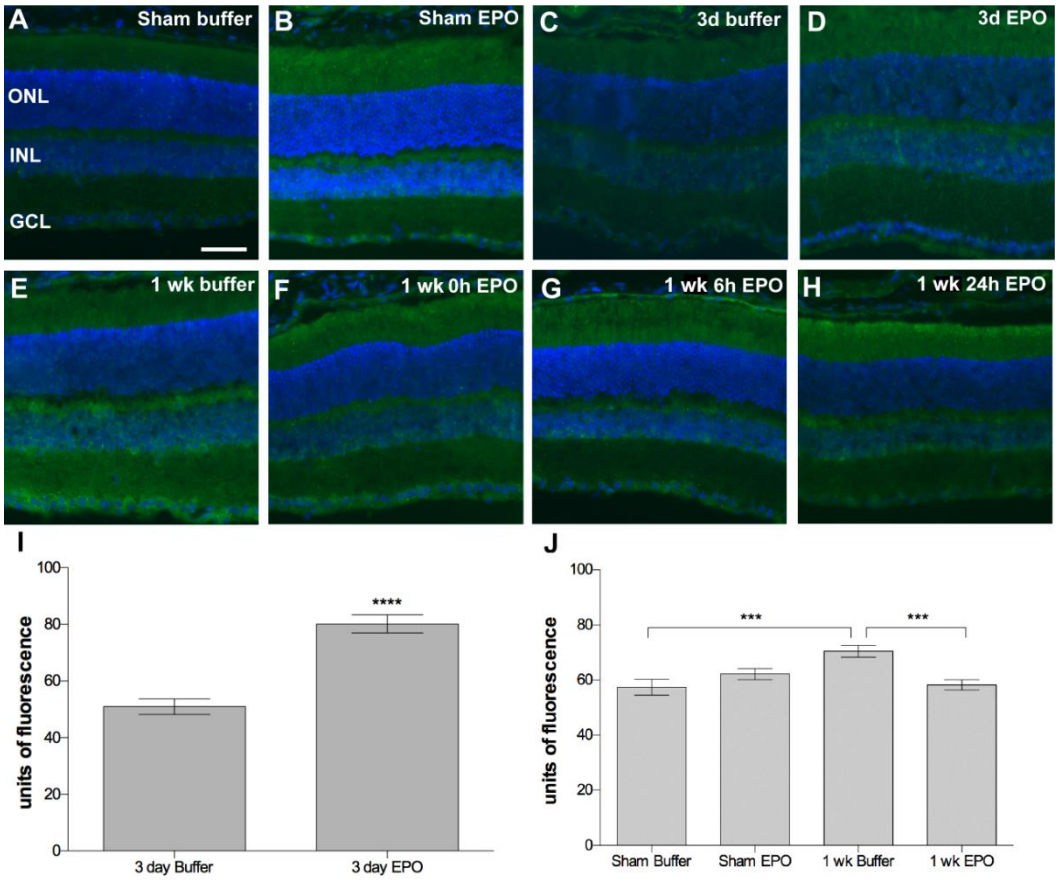

Figure 3.5. Treatment with EPO beginning at 24h post-blast decreases oxidative stress at 1 week, but not 3 days post-blast in the DBA/2J mouse. Representative fluorescence micrographs of nitrotyrosine immunolabeling in retinas from: sham blast mice injected with buffer (A) or EPO (B); 3 day post-blast mice treated with buffer (C) or EPO (D); and 1 week post-blast mice treated with buffer (E) or EPO beginning at 0h (F), 6h (G), or 24h (H) post-blast. Nitrotyrosine (green), DAPI (blue). Scale bar represents 50μm and applies to all images. Bar graphs of quantification of the mean anti-nitrotyrosine immunofluorescence intensity in the inner retina of 3-day post-blast DBA/2J mice (I) and 7 day sham and post-blast DBA/2J mice treated with buffer or EPO at 24, 48, and 72h after blast (J). ***$p<0.001$, ****$p<0.0001$.

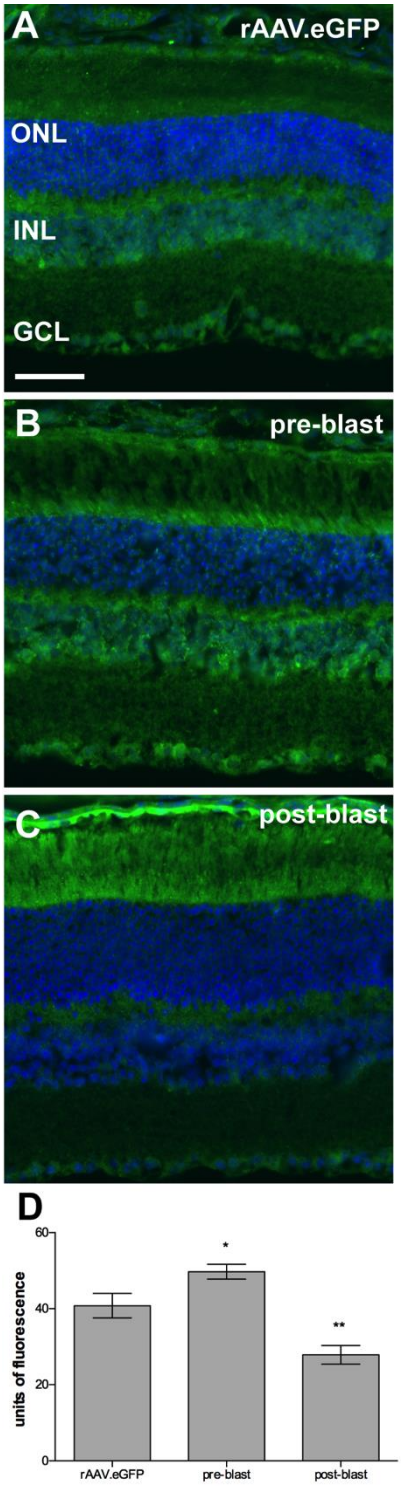

Figure 3.6. Treatment with rAAV.EpoR76E alters nitrotyrosine immunofluorescence in the inner retina of Balb/c mice after blast. Representative fluorescence micrographs of nitrotyrosine immunolabeling in retinas from mice injected with rAAV.eGFP (A), rAAV.EpoR76E prior to blast (B), or rAAV.EpoR76E after blast (C). Scale bar represents 50μm and applies to all images. Bar graph of quantification of anti-nitrotyrosine immunofluorescence in the inner retina at 1-month post-blast. *p<0.05, **p<0.01.

Immunolabeling for nitrotyrosine was also evident at 1-month post-blast in the Balb/c mice (Figure 3.6A-C). Nitrotyrosine immunofluorescence was increased in the pre-blast rAAV.EpoR76E group, $p<0.05$, and decreased in the post-blast rAAV.EpoR76E group, $p<0.01$, as compared to rAAV.eGFP injected Balb/c mice (Figure 3.6D).

EPO therapy increases hematocrit and retinal ferritin levels

In the 3-day post-blast mice the hematocrit increased from 43 ± 3.1% (avg ± sd) in buffer-injected mice to 46 ± 2.2% in EPO-injected mice, $p<0.01$ (Figure 4.7A). In the 7-day post-blast mice, the hematocrit was increased from 42 ± 2.1% in the buffer-injected mice to 50.5 ± 3.4%, 48.5 ± 3.0%, and 47.6 ± 2.1% in the 0h, 6h, and 24h EPO-treated mice, respectively, $p<0.0001$ compared to buffer (Figure 3.7B). The hematocrit was also statistically significantly higher in the 0h EPO group as compared to the 24h EPO group, $p<0.05$.

We then performed anti-ferritin immunolabeling and quantification of fluorescence to determine if these slight increases in hematocrit were sufficient to cause an increase in retinal iron levels. The anti-ferritin labeled the photoreceptor inner segments, inner nuclear layer, and punctate structures in the inner plexiform layer (Figure 3.7). Ferritin immunolabeling appeared similar in buffer-treated, sham and blast-exposed mice (Figure 3.7C, E, G). However, the amount of labeling appeared increased in retinas of mice that received EPO (Figure 3.7D, F, H-J) regardless of exposure to blast. Quantification confirmed an increase in ferritin levels in the retinas from EPO treated 3-day post-blast retinas as compared to buffer-injected mice, $p<0.0001$ (Figure

3.7K). This increase was primarily due to EPO and not blast since a large increase was detected in sham blast mice treated with EPO as compared to buffer injected sham mice, $p<0.0001$ (Figure 3.7L). Like the 3-day post-blast result, there was also an increase in ferritin immunolabeling in the EPO treated 7-day post-blast retinas as compared to buffer-injected 7-day blast mice, $p<0.0001$ (Figure 3.7L).

Despite expressing Epo-R76E rather than wild-type EPO, the Balb/c mice exhibited a rise in hematocrit similar to what we detected in the short-term EPO protein study in the DBA/2J mice. The hematocrit in mice injected with rAAV.eGFP was 45 ± 4.0%. In contrast mice treated with rAAV.EpoR76E had a hematocrit of 50 ± 5.0% (pre-blast cohort) and 57 ± 11% (post-blast cohort), $p<0.05$ as compared to rAAV.eGFP mice. The ferritin immunolabeling pattern in Balb/c mouse retinas appeared similar in all post-blast groups regardless of treatment (data not shown). Quantification confirmed that there was no difference in ferritin levels between the pre-blast rAAV.eGFP and rAAV.EpoR76E groups (data not shown). In contrast, despite an elevated hematocrit, ferritin immunolabeling levels were lower in the post-blast rAAV.EpoR76E group, 53 ± 1.8 (mean fluorescence ± SEM), as compared to the post-blast rAAV.eGFP group, 69 ± 2.1, $p<0.0001$.

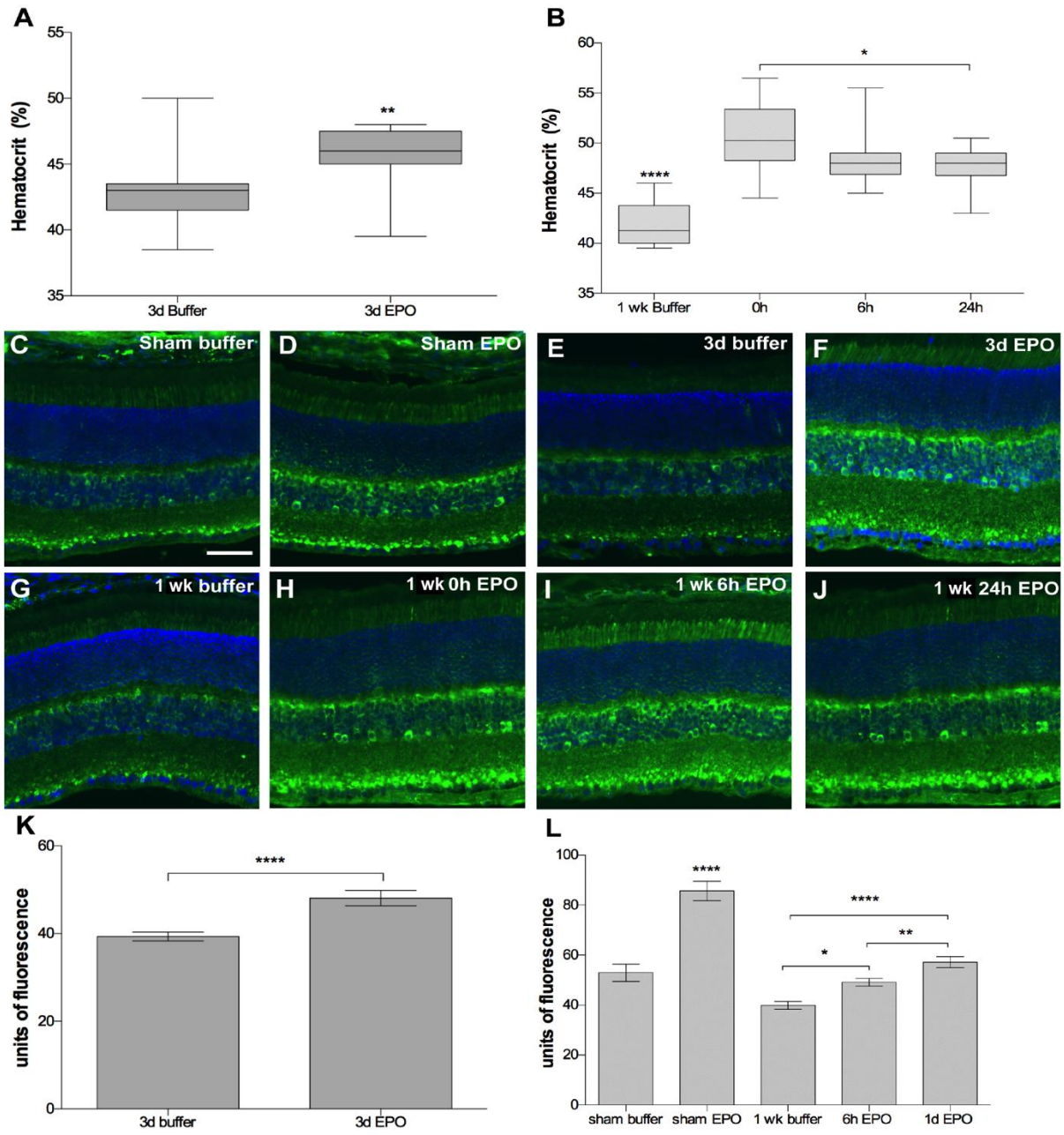

Figure 3.7. EPO increases hematopoiesis and retinal ferritin in the DBA/2J mouse. Box plots of hematocrit level at 3 days (A) or 1 week post-blast (B) showing an increase in all EPO treated mice. ****p<0.0001. *p<0.05, **p<0.01. Representative fluorescence micrographs of retinas labeled with anti-H-ferritin from sham blast mice injected with buffer (C) or EPO (D); 3 day post-blast mice injected with buffer (E), or EPO (F); 7 day post-blast mice injected with buffer (G), or EPO beginning at 0h (H), 6h (I), or 24h after blast (J). H-ferritin (green), DAPI (blue). Scale bar represents 50μm and applies to all images. Bar graphs of the mean anti-ferritin immunofluorescence intensity in retinas from 3 days post-blast DBA/2J mice (K), ****p<0.0001, and sham and 7 days post-blast DBA/2J mice (L), *p<0.05, **p<0.01, ****p<0.0001.

EPO and blast exposure alter oxidative stress gene expression in the DBA/2J mouse

In the 3 day post-blast, buffer-injected retinas there were increases in the mRNA levels of several NADPH oxidases (Figure 3.8A). In particular, Nox4 transcript was increased. In addition, expression of Nox 1, Noxa1, and Noxo1 were also increased. The expression of these proteins returned to sham levels at 1 week post-blast, however, mRNA levels of cytochrome b-245 alpha (Cyba), a NOX interacting protein, were increased at that time-point. EPO did not appear to alter expression levels of any of these proteins with the exception of decreasing Cyba message levels at 1 week post-blast.

The mRNAs were organized into functional groups and plotted to assess trends (Figure 3.8B). There was an increase in expression of peroxireductases (Prdx) and superoxide dismutases in the 3 day post-blast, buffer-injected retinas, suggestive of an endogenous protective mechanism. In contrast, in all groups there was a decrease in gene expression in the EPO-treated 3 day post-blast retinas as compared to the buffer group.

At 1 week post-blast gene expression levels of the antioxidant enzymes were comparable to or higher than the 3 day post-blast group. At 1 week post-blast, EPO again appeared to cause a decrease in expression of most of these enzymes, although levels were higher than in the EPO-treated 3 day post-blast group. One notable exception was an increase in Prdx in the EPO-treated 1 week post-blast group. In order to further investigate this effect, the expression of individual mRNAs with changes from sham of greater than 2-fold was graphed (Figure 3.8C). The increase in Prdx overall is

due to increases specifically in Prdx2 and Prdx6. This individual analysis also showed increases of 2-fold or greater in Gpx4, Gclm, Sod1, and Sod3 in buffer-injected post-blast mice at 3 days and/or 1 week and not in the EPO-treated 1 week post-blast retinas.

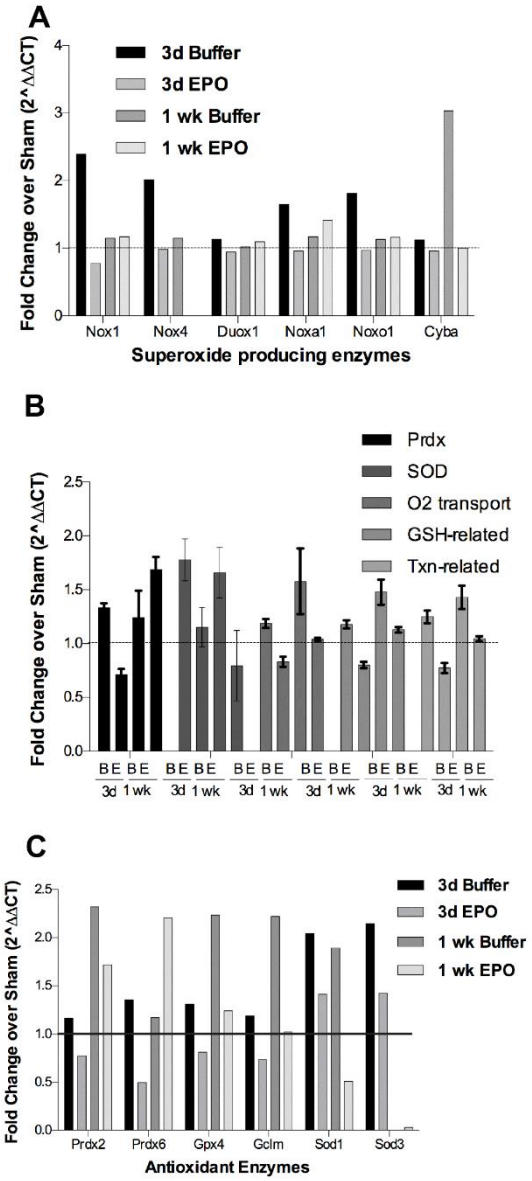

Figure 3.8. Both blast exposure and EPO treatment induce expression changes in oxidative stress-related genes. Bar graph of message levels of superoxide ion producing enzymes (A). Bar graph of message levels of antioxidant enzymes grouped into functional families (B). B= buffer, E=EPO. Bar graph of mRNA transcripts at least 2-fold different from the sham controls (C).

Discussion

In agreement with TBI studies, we detected less cell death, optic nerve degeneration, glial reactivity, and oxidative stress by systemic injection of EPO (Peng et al., 2014). Further, as in other models, we also detected efficacy with EPO when treatment was delayed until 24h post-injury (Gawad et al., 2009; Xiong et al., 2010). However, the effect was timing specific with efficacy only detected when treatment was initiated at least 1 day post-injury and assessed at 1 week or 1 month post-injury. When treatment was initiated or stopped earlier, no benefit was found. This effect was not strain-specific since we also detected protection in the Balb/c mouse when treatment was initiated 3 weeks after blast, but not when it was initiated prior to blast.

A surprise finding was the lack of protection in 1 week post-blast retinas treated with EPO beginning at 0 or 6h post-blast. In these groups the last EPO injection was performed at or before 54h post-injury. Erythropoiesis was increased in all EPO-treated mice, causing a correlative increase in retina ferritin levels. The increase in iron could promote the Fenton reaction, converting hydrogen peroxide to the much more damaging hydroxyl radical and causing greater cell death. The peak of cell death after an eye-directed blast in the D2 mouse is 3 days post-blast (Bricker-Anthony et al., 2014a). EPO has a rapid systemic half-life of approximately 2.5h in rodents (Fisher, 2003; Lee et al., 2006a). Thus, in addition to having elevated tissue iron levels from an increased hematocrit, these mice likely did not have sufficient levels of EPO in the retina during the peak of cell death to induce expression of antioxidant enzymes and counteract the ongoing oxidative stress. EPO can activate Nrf2 within neuronal tissue to induce transcription from the antioxidant response element resulting in increased levels

of many antioxidant enzymes (Bond and Rex, 2014). In agreement with this analysis, the oxidative stress microarray showed low levels of all tested antioxidant enzymes in the EPO-treated 3 day post-blast retinas. This lack of increase in antioxidant enzymes likely also explains the lack of benefit in the EPO-treated retinas at 3 days post-blast. These results suggest that the benefit of EPO treatment at 1 week post-blast was in spite of greater damage at 3 days post-blast.

Based on these results, greater therapeutic benefit would be expected by treatment with EPO if increased erythropoiesis is reduced. This can be achieved either through local delivery of EPO (King et al., 2007; Rex et al., 2009; Tsai et al., 2005; Weishaupt et al., 2004) or by systemic delivery of forms of EPO that have attenuated erythropoietic activity and yet maintain their neuroprotective function (Dumont and Bischoff, 2010; Leist et al., 2004; Sullivan et al., 2012, 2010, 2011a). To test this hypothesis, we treated mice with rAAV.EpoR76E and we detected less cell death when therapy was initiated after injury, but not prior to injury. EPO-R76E does induce a slight rise in hematocrit that is comparable, or lower, than what was induced by EPO treatment in the DBA/2J mice. Retinal ferritin levels were not increased in the pre-blast treatment group, and were surprisingly decreased in the post-blast group. The greater benefit in the post-blast group demonstrates that providing therapeutic levels of EPO as late as 3 weeks after blast is still effective.

In terms of clinical translation, these results suggest that: 1) oxidative stress is an important early component of retinal damage after blast trauma, 2) rapid treatment is not critical, 3) intraocular treatment with EPO maybe more effective than systemic

therapy as it would avoid induction of erythropoiesis and 4) EPO is protective to retinal neurons and axons in the optic nerve after ocular blast trauma.

CHAPTER 4

GULO$^{-/-}$ MICE ARE SIMILAR TO BL/6 MICE AFTER BLAST EXPOSURE

Introduction

Oxidative and nitrosative stress play a significant role in the pathogenesis of ocular disease and injury (Ethen et al., 2007; Leal et al., 2007; Neufeld et al., 1999; Tanito et al., 2005). Elevations in oxidative stress also occur in both human patients with traumatic brain injury (Cernak et al., 2000) and animal models of traumatic brain injury (Readnower et al., 2010; Tyurin et al., 2000). The high metabolic activity of the outer retina predisposes both photoreceptors and the RPE to damage from these stressors (Strauss, 2005). However, the inner retina is not immune to these stressors either, as levels of reactive oxygen species (ROS) in glaucomatous eyes can make the difference between cell survival and cell death (Tezel, 2006).

High levels of ROS can initiate lipid peroxidation within a cell membrane, which ripples through the membrane as one lipid radical steals electrons from a neighboring lipid, creating another lipid radical and threatening membrane integrity (Halliwell and Chirico, 1993). 4-HNE, a product of lipid peroxidation, modifies several proteins in the retina and RPE, including α enolase, triosephosphate isomerase and βB2 crystallin (Kapphahn et al., 2006). Modification of α enolase and triosephosphate, which are involved in glycolysis and gluconeogenesis, respectively, implies that 4-HNE may compromise cellular metabolism, while the impact of βB2 crystallin modification is currently unclear (Kapphahn et al., 2006). Modification of photoreceptor outer segments

with 4-HNE and malondialdehyde resulted in accumulation of shed outer segments within lysosomal compartments of the RPE *in vitro* (Kaemmerer et al., 2007).

In a similar manner, elevations in iNOS within the retina can lead to the formation of 3-nitrotyrosine residues on adolase A, another enzyme involved in energy metabolism (Koeck et al., 2004). Increased iNOS production is also linked to inner retinal cell death in ischemic injury and capillary damage in diabetic retinopathy (Sennlaub et al., 2002; Zheng et al., 2007). There is evidence of both lipid peroxidation (Mohan et al., 2013) and nitrosative stress (Bricker-Anthony et al., 2014b; a, 2016b) in the retina after ocular blast trauma. If 4-HNE and iNOS act on similar proteins and pathways in ocular blast trauma, then there is a strong possibility that energy metabolism will be impaired in both the retina and RPE. Additionally, photoreceptor outer segment turnover could also be impaired within the RPE due to 4-HNE adducts. Together, iNOS and 4-HNE can potentially exacerbate retinal injury following ocular blast trauma and should be considered when designing a therapeutic strategy.

To investigate the role of oxidative stress in ocular blast injury, we used gulonolactone oxidase knockout mice ($Gulo^{-/-}$). The $Gulo^{-/-}$ mice lack the enzyme necessary for vitamin C synthesis and must receive vitamin C in their diet, like humans (Maeda et al., 2000). In the retina, vitamin C directly scavenges reactive oxygen species and regenerates vitamin E (Stoyanovsky et al., 1995). Additionally, $Gulo^{-/-}$ mice maintained on a low vitamin C diet exhibit increased levels of oxidative stress in neuronal tissue (Harrison et al., 2010), making them an ideal model for exploring the role of oxidative stress in ocular blast injury.

Materials and Methods

Animals

Gulonolactone (L-) oxidase knockout mice ($Gulo^{-/-}$, n=8) were generously provided by Dr. Fiona Harrison. $Gulo^{-/-}$ mice were maintained on a low vitamin C diet comprised of 0.033 g/l ascorbic acid (Sigma Aldrich, St. Louis, MO) mixed into their deionized drinking water, along with 20 µl EDTA to stabilize the ascorbic acid in solution. All experimental procedures were approved by the Institutional Animal Care and Use Committee of Vanderbilt University, according to AALAC guidelines. Age-matched Bl/6 animals were used throughout the study.

Ocular Blast Injury

Isofluorane anesthetized mice were secured and padded within a housing chamber that was placed within a larger tube, which shielded the body and head of the mouse from blast. The left eye of the mouse was positioned against a hole in the tube and was aligned with the barrel of the blast device. An overpressure air-wave with a peak pressure of 26psi was produced by a modified paintball marker (Empire Paintball, Sewell, NJ).

Ascorbic acid quantification

The Harrison laboratory measured ascorbic acid concentration in the cortex and liver of $Gulo^{-/-}$ mice. Tissue samples were weighed and homogenized in a 1.5 ml microfuge tube with 25% (w/v) aqueous metaphosphoric acid and 100 mM sodium phosphate buffer containing 5 mM EDTA (pH 8.0), mixed together in a ratio of 2:7. A

total of 10 µl of buffer solutions was used for each mg of tissue. The samples were then centrifuged at 13,600 g for 4 min at 3° C, and aliquots of the clear supernatant were taken for assay of ascorbic acid with ion pair HPLC.

Visual acuity

Photopic spatial frequency thresholds (i.e. visual acuity) were assessed by optokinetic nystagmus (OKN) (OptoMotry, Canada) in awake mice at baseline and post-blast or sham. A step-wise, masked paradigm was used. Mice were acclimated to the testing chamber for 5 min prior to the initiation of each test. The speed of sinusoidal grating rotation and contrast were maintained at 0.042 c/d and 100%, respectively.

Electroretinogram (ERG)

Flash ERGs were performed at baseline and 28 days post-blast in mice dark-adapted overnight, anesthetized with ketamine/xylazine, dilated with 1% tropicamide, and placed on a heated mouse platform within the Ganzfeld dome of a Diagnosys LLC Espion Electrophysiology system (Lowell, MA). Mice were exposed to flashes of light ranging from -2 to 2.88 log cd*s/m^2 with a flash frequency of 2000Hz. For flashes below -1 log cd*s/m^2, the inter sweep delay was 10 sec, for the -1 log cd*s/m^2 flash it was 15sec, and for all remaining flashes, the delay was 20 sec. Oscillatory potentials (OPs) were measured at 3 log cd*s/m^2 sampled at 2000Hz with an inter sweep delay of 15sec. Amplitudes were measured from trough to peak.

Tissue collection

Mice were euthanized by an overdose of avertin delivered via intraperitoneal injection and transcardially perfused with 4% paraformaldehyde (PFA, Electron Microscopy Sciences, Hatfield, PA) and phosphate buffered saline (PBS). The tissues were collected and stored in 4% PFA. All mice were collected at 1 month post-injury to coincide with the peak of cell death and oxidative stress in the Bl/6 mouse (Bricker-Anthony et al., 2014b)

Statistical analysis

The mean and standard error of the mean were calculated and presented for each data set. We performed a two-way ANOVA with a Bonferroni's post-hoc test on the visual acuity and ERG data using GraphPad Prism software (GraphPad, La Jolla, CA).

Results

Low vitamin C gulo$^{-/-}$ mice and bl/6 mice exhibit similar responses to ocular blast trauma

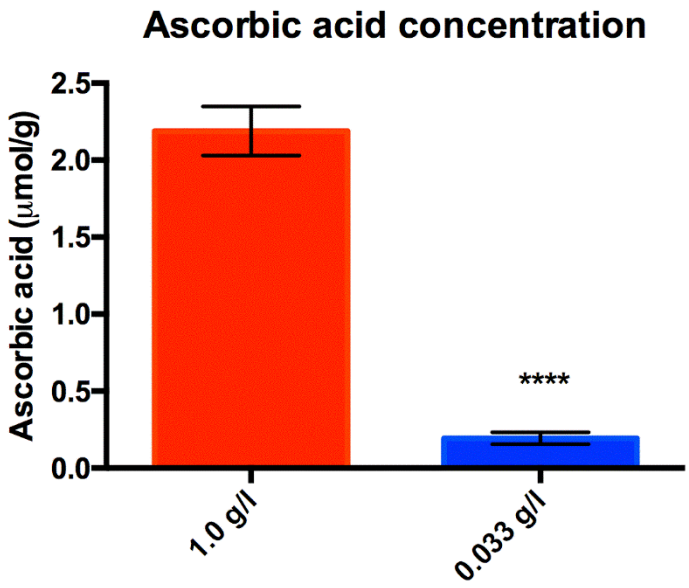

Figure 4.1. Confirmation of low ascorbic acid levels by HPLC. Ascorbic acid levels in the livers of mice on a low ascorbic acid diet (0.033 g/l) are significantly lower than those of mice on a high ascorbic acid diet (1.0 g/l). Values represent the mean ± SEM. ****p<0.0001

To make the Gulo$^{-/-}$ mice vulnerable to oxidative stress, we placed them on a low vitamin C diet (0.033 g/l in their drinking water) 1 month prior to any baseline assessments. The Harrison laboratory confirmed the low vitamin C levels using HPLC on liver homogenates and found that mice on a low vitamin C diet had significantly lower levels than those maintained on a high vitamin C diet (1.0 g/l; Figure 4.1). Despite their diminished defenses against oxidative stress, the Gulo$^{-/-}$ mice only exhibited slightly diminished visual acuity at 1 month post-blast when compared to Bl/6 mice (Figure 4.2).

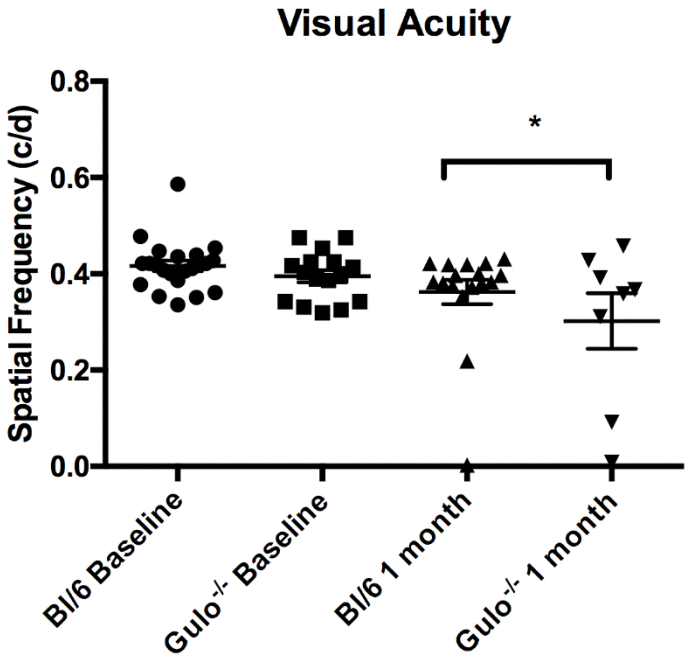

Figure 4.2. Gulo$^{-/-}$ mice exhibit modest deficits in visual acuity at 1 month post-blast when compared to Bl/6 mice. Values represent the mean ± SEM. *p<0.05.

We also measured ERG amplitudes at baseline and 1 month post-blast in the Gulo$^{-/-}$ mice. There were no statistically significant differences between blast-exposed Bl/6 mice and Gulo$^{-/-}$ mice at 1 month post-injury (Figure 4.3).

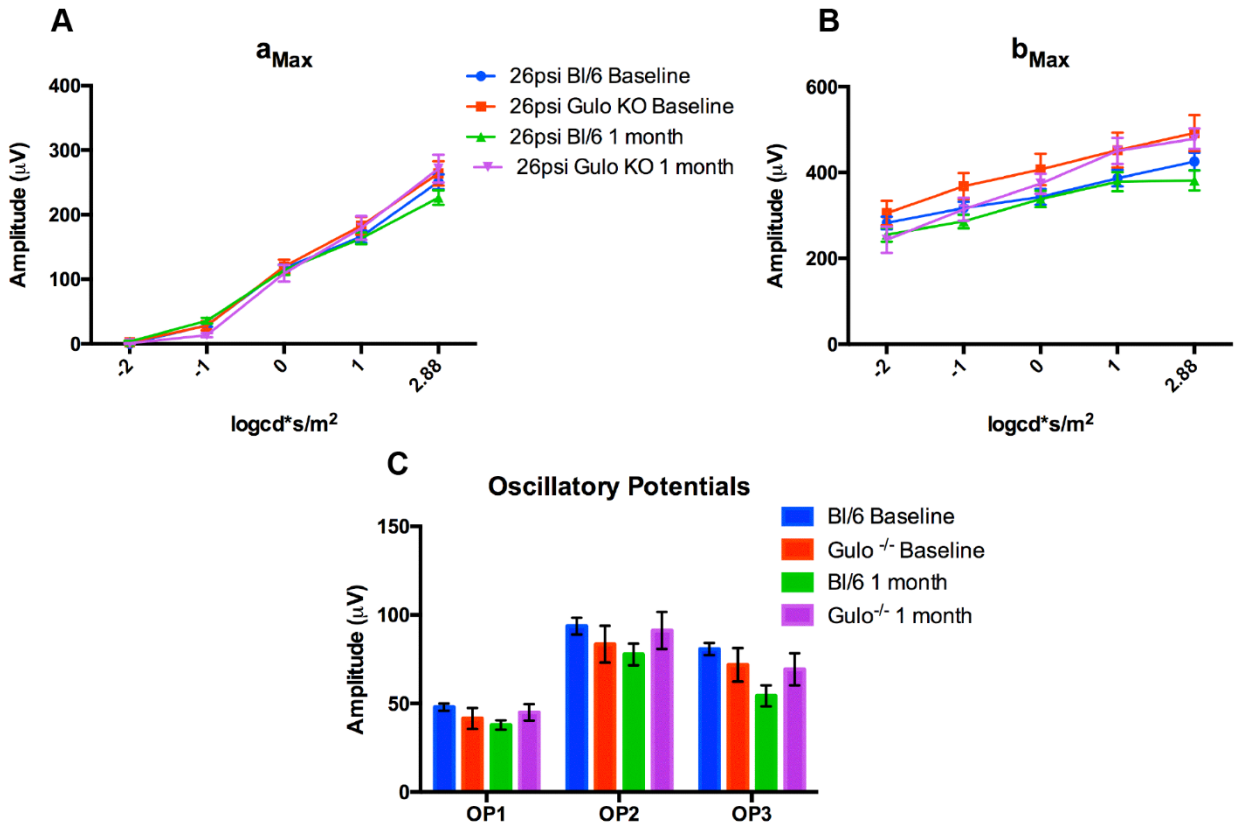

Figure 4.3. Gulo$^{-/-}$ ERG amplitudes don't change after blast exposure. The ERG a_{max} (A), b_{max} (B) and oscillatory potentials (C) in Bl/6 and Gulo$^{-/-}$ mice at baseline and 1 month post-blast. Values represent the mean ± SEM.

Discussion

These initial findings in the Gulo$^{-/-}$ mice suggest that vitamin C deficiency is insufficient to exacerbate visual dysfunction after ocular blast trauma. However, these are preliminary results based on a small number of mice and we still need to perform immunolabeling on the retinas to see if vitamin C deficiency results in increased nitrosative stress and cell death. Given these results, a review of the role of vitamin C in the regulation of retinal oxidative stress is warranted.

Among the various cells and tissues in the body, vitamin C levels are highest in leukocytes, eyes, adrenal glands, pituitary gland and the brain (Office of Dietary Supplements - Vitamin C, 2016). In the eye, vitamin C levels are highest in the retina, aqueous humor, lens, retinal pigment epithelium and choroid (Woodford et al., 1983). Previous studies have demonstrated that vitamin C supplementation protects the retina from light-induced damage in animal models (Woodford et al., 1983; Li et al., 1985) and potentially lowers the risk of age-related macular degeneration (AMD) in human patients (Seddon et al., 1994; Age-Related Eye Disease Study Research Group, 2001). Vitamin C in the aqueous humor can also inhibit neutrophil secretion of myeloperoxidase, which contributes to and serves as a marker of oxidative stress (Rosenbaum et al., 1985), but we did not observe any invading neutrophils in the Bl/6 eye after blast, so this protective mechanism is not relevant for the Gulo$^{-/-}$.

The pathogenesis of both light-induced retinal damage and AMD are unlike the pathogenesis of ocular blast injury. Retinal light damage causes increased oxidative stress that can cause cell death in the outer retina, but its pathogenesis is primarily mediated by RPE65 recycling of rhodopsin (Wenzel et al., 2001). AMD is also

characterized by increased oxidative stress in the outer retina, but one of the strongest risk factors for developing the disease is a common polymorphism in the complement factor H gene (Klein et al., 2005). Oxidative stress from retinal light damage and AMD often causes lipid peroxidation in the photoreceptor outer segments, which can be blocked by vitamin C (Woodford et al., 1983; Bendich et al., 1986; Pennesi et al., 2012). However, we have performed some preliminary immunolabeling for 4-HNE in blast exposed retinas from Bl/6 mice and have not observed positive immunolabeling. Thus, if lipid peroxidation does not contribute to the pathogenesis of ocular blast injury, loss of vitamin C would not exacerbate the injury.

Vitamin C also functions as a direct scavenger of superoxide, singlet oxygen and hydroxyl radicals (Bendich et al., 1986). We showed that markers of superoxide and reactive oxygen species increased *in vivo* in the Balb/cJ retina after blast (Bricker-Anthony et al., 2016b). While we have not tested those markers in the Bl/6 or Gulo$^{-/-}$ retinas after blast, we do know that peroxynitrite is likely elevated after blast injury in the Bl/6 retina (Bricker-Anthony et al., 2014b) because we observed increased immunolabeling for 3-nitrotyrosine.

Peroxynitrite, produced by the interaction of superoxide anions with nitric oxide, causes the formation of 3-nitrotyrosine (Ahsan, 2013). Interestingly, vitamin C is inefficient at competing with nitric oxide for superoxide to block peroxynitrite formation at physiological levels (1 mmol/L) and is only partially effective at blocking peroxynitrite formation well beyond physiological levels (10 mmol/L) *in vitro* (Jackson et al., 1998). In turn, elevated peroxynitrite can deplete both vitamin C and vitamin E through oxidation and then uncouple oxidative phosphorylation in the mitochondria (Vatassery et al.,

2004). These reactions are incredibly damaging for several reasons. First, oxidation of vitamin C prevents it from scavenging reactive oxygen species and blocks its ability to regenerate vitamin E (Bendich et al., 1986). Second, depletion of vitamin C causes depletion of glutathione (Henning et al., 1991), a critical antioxidant for both lens and retinal health (Ganea and Harding, 2006). Third, loss of vitamin E increases lipid peroxidation in the retina, which causes photoreceptor cell loss and oxidative damage to the RPE (Robison et al., 1979). Finally, uncoupling oxidative phosphorylation in the mitochondria reduces ATP production (Vatassery et al., 2004).

If vitamin C is inefficient at blocking the formation of peroxynitrite at normal physiological levels, then low levels of vitamin C are unlikely to exacerbate ocular blast injury. Thus, to assess the role of oxidative stress in ocular blast injury, we will need to examine the effects of losing an antioxidant that efficiently blocks peroxynitrite formation. One such candidate is manganese superoxide dismutase (SOD2), which can scavenge reactive oxygen species and effectively prevent formation of peroxynitrite in the presence of elevated nitric oxide (Jackson et al., 1998). Mice with only one copy of the Sod2 gene exhibit increased oxidative stress in the brain (Liang and Patel, 2004), as well as cell loss and mitochondrial abnormalities in the retina (Sandbach et al., 2001). Using the $Sod2^{+/-}$ mouse moving forward may provide us with a clearer picture of how oxidative stress contributes to the pathogenesis of ocular blast injury.

CHAPTER 5

DISCUSSION

Mechanisms of vision loss after ocular blast injury

Vision loss is a common consequence of ocular blast injuries in both civilians and members of the military (Alam et al., 2012; Erdurman et al., 2011; Thach et al., 2008; Weichel et al., 2008; Yonekawa et al., 2014; Phillips et al., 2013). We also demonstrated that vision loss occurs in both Bl/6 (Bricker-Anthony et al., 2014b) and D2 (Bricker-Anthony et al., 2014a) mice after ocular blast trauma. We do not know the specific mechanisms underlying vision loss after blast exposure, but there are several possibilities.

During the first week post-injury, visual acuity deficits occurred in both Bl/6 and D2 mice and ERG deficits occurred in the D2 mice. These alterations in visual function coincided with multiple pathological changes in the eye, including RPE vacuoles, accumulated debris in the RPE, photoreceptor outer segment damage and accumulation in the subretinal space, retinal detachments, photoreceptor cell death and increased nitrosative stress. The RPE is critical for visual function in the outer retina, due to its role in photoreceptor outer segment phagocytosis, transfer of oxygen and nutrients from the choriocapillaris to the photoreceptors, retinoid metabolism and forming part of the blood-retinal barrier (Schraermeyer and Heimann, 1999). We observed RPE vacuoles throughout the eye in all mouse strains studied; these vacuoles are indicative of oxidative stress (Fujihara et al., 2008). Oxidative stress in the RPE is

associated with cell death (Garg and Chang, 2003), disruption of tight junctions and loss of the blood-retinal barrier (Bailey et al., 2004) and mitochondrial DNA damage and impaired energy production (Liang and Godley, 2003). Oxidative stress-induced damage to the RPE could also potentially impair retinoid metabolism and could explain why we observed a transient decrease in visual acuity in both the D2 and Bl/6 mice during the first week post-blast and the transient decrease in the ERG a wave amplitude in the D2 mice during the first week post-blast, as both mouse strains exhibited extensive RPE damage in the first week post-blast that resolved by 1 month post-blast.

However, RPE damage does not explain why we observed decreases in the ERG b wave and visual acuity in the D2 mice at 1 month post-blast. It is possible that visual dysfunction at 1 month post-blast in the D2 mice was driven by inner retinal changes, as damage to the inner retina is associated with reductions in the ERG b wave (Block and Schwarz, 1998; Li et al., 2002) and oscillatory potential amplitudes (Holcombe et al., 2008). We also observed cell death and nitrosative stress in the inner retina at 1 month post-blast in the D2 mice that could have negatively impacted the ERG b wave, oscillatory potentials and visual acuity. Since we also observed optic nerve degeneration after retinal ganglion cell loss in the D2 retina after blast, transmission of visual information to the primary visual cortex may also be impaired after blast, which could be assessed using visually evoked potentials (Creel, 2012). Altogether, these findings suggest that inner retinal damage and dysfunction may drive long-term visual deficits after blast, which is supported by findings in Mohan and colleagues' blast model (Mohan et al., 2013) and by deficits in visually evoked potentials in patients with traumatic brain injury (Freed and Fishman-Hellerstein, 1997).

Translating mechanical insults into pathological changes

While we successfully recapitulated features of ocular blast trauma in three different inbred strains of mice and determined how EPO influences neuronal survival through modulation of oxidative stress after ocular blast injury, we still lack a true mechanistic understanding of what happens in the eye during blast exposure. Specifically, we do not know how exposure to a blast wave causes elevations in oxidative stress and focal cell death in the retina. However, we can place our data in the context of known mechanisms in traumatic brain injury and other biomechanical insults to piece together an understanding of what occurs when the eye is exposed to blast.

In our injury model, the first event is the impact of the overpressure air-wave. Finite element modeling, a computational method used to simulate physics problems, has been used to model the impact of an overpressure air-wave on the eye (Rossi et al., 2012). The finite element model of blast injury to the eye showed that the pressure wave initially impacted the cornea and anterior chamber, caused globe deformation, traveled through the vitreous and hit the posterior pole of the eye, as well the bony orbit surrounding the eye. Interestingly, the blast wave didn't stop when it hit the posterior pole and orbit, but reverberated throughout the globe, causing small sinusoidal waves of positive pressure and negative pressure to impact various posterior structures, such as the retina, optic nerve head, RPE and choroid. The reverberation of these small waves throughout the posterior chamber could potentially explain why we observed focal pockets of damage in the mid-peripheral and central retina instead of uniform damage at a single point. This pattern of damage was also seen in blunt ocular trauma (Giovinazzo, 1986) and ocular blast trauma (Cockerham et al., 2011) in human patients.

Demonstrating that these pressure waves occur in the eye *in vivo* may be technically challenging, but is not impossible. Recent advances in fabrication of pressure sensing devices led to the creation of implantable devices capable of measuring intraocular pressure in both mouse (Ha et al., 2012) and human (Melki et al., 2014) eyes. An implantable device could potentially measure oscillations in intraocular pressure produced by a blast wave in the living mouse eye.

Reverberating pressure waves in the eye likely subject ocular tissues, including the retina, vasculature, optic nerve head, RPE and choroid, to significant mechanical stress (Rossi et al., 2012). In our injury model, the gross pathological features of mechanical damage were manifested by retinal detachments, photoreceptor outer segment damage and RPE damage, which are observed in both blunt ocular trauma (Johnston, 1991; Sarrazin et al., 2004) and ocular blast trauma (Erdurman et al., 2011; Weichel et al., 2008). Physical separation of the photoreceptor outer segments from the RPE disrupts the flow of oxygen and nutrients from the RPE to the photoreceptors and causes hypoxia and apoptosis of the photoreceptors within 3 days (Cook et al., 1995; Mervin et al., 1999). Retinal detachment also places significant stress upon the RPE cells (Mervin et al., 1999), which might explain the extensive vacuolization. However, the retinal detachments in our injury model were infrequent in all three mouse strains. We also did not observe evidence of apoptotic cell death in the retina after blast, even in the photoreceptors. Additionally, RPE damage also occurred in the absence of retinal detachments, which is suggestive of direct injury from the blast or cytotoxic stress from another source. If photoreceptors underwent necrosis directly in response to blast, which has been observed in traumatic brain injury (Zhou et al., 2012), the process

would generate reactive oxygen species, extracellular ATP and TNF-α and stress the neighboring RPE cells (Zhang et al., 2009). However, this explanation is unlikely as we mostly saw positive immunolabeling for markers of necrosis in the Bl/6 and D2 after the resolution of RPE damage at 1 month. Therefore, blast likely directly damaged the RPE.

Direct mechanical stress from the blast could have also induced pathological changes in the retinal vasculature. Endothelial cells are capable of transducing mechanical stress into biochemical cascades through ion channels, integrins and caveolae (Traub and Berk, 1998). In response to mechanical stress and ischemia/reperfusion injury, endothelial cells released nitric oxide (Traub and Berk, 1998; Topper et al., 1996; Goldstein et al., 1996). This provides a potential explanation for the increased nitrotyrosine immunolabeling in the inner retina within days of blast injury in our model, as nitric oxide contributes to the formation of peroxynitrite (Pacher et al., 2007). Possible contributions of the retinal vasculature to the pathogenesis of ocular blast injury could be assessed using an endothelial nitric oxide knockout mouse (Le Gouill et al., 2007).

Müller glia (Lindqvist et al., 2010) and microglia (Sappington and Calkins, 2008) are also capable of transducing mechanical stress into signaling cascades that could contribute to the pathogenesis of ocular blast trauma. Mechanical stress induced elevated intracellular calcium and changes in gene expression in Müller glia (Lindqvist et al., 2010); these changes could lead to Müller glia reactivity, disruption of ion and neurotransmitter homeostasis and promotion of retinal degeneration after blast (Bringmann et al., 2006). Müller glial reactivity occurred within days of blast injury in our model and could have possibly been initiated by direct mechanical strain from the blast.

Previous research also demonstrated that microglial transduce mechanical stimuli through the TRPV1 receptor, which caused increased intracellular calcium, changes in gene expression and secretion of Il-6 (Sappington and Calkins, 2008). In another study, TRPV1 receptor activation caused microglia to secrete reactive oxygen species, indicating that TRPV1 activation might promote microglial reactivity (Schilling and Eder, 2009). We observed some microglia with morphology suggestive of reactivity in conjunction with nitrosative stress and cell death after blast injury in our model, but we would need to conduct additional studies to confirm their reactive status. Thus, blast injury may have also directly induced microglial reactivity in our model and contributed to elevated oxidative stress levels. Since transduction of mechanical stress in both Müller glia and microglia appears to be mediated by calcium influx (Lindqvist et al., 2010; Sappington and Calkins, 2008), intraocular injection of a calcium chelator after blast could be used to test the hypotheses that glial reactivity is directly induced by mechanical stress from blast and results in elevated oxidative stress post-blast.

Moving forward, more research is needed to provide a comprehensive understanding of the pathological mechanisms of blast injury to the eye. Multiple tissues in the retina are affected by blast and may drive excess production of oxidative stress after injury, which likely caused the cell death, inflammation and vision loss that we observed in our model. Hopefully, this research will inform the development of therapeutic agents for the treatment of ocular injuries, as over 2 million people experience ocular trauma and related vision loss every year (Kuhn et al., 2006).

Potential sources of oxidative stress after blast injury

Oxidative stress is common after blast-induced traumatic brain injury in both animal models (Readnower et al., 2010; Abdul-Muneer et al., 2013) and human patients (Cernak et al., 2000). Due to its heavy oxygen consumption, light exposure and enrichment in chromophores and polyunsaturated fatty acids (Beatty et al., 2000), the retina is naturally prone to oxidative stress. We also demonstrated that oxidative stress increased in the retina after blast injury. There are multiple potential sources of increased oxidative stress after blast injury to the eye, which I describe below.

The retina vasculature could contribute to elevated oxidative stress after blast injury. As mentioned in the previous section, endothelial cells secrete nitric oxide in response to mechanical stress (Traub and Berk, 1998). There are three known isoforms of nitric oxide synthase, including endothelial nitric oxide synthase (eNOS), neuronal nitric oxide synthase (nNOS) and inducible nitric oxide synthase (iNOS) (Goldstein et al., 1996). eNOS and nNOS are produced constitutively and play important roles in vasodilation and synaptic transmission, respectively, while iNOS is produced in response to inflammatory stimuli such as TNF-α (Goldstein et al., 1996). eNOS and nNOS typically produce small amounts of nitric oxide for a few hours, but iNOS produces relatively large amounts of nitric oxide for several days (Goldstein et al., 1996). All three isoforms of nitric oxide synthase can contribute to the formation of reactive nitrogen species like peroxynitrite, which causes 3-nitroyrosine formation (Fink et al., 1999). Elevated intraocular pressure (Rokicki et al., 2015) or exposure to inflammatory cytokines (Chakravarthy et al., 1995) can trigger iNOS expression in endothelial cells. Additionally, superoxide is also required for the formation of

peroxynitrite (Pacher et al., 2007). One potential source of superoxide after blast injury is red blood cells (Elsayed et al., 1997). Blast exposure was previously shown to induce lysis of red blood cells, which subsequently released superoxide (Elsayed et al., 1997). Reactive microglial cells also secrete superoxide (Schilling and Eder, 2009). Elevated superoxide was also present in the retina after blast injury in our model. The combination of superoxide released from damaged red blood cells and reactive microglial cells with nitric oxide from the endothelial cells could lead to peroxynitrite formation in the inner retina. Peroxynitrite is also capable of diffusing through cell membranes (Pacher et al., 2007) and could initiate the spread of injury from focal pockets of damage in the retina.

Mitochondria could also contribute to elevated oxidative stress after blast injury. Numerous studies have demonstrated that mitochondrial dysfunction contributes to neuronal death and oxidative stress in the aftermath of traumatic brain injury (Xiong et al., 1997; Lifshitz et al., 2004; Singh et al., 2006). These effects appear to be primarily mediated by an influx of calcium into neurons after injury, which depolarizes the mitochondrial membrane and uncouples the electron transport chain, resulting in increased production of mitochondrial reactive oxygen species (Singh et al., 2006). We do not have any data on calcium homeostasis after blast injury to the retina, but it is possible that changes in intraocular pressure during blast exposure could activate TRP channels and cause an influx of calcium that disrupts the electron transport chain. The TRP channels are mechanoreceptors that are expressed throughout the retina (Gilliam and Wensel, 2011); in response to mechanical stress, the TRP channels open and allow calcium to the enter the cell (Yin and Kuebler, 2010). Interestingly, one of the TRP

family members, TRPM1, is necessary for the ON-bipolar cell response that drives the ERG b wave (Shen et al., 2009). Changes in TRPM1 activation could contribute to the ERG b wave deficits we observed in the D2 mice.

Another potential source of post-blast oxidative stress is the necroptosis pathway. RIP1 and RIP3, markers of necroptosis, were both increased in the retina after blast in both Bl/6 and D2 mice. Downstream of TNF-α receptor activation, RIP1 and RIP3 form a complex called the necrosome (Li et al., 2012). RIP3 directly interacts with several enzymes involved in cellular energy metabolism, specifically glycogen phosphorylase L, glutamate ammonia ligase and glutamate dehydrogenase (Zhang et al., 2009). Interaction with RIP3 pushes these enzymes into overdrive and causes increased production of reactive oxygen species, depletion of ATP and necrosis (Zhang et al., 2009; Moriwaki and Chan, 2013). The necroptosis pathway can also increase microglial reactivity and further exacerbate oxidative stress (Trichonas et al., 2010).

Finally, we also identified another set of contributors to post-blast oxidative stress in the D2 mice: the NADPH oxidases (Bricker-Anthony et al., 2016a). The NADPH oxidase family, which consists of NOX1-5 and DUOX1-2, was first discovered in immune cells (Donkó et al., 2005). In neutrophils, NADPH oxidases were shown to catalyze the transfer of electrons from NADPH to molecular oxygen, which generated superoxide radicals that the neutrophil utilized to attack foreign invaders (Donkó et al., 2005). Since their initial characterization in peripheral immune cells, the NADPH oxidases have also been identified in other cell types throughout the body and the retina, including RGCs, Müller glia and microglia (Deliyanti and Wilkinson-Berka, 2015). In response to increased intraocular pressure or retinal ischemia, RGCs, microglia and

Müller glia upregulate expression of the NADPH oxidases, resulting in excess production of reactive oxygen species and cell death (Deliyanti and Wilkinson-Berka, 2015; Dvoriantchikova et al., 2012). Interestingly, the NADPH oxidases are activated by increased intracellular calcium (Nauseef, 2008), which could be one the first signals that initiates neurodegenerative changes after blast.

Summary

These studies demonstrate several things. First, ocular blast trauma induces both acute and long-term changes in the retina and optic nerve. Our findings indicate that cell death, inflammation and oxidative stress are persistent up to 2 months post-injury and may continue over time without therapeutic intervention. We also demonstrated that we can model various degrees of injury using genetically distinct mouse strains, with the Bl/6 representing a mild closed-globe injury phenotype, the D2 representing a severe open-globe like phenotype and the Balb/cJ representing a closed-globe phenotype with features of traumatic optic neuropathy.

Secondly, we showed that erythropoietin reduces cell death, nitrosative stress and optic nerve damage after injury. However, the timing and treatment delivery method are critical. Acute systemic treatment with EPO boosts retinal iron levels and further increases oxidative stress in the retina through the Fenton reaction. To avoid these damaging side effects, less hematopoietic forms of EPO should be delivered intraocularly to prevent increased systemic hematopoiesis.

Finally, our preliminary results with the $Gulo^{-/-}$ mice suggest that vitamin C depletion is not sufficient to exacerbate ocular blast injuries. Oxidative stress is common

after blast in all three of our mouse models and appears to contribute to worse outcomes with acute EPO treatment. It is possible that the increased oxidative stress in the Gulo$^{-/-}$ retina is too mild to exacerbate the injury. However, we need still need to quantify oxidative stress in the Gulo$^{-/-}$ after blast.

Together, these findings demonstrate that we can effectively model various aspects of ocular blast trauma and test potential treatments for injury, which are greatly needed.

REFERENCES

Abbotts, R., Harrison, S., and Cooper, G., 2007. Primary blast injuries to the eye: a review of the evidence. *Journal of the Royal Army Medical Corps*, 153(2), pp.119–123.

Abdul-Muneer, P., Schuetz, H., Wang, F., Skotak, M., Jones, J., Gorantla, S., Zimmerman, M.C., Chandra, N., and Haorah, J., 2013. Induction of oxidative and nitrosative damage leads to cerebrovascular inflammation in an animal model of mild traumatic brain injury induced by primary blast. *Free Radical Biology and Medicine*, 60, pp.282–291.

Abecasis, G.R., Yashar, B.M., Zhao, Y., Ghiasvand, N.M., Zareparsi, S., Branham, K.E., Reddick, A.C., Trager, E.H., Yoshida, S., Bahling, J., and others 2004. Age-related macular degeneration: a high-resolution genome scan for susceptibility loci in a population enriched for late-stage disease. *The American Journal of Human Genetics*, 74(3), pp.482–494.

Agapova, O.A., Ricard, C.S., Salvador-Silva, M., and Hernandez, M.R., 2001. Expression of matrix metalloproteinases and tissue inhibitors of metalloproteinases in human optic nerve head astrocytes. *Glia*, 33(3), pp.205–216.

Age-Related Eye Disease Study Research Group 2001. A randomized, placebo-controlled, clinical trial of high-dose supplementation with vitamins C and E, beta carotene, and zinc for age-related macular degeneration and vision loss: AREDS report no. 8. *Archives of Ophthalmology*, 119(10), p.1417.

Ahsan, H., 2013. 3-Nitrotyrosine: a biomarker of nitrogen free radical species modified proteins in systemic autoimmunogenic conditions. *Human Immunology*, 74(10), pp.1392–1399.

Alam, M., Iqbal, M., Khan, A., and Khan, S.A., 2012. Ocular injuries in blast victims. *JPMA-Journal of the Pakistan Medical Association*, 62(2), p.138.

Anderson, M.G., Smith, R.S., Hawes, N.L., Zabaleta, A., Chang, B., Wiggs, J.L., and John, S.W., 2002. Mutations in genes encoding melanosomal proteins cause pigmentary glaucoma in DBA/2J mice. *Nature Genetics*, 30(1), pp.81–85.

Anon, 2016. *Office of Dietary Supplements - Vitamin C*. Vitamin C.

Bailey, T.A., Kanuga, N.,, Romero, I.A., Greenwood, J., Luthert, P.J., and Cheetham, M.E., 2004. Oxidative stress affects the junctional integrity of retinal pigment epithelial cells. *Investigative Ophthalmology & Visual Science*, 45(2), pp.675–684.

Barbero, S., Bajetto, A., Bonavia, R., Porcile, C., Piccioli, P., Pirani, P., Ravetti, J.L., Zona, G., Spaziante, R., Florio, T., and others 2002. Expression of the chemokine receptor CXCR4 and its ligand stromal cell-derived factor 1 in human brain tumors and their involvement in glial proliferation in vitro. *Annals of the New York Academy of Sciences*, 973(1), pp.60–69.

Bass, C.R., Panzer, M.B., Rafaels, K.A., Wood, G., Shridharani, J., and Capehart, B., 2012. Brain injuries from blast. *Annals of Biomedical Engineering*, 40(1), pp.185–202.

Beatty, S., Koh, H.H., Phil, M., Henson, D., and Boulton, M., 2000. The role of oxidative stress in the pathogenesis of age-related macular degeneration. *Survey of Ophthalmology*, 45(2), pp.115–134.

Bendich, A., Machlin, L., Scandurra, O., Burton, G., and Wayner, D., 1986. The antioxidant role of vitamin C. *Advances in Free Radical Biology & Medicine*, 2(2), pp.419–444.

Bergsbaken, T., Fink, S.L., and Cookson, B.T., 2009. Pyroptosis: host cell death and inflammation. *Nature Reviews Microbiology*, 7(2), pp.99–109.

Blanch, R.J., Ahmed, Z., Sik, A., Snead, D.R., Good, P.A., O'Neill, J., Berry, M., Scott, R.A., and Logan, A., 2012. Neuroretinal cell death in a murine model of closed globe injury: pathological and functional characterization. *Investigative Ophthalmology & Visual Science*, 53(11), pp.7220–7226.

Blight, R., and Hart, J., 1977. Structural changes in the outer retinal layers following blunt mechanical non-perforating trauma to the globe: an experimental study. *British Journal of Ophthalmology*, 61(9), pp.573–587.

Block, F., and Schwarz, M., 1998. The b-wave of the electroretinogram as an index of retinal ischemia. *General Pharmacology: The Vascular System*, 30(3), pp.281–287.

Bloemendal, H., de Jong, W., Jaenicke, R., Lubsen, N.H., Slingsby, C., and Tardieu, A., 2004. Ageing and vision: structure, stability and function of lens crystallins. *Progress in Biophysics and Molecular Biology*, 86(3), pp.407–485.

Bogdan, C., Paik, J., Vodovotz, Y., and Nathan, C., 1992. Contrasting mechanisms for suppression of macrophage cytokine release by transforming growth factor-beta and interleukin-10. *Journal of Biological Chemistry*, 267(32), pp.23301–23308.

Bond, W.S., and Rex, T.S., 2014. Evidence that erythropoietin modulates neuroinflammation through differential action on neurons, astrocytes, and microglia. *Frontiers in Immunology*, 5, p.523.

Bonni, A., Brunet, A., West, A.E., Datta, S.R., Takasu, M.A., and Greenberg, M.E., 1999. Cell survival promoted by the Ras-MAPK signaling pathway by transcription-dependent and-independent mechanisms. *Science*, 286(5443), pp.1358–1362.

Bosco, A., Steele, M.R., and Vetter, M.L., 2011. Early microglia activation in a mouse model of chronic glaucoma. *Journal of Comparative Neurology*, 519(4), pp.599–620.

Bricker-Anthony, C., D'Surney, L., Lunn, B., Hines-Beard, J., Jo, M., Bernardo-Colon, A., and Rex, T.S., 2016a. Erythropoietin either Prevents or Exacerbates Retinal Damage from Eye Trauma Depending on Treatment Timing. *Optometry and Vision Science: Official Publication of the American Academy of Optometry*.

Bricker-Anthony, C., Hines-Beard, J., D'Surney, L., and Rex, T.S., 2014a. Exacerbation of blast-induced ocular trauma by an immune response. *Journal of Neuroinflammation*, 11(192).

Bricker-Anthony, C., Hines-Beard, J., and Rex, T.S., 2016b. Eye-Directed Overpressure Airwave-Induced Trauma Causes Lasting Damage to the Anterior and Posterior Globe: A Model for Testing Cell-Based Therapies. *Journal of Ocular Pharmacology and Therapeutics*.

Bricker-Anthony, C., Hines-Beard, J., and Rex, T.S., 2014b. Molecular changes and vision loss in a mouse model of closed-globe blast trauma. *Investigative Ophthalmology & Visual Science*, 55(8), pp.4853–4862.

Brines, M., and Cerami, A., 2012. The receptor that tames the innate immune response. *Molecular Medicine*, 18(1), pp.486–496.

Brines, M., Grasso, G., Fiordaliso, F., Sfacteria, A., Ghezzi, P., Fratelli, M., Latini, R., Xie, Q., Smart, J., Su-Rick, C., and others, 2004. Erythropoietin mediates tissue protection through an erythropoietin and common β-subunit heteroreceptor. *Proceedings of the National Academy of Sciences of the United States of America*, 101(41), pp.14907–14912.

Bringmann, A., Pannicke, T., Grosche, J., Francke, M., Wiedemann, P., Skatchkov, S.N., Osborne, N.N., and Reichenbach, A., 2006. Müller cells in the healthy and diseased retina. *Progress in Retinal and Eye Research*, 25(4), pp.397–424.

Brunet, A., Datta, S.R., and Greenberg, M.E., 2001. Transcription-dependent and-independent control of neuronal survival by the PI3K–Akt signaling pathway. *Current Opinion in Neurobiology*, 11(3), pp.297–305.

Bunt-Milam, A.H., Black, R.A., and Bensinger, R.E., 1986. Breakdown of the outer blood-retinal barrier in experimental commotio retinae. *Experimental Eye Research*, 43(3), pp.397–412.

Burne, M.J., Haq, M., Matsuse, H., Mohapatra, S., and Rabb, H., 2000. Genetic susceptibility to renal ischemia reperfusion injury revealed in a murine model. *Transplantation*, 69(5), pp.1023–1025.

Callegan, M.C., Engelbert, M., Parke, D.W., Jett, B.D., and Gilmore, M.S., 2002. Bacterial endophthalmitis: epidemiology, therapeutics, and bacterium-host interactions. *Clinical Microbiology Reviews*, 15(1), pp.111–124.

Calvert, P., Krasnoperova, N., Lyubarsky, A., Isayama, T., Nicolo, M., Kosaras, B., Wong, G., Gannon, K., Margolskee, R., Sidman, R., and others 2000. Phototransduction in transgenic mice after targeted deletion of the rod transducin α-subunit. *Proceedings of the National Academy of Sciences*, 97(25), pp.13913–13918.

Capó-Aponte, J.E., Jurek, G.M., Walsh, D.V., Temme, L.A., Ahroon, W.A., and Riggs, D.W., 2015. Effects of repetitive low-level blast exposure on visual systems and ocular structures. *Journal of Rehabilitation Research and Development*, 52(3), pp.273–290.

Carter-Dawson, L.D., and Lavail, M.M., 1979. Rods and cones in the mouse retina. I. Structural analysis using light and electron microscopy. *Journal of Comparative Neurology*, 188(2), pp.245–262.

Cebulla, C.M., and Flynn, H.W., 2009. Endophthalmitis after open globe injuries. *American Journal of Ophthalmology*, 147(4), pp.567–568.

Cernak, I., Savic, V.J., Kotur, J., Prokic, V., Veljovik, M., and Grbovic, D., 2000. Characterization of plasma magnesium concentration and oxidative stress following graded traumatic brain injury in humans. *Journal of Neurotrauma*, 17(1), pp.53–68.

Chakravarthy, U., Stitt, A.W., Mcnally, J., Bailie, J.R., Hoey, E.M., and Duprex, P., 1995. Nitric oxide synthase activity and expression in retinal capillary endothelial cells and pericytes. *Current Eye Research*, 14(4), pp.285–294.

Chang, Z.-Y., Yeh, M.K., Chiang, C.H., Chen, Y.H., and Lu, D.W., 2013. Erythropoietin protects adult retinal ganglion cells against NMDA, trophic factor withdrawal, and TNF-α-induced damage. *PloS One*, 8(1), p.e55291.

Chattopadhyay, S., O'Rourke, J., and Cone, R.E., 2008. Implication for the CD94/NKG2A-Qa-1 system in the generation and function of ocular-induced splenic CD8+ regulatory T cells. *International Immunology*, 20(4), pp.509–516.

Cheetham, J.C., Smith, D.M., Aoki, K.H., Stevenson, J.L., Hoeffel, T.J., Syed, R.S., Egrie, J., and Harvey, T.S., 1998. NMR structure of human erythropoietin and a comparison with its receptor bound conformation. *Nature Structural & Molecular Biology*, 5(10), pp.861–866.

Chevallier, A., Mialot, A., Petit, J.M., Fernandez-Salguero, P., Barouki, R., Coumoul, X., and Beraneck, M., 2013. Oculomotor deficits in aryl hydrocarbon receptor null mouse. *PloS One*, 8(1), p.e53520.

Cho, C., and Miller, R.J., 2002. Chemokine receptors and neural function. *Journal of Neurovirology*, 8(6), pp.573–584.

Cockerham, G.C., Goodrich, G.L., Weichel, E.D., Orcutt, J.C., Rizzo, J.F., Bower, K.S., and Schuchard, R.A., 2009. Eye and visual function in traumatic brain injury. *Journal of Rehabilitation Research & Development*, 46(6).

Cockerham, G.C., Lemke, S., Glynn-Milley, C., Zumhagen, L., and Cockerham, K.P., 2013. Visual performance and the ocular surface in traumatic brain injury. *Clinical Practice*, 11(1), pp.225–34.

Cockerham, G.C., Rice, T.A., Hewes, E.H., Cockerham, K.P., Lemke, S., Wang, G., Lin, R.C., Glynn-Milley, C., and Zumhagen, L., 2011. Closed-eye ocular injuries in the Iraq and Afghanistan wars. *New England Journal of Medicine*, 364(22), pp.2172–2173.

Cone, F.E., Gelman, S.E., Son, J.L., Pease, M.E., and Quigley, H.A., 2010. Differential susceptibility to experimental glaucoma among 3 mouse strains using bead and viscoelastic injection. *Experimental Eye Research*, 91(3), pp.415–424.

Cook, B., Lewis, G.P., Fisher, S.K., and Adler, R., 1995. Apoptotic photoreceptor degeneration in experimental retinal detachment. *Investigative Ophthalmology and Visual Science*, 36(6), pp.990–996.

Crawley, J.N., Belknap, J.K., Collins, A., Crabbe, J.C., Frankel, W., Henderson, N., Hitzemann, R.J., Maxson, S.C., Miner, L.L., Silva, A.J., and others 1997. Behavioral phenotypes of inbred mouse strains: implications and recommendations for molecular studies. *Psychopharmacology*, 132(2), pp.107–124.

Creel, D., Witkop, C.J., and King, R.A., 1974. Asymmetric visually evoked potentials in human albinos: evidence for visual system anomalies. *Investigative Ophthalmology & Visual Science*, *13*(6), pp.430-440.

Cunha, F., Mohcada, S., and Liew, F., 1992. Interleukin-10 (IL-10) inhibits the induction of nitric oxide synthase by interferon-γ in murine macrophages. *Biochemical and Biophysical Research Communications*, 182(3), pp.1155–1159.

Curcio, C.A., and Allen, K.A., 1990. Topography of ganglion cells in human retina. *Journal of Comparative Neurology*, 300(1), pp.5–25.

Curcio, C.A., Sloan, K.R., Kalina, R.E., and Hendrickson, A.E., 1990. Human photoreceptor topography. *Journal of Comparative Neurology*, 292(4), pp.497–523.

Danesh-Meyer, H.V., Kerr, N.M., Zhang, J., Eady, E.K., O'Carroll, S.J., Nicholson, L.F., Johnson, C.S., and Green, C.R., 2012. Connexin43 mimetic peptide reduces vascular leak and retinal ganglion cell death following retinal ischaemia. *Brain*, 135(2), pp.506–520.

Deliyanti, D., and Wilkinson-Berka, J.L., 2015. Inhibition of NOX1/4 with GKT137831: a potential novel treatment to attenuate neuroglial cell inflammation in the retina. *Journal of Neuroinflammation*, 12(1), p.1.

Dentchev, T., Milam, A.H., Lee, V.M.Y., Trojanowski, J.Q., and Dunaief, J.L., 2003. Amyloid-β is found in drusen from some age-related macular degeneration retinas, but not in drusen from normal retinas. *American Journal of Ophthalmology*, 136(4), pp.787–787.

DePalma, R.G., Burris, D.G., Champion, H.R., and Hodgson, M.J., 2005. Blast injuries. *New England Journal of Medicine*, 352(13), pp.1335–1342.

De Vos, J., Jourdan, M., Tarte, K., Jasmin, C., and Klein, B., 2000. JAK2 tyrosine kinase inhibitor tyrphostin AG490 downregulates the mitogen-activated protein kinase (MAPK) and signal transducer and activator of transcription (STAT) pathways and induces apoptosis in myeloma cells. *British Journal of Haematology*, 109(4), pp.823–828.

Digicaylioglu, M., and Lipton, S.A., 2001. Erythropoietin-mediated neuroprotection involves cross-talk between Jak2 and NF-κB signalling cascades. *Nature*, 412(6847), pp.641–647.

Donkó, Á., Péterfi, Z., Sum, A.,, Leto, T., and Geiszt, M., 2005. Dual oxidases. *Philosophical Transactions of the Royal Society of London B: Biological Sciences*, 360(1464), pp.2301–2308.

Douglas, R., Alam, N., Silver, B., McGill, T., Tschetter, W., and Prusky, G., 2005. Independent visual threshold measurements in the two eyes of freely moving rats and mice using a virtual-reality optokinetic system. *Visual Neuroscience*, 22(05), pp.677–684.

Dumont, F., and Bischoff, P., 2010. Non-erythropoietic tissue-protective peptides derived from erythropoietin: WO2009094172. *Expert Opinion on Therapeutic Patents*, 20(5), pp.715–723.

Dvoriantchikova, G., Grant, J., Santos, A.R.C., Hernandez, E., and Ivanov, D., 2012. Neuronal nad(p)h oxidases contribute to ros production and mediate rgc death after ischemia role of neuronal nad(p)h oxidases in rgc death. *Investigative Ophthalmology & Visual Science*, 53(6), pp.2823–2830.

Egan, D.J., Peak, D.A., and Peters, J.R., 2016. Endophthalmitis: background, pathophysiology, epidemiology.

Elliott, S., Busse, L., Bass, M.B., Lu, H., Sarosi, I., Sinclair, A.M., Spahr, C., Um, M., Van, G., and Begley, C.G., 2006. Anti-epo receptor antibodies do not predict Epo receptor expression. *Blood*, 107(5), pp.1892–1895.

Elsayed, N.M., Gorbunov, N.V., and Kagan, V.E., 1997. A proposed biochemical mechanism involving hemoglobin for blast overpressure-induced injury. *Toxicology*, 121(1), pp.81–90.

Erdurman, F., Hurmeric, V., Gokce, G., Durukan, A., Sobaci, G., and Altinsoy, H., 2011. Ocular injuries from improvised explosive devices. *Eye*, 25(11), pp.1491–1498.

Eschbach, J.W., Egrie, J.C., Downing, M.R., Browne, J.K., and Adamson, J.W., 1987. Correction of the anemia of end-stage renal disease with recombinant human erythropoietin. *New England Journal of Medicine*, 316(2), pp.73–78.

Ethen, C.M., Reilly, C., Feng, X., Olsen, T.W., and Ferrington, D.A., 2007. Age-related macular degeneration and retinal protein modification by 4-hydroxy-2-nonenal. *Investigative Ophthalmology & Visual Science*, 48(8), pp.3469–3479.

Fink, K., Andrews, L., Butler, W., Ona, V., Li, M., Bogdanov, M., Endres, M., Khan, S., Namura, S., Stieg, P., and others 1999. Reduction of post-traumatic brain injury and free radical production by inhibition of the caspase-1 cascade. *Neuroscience*, 94(4), pp.1213–1218.

Fisher, J.W., 2003. Erythropoietin: physiology and pharmacology update. *Experimental Biology and Medicine*, 228(1), pp.1–14.

Freed, S., and Fishman-Hellerstein, L., 1997. Visual electrodiagnostic findings in mild traumatic brain injury. *Brain Injury*, 11(1), pp.25–36.

Friedman, G., Froom, P., Sazbon, L., Grinblatt, I., Shochina, M., Tsenter, J., Babaey, S., Yehuda, A.B., and Groswasser, Z., 1999. Apolipoprotein E-ε4 genotype predicts a poor outcome in survivors of traumatic brain injury. *Neurology*, 52(2), pp.244–244.

Fujihara, M., Nagai, N., Sussan, T.E., Biswal, S., and Handa, J.T., 2008. Chronic cigarette smoke causes oxidative damage and apoptosis to retinal pigmented epithelial cells in mice. *PLoS One*, 3(9), p.e3119.

Ganea, E., and Harding, J.J., 2006. Glutathione-related enzymes and the eye. *Current Eye Research*, 31(1), pp.1–11.

Garg, T.K., and Chang, J.Y., 2003. Oxidative stress causes erk phosphorylation and cell death in cultured retinal pigment epithelium: prevention of cell death by ag126 and 15-deoxy-delta 12, 14-pgj 2. *BMC Ophthalmology*, 3(1), p.1.

Garman, R.H., Jenkins, L.W., Switzer III, R.C., Bauman, R.A., Tong, L.C., Swauger, P.V., Parks, S.A., Ritzel, D.V., Dixon, C.E., Clark, R.S., and others 2011. Blast exposure in rats with body shielding is characterized primarily by diffuse axonal injury. *Journal of Neurotrauma*, 28(6), pp.947–959.

Gawad, A., Schlichting, L., Strauss, O., and Zeitz, O., 2009. Antiapoptotic properties of erythropoietin: novel strategies for protection of retinal pigment epithelial cells. *Eye*, 23(12), pp.2245–2250.

Gilliam, J.C., and Wensel, T.G., 2011. TRP channel gene expression in the mouse retina. *Vision Research*, 51(23), pp.2440–2452.

Giovinazzo, V., 1986. The ocular sequelae of blunt trauma. *Advances in Ophthalmic Plastic and Reconstructive Surgery*, 6, pp.107–114.

Goldstein, I.M., Ostwald, P., and Roth, S., 1996. Nitric oxide: a review of its role in retinal function and disease. *Vision Research*, 36(18), pp.2979–2994.

Goldstein, L.E., Fisher, A.M., Tagge, C.A., Zhang, X.L., Velisek, L., Sullivan, J.A., Upreti, C., Kracht, J.M., Ericsson, M., Wojnarowicz, M.W., and others 2012. Chronic traumatic encephalopathy in blast-exposed military veterans and a blast neurotrauma mouse model. *Science Translational Medicine*, 4(134), p.13460.

Gregory, T., Yu, C., Ma, A., Orkin, S.H., Blobel, G.A., and Weiss, M.J., 1999. GATA-1 and erythropoietin cooperate to promote erythroid cell survival by regulating bcl-xL expression. *Blood*, 94(1), pp.87–96.

Grimm, C., Wenzel, A., Groszer, M., Mayser, H., Seeliger, M., Samardzija, M., Bauer, C., Gassmann, M., and Remé, C.E., 2002. HIF-1-induced erythropoietin in the hypoxic retina protects against light-induced retinal degeneration. *Nature Medicine*, 8(7), pp.718–724.

Gunnarson, E., Song, Y., Kowalewski, J.M., Brismar, H., Brines, M., Cerami, A.,, Andersson, U., Zelenina, M., and Aperia, A., 2009. Erythropoietin modulation of astrocyte water permeability as a component of neuroprotection. *Proceedings of the National Academy of Sciences*, 106(5), pp.1602–1607.

Ha, D., de Vries, W.N., John, S.W., Irazoqui, P.P., and Chappell, W.J., 2012. Polymer-based miniature flexible capacitive pressure sensor for intraocular pressure (IOP) monitoring inside a mouse eye. *Biomedical Microdevices*, 14(1), pp.207–215.

Halliwell, B., and Chirico, S., 1993. Lipid peroxidation: its mechanism, measurement, and significance. *The American Journal of Clinical Nutrition*, 57(5), p.715S–724S.

Hall, L.R., Diaconu, E., Patel, R., and Pearlman, E., 2001. CXC chemokine receptor 2 but not CC chemokine receptor 1 expression is essential for neutrophil recruitment to the cornea in helminth-mediated keratitis (river blindness). *The Journal of Immunology*, 166(6), pp.4035–4041.

Hampson, E., Vaney, D.I., and Weiler, R., 1992. Dopaminergic modulation of gap junction permeability between amacrine cells in mammalian retina. *The Journal of Neuroscience*, 12(12), pp.4911–4922.

Hardy, J., and Selkoe, D.J., 2002. The amyloid hypothesis of Alzheimer's disease: progress and problems on the road to therapeutics. *Science*, 297(5580), pp.353–356.

Harrison, F.E., Meredith, M.E., Dawes, S.M., Saskowski, J.L., and May, J.M., 2010. Low ascorbic acid and increased oxidative stress in gulo (-/-) mice during development. *Brain Research*, 1349, pp.143–152.

Haverkamp, S., and Wässle, H., 2000. Immunocytochemical analysis of the mouse retina. *Journal of Comparative Neurology*, 424(1), pp.1–23.

He, H., Yang, P., Jiang, L., Zhang, J., Zhao, C., Chen, L., Lin, X., Zhou, H., and Kijlstra, A., 2008. Upregulation of CD94 on CD8+ T cells in anterior chamber-associated immune deviation. *BMC Immunology*, 9(1), p.53.

Helga Kolb, 2016. Roles of Amacrine Cells. *Webvision*.

Henning, S.M., Zhang, J.Z., McKee, R.W., Swendseid, M.E., and Jacob, R.A., 1991. Glutathione blood levels and other oxidant defense indices in men fed diets low in vitamin C. *The Journal of Nutrition*, 121(12), pp.1969–1975.

Hernandez, M.R., 1992. Ultrastructural immunocytochemical analysis of elastin in the human lamina cribrosa. Changes in elastic fibers in primary open-angle glaucoma. *Investigative Ophthalmology & Visual Science*, 33(10), pp.2891–2903.

Hetling, J.R., and Pepperberg, D.R., 1999. Sensitivity and kinetics of mouse rod flash responses determined in vivo from paired-flash electroretinograms. *The Journal of Physiology*, 516(2), pp.593–609.

Hilber 2011. *Eye injuries, active component, US Armed Forces, 2000-2010*. Medical Surveillance Monthly Report. Armed Forces Health Surveillance Center, pp.2–7.

Hines-Beard, J., Marchetta, J., Gordon, S., Chaum, E., Geisert, E.E., and Rex, T.S., 2012. A mouse model of ocular blast injury that induces closed globe anterior and posterior pole damage. *Experimental Eye Research*, 99, pp.63–70.

Holcombe, D.J., Lengefeld, N., Gole, G.A., and Barnett, N.L., 2008. Selective inner retinal dysfunction precedes ganglion cell loss in a mouse glaucoma model. *British Journal of Ophthalmology*, 92(5), pp.683–688.

Howell, G.R., Soto, I., Ryan, M., Graham, L.C., Smith, R.S., and John, S.W., 2013. Deficiency of complement component 5 ameliorates glaucoma in DBA/2J mice. *Journal of Neuroinflammation*, 10(1), p.1.

Huberman, A.D., and Niell, C.M., 2011. What can mice tell us about how vision works? *Trends in Neurosciences*, 34(9), pp.464–473.

Hu, L., Luo, Y., Zhang, J., Lei, X., Shen, J., Wu, Y., Qin, M., Unver, Y., Zhong, Y., Xu, G., and others, 2010. EPO reduces reactive gliosis and stimulates neurotrophin expression in Muller cells. *Frontiers in Bioscience (Elite edition)*, 3, pp.1541–1555.

Humphries, M.M., Rancourt, D., Farrar, G.J., Kenna, P., Hazel, M., Bush, R.A., Sieving, P.A., Sheils, D.M., McNally, N., Creighton, P., and others 1997. Retinopathy induced in mice by targeted disruption of the rhodopsin gene. *Nature Genetics*, 15(2), pp.216–219.

Jackson, T.S., Xu, A., Vita, J.A., and Keaney, J.F., 1998. Ascorbate prevents the interaction of superoxide and nitric oxide only at very high physiological concentrations. *Circulation Research*, 83(9), pp.916–922.

Jen, L., Hart, A., Jen, A., Relvas, J., Gentleman, S., Garey, L., and Patel, A., 1998. Alzheimer's peptide kills cells of retina in vivo. *Nature*, 392(6672), pp.140–141.

Jin, C., and Flavell, R.A., 2010. Molecular mechanism of NLRP3 inflammasome activation. *Journal of Clinical Immunology*, 30(5), pp.628–631.

Johnson, V.E., Stewart, W., and Smith, D.H., 2013. Axonal pathology in traumatic brain injury. *Experimental Neurology*, 246, pp.35–43.

John, S., Smith, R.S., Savinova, O.V., Hawes, N.L., Chang, B., Turnbull, D., Davisson, M., Roderick, T.H., and Heckenlively, J.R., 1998. Essential iris atrophy, pigment dispersion, and glaucoma in DBA/2J mice. *Investigative Ophthalmology & Visual Science*, 39(6), pp.951–962.

Johnston, P., 1991. Traumatic retinal detachment. *British Journal of Ophthalmology*, 75(1), pp.18–21.

Julius, D., and Basbaum, A.I., 2001. Molecular mechanisms of nociception. *Nature*, 413(6852), pp.203–210.

Kaemmerer, E., Schutt, F., Krohne, T.U., Holz, F.G., and Kopitz, J., 2007. Effects of lipid peroxidation-related protein modifications on RPE lysosomal functions and POS phagocytosis. *Investigative Ophthalmology & Visual Science*, 48(3), pp.1342–1347.

Kapphahn, R.J., Giwa, B.M., Berg, K.M., Roehrich, H., Feng, X., Olsen, T.W., and Ferrington, D.A., 2006. Retinal proteins modified by 4-hydroxynonenal: identification of molecular targets. *Experimental Eye Research*, 83(1), pp.165–175.

Kapur, G.B., Hutson, H.R., Davis, M.A., and Rice, P.L., 2005. The United States twenty-year experience with bombing incidents: implications for terrorism preparedness and medical response. *Journal of Trauma and Acute Care Surgery*, 59(6), pp.1436–1444.

Kilic, E., Kilic, Ü., Soliz, J., Bassetti, C.L., Gassmann, M., and Hermann, D.M., 2005. Brain-derived erythropoietin protects from focal cerebral ischemia by dual activation of ERK-1/-2 and Akt pathways. *The FASEB Journal*, 19(14), pp.2026–2028.

Kilmartin, D.J., Wilson, D., Liversidge, J., Dick, A.D., Bruce, J., Acheson, R.W., Urbaniak, S.J., and Forrester, J.V., 2001. Immunogenetics and clinical phenotype of sympathetic ophthalmia in British and Irish patients. *British Journal of Ophthalmology*, 85(3), pp.281–286.

King, C.E., Rodger, J., Bartlett, C., Esmaili, T., Dunlop, S.A., and Beazley, L.D., 2007. Erythropoietin is both neuroprotective and neuroregenerative following optic nerve transection. *Experimental Neurology*, 205(1), pp.48–55.

Kipnis, J., Yoles, E., Schori, H., Hauben, E., Shaked, I., and Schwartz, M., 2001. Neuronal survival after CNS insult is determined by a genetically encoded autoimmune response. *The Journal of Neuroscience*, 21(13), pp.4564–4571.

Klein, R.J., Zeiss, C., Chew, E.Y., Tsai, J.Y., Sackler, R.S., Haynes, C., Henning, A.K., SanGiovanni, J.P., Mane, S.M., Mayne, S.T., and others 2005. Complement factor H polymorphism in age-related macular degeneration. *Science*, 308(5720), pp.385–389.

Koeberle, P., Gauldie, J., and Ball, A., 2004. Effects of adenoviral-mediated gene transfer of interleukin-10, interleukin-4, and transforming growth factor-β on the survival of axotomized retinal ganglion cells. *Neuroscience*, 125(4), pp.903–920.

Koeck, T., Levison, B., Hazen, S.L., Crabb, J.W., Stuehr, D.J., and Aulak, K.S., 2004. Tyrosine nitration impairs mammalian aldolase A activity. *Molecular & Cellular Proteomics*, 3(6), pp.548–557.

Koliatsos, V.E., Cernak, I., Xu, L., Song, Y., Savonenko, A., Crain, B.J., Eberhart, C.G., Frangakis, C.E., Melnikova, T., Kim, H., and others 2011. A mouse model of blast injury to brain: initial pathological, neuropathological, and behavioral characterization. *Journal of Neuropathology & Experimental Neurology*, 70(5), pp.399–416.

Kuhn, F., Morris, R., Witherspoon, C.D., and Mann, L., 2006. Epidemiology of blinding trauma in the United States eye injury registry. *Ophthalmic Epidemiology*, 13(3), pp.209–216.

Leal, E.C., Manivannan, A., Hosoya, K.I., Terasaki, T., Cunha-Vaz, J., Ambrósio, A.F., and Forrester, J.V., 2007. Inducible nitric oxide synthase isoform is a key mediator of leukostasis and blood-retinal barrier breakdown in diabetic retinopathy. *Investigative Ophthalmology & Visual Science*, 48(11), pp.5257–5265.

Ledeboer, A., Breve, J.J., Poole, S., Tilders, F.J., and Van Dam, A.M., 2000. Interleukin-10, interleukin-4, and transforming growth factor-β differentially regulate lipopolysaccharide-induced production of pro-inflammatory cytokines and nitric oxide in co-cultures of rat astroglial and microglial cells. *Glia*, 30(2), pp.134–142.

Lee, D.E., Son, W., Ha, B.J., Oh, M.S., and Yoo, O.J., 2006a. The prolonged half-lives of new erythropoietin derivatives via peptide addition. *Biochemical and Biophysical Research Communications*, 339(1), pp.380–385.

Lee, S.T., Chu, K., Sinn, D.I., Jung, K.H., Kim, E.H., Kim, S.J., Kim, J.M.,, Ko, S.Y., Kim, M., and Roh, J.K., 2006b. Erythropoietin reduces perihematomal inflammation and cell death with eNOS and STAT3 activations in experimental intracerebral hemorrhage. *Journal of Neurochemistry*, 96(6), pp.1728–1739.

Le Gouill, E., Jimenez, M., Binnert, C., Jayet, P.Y., Thalmann, S., Nicod, P., Scherrer, U., and Vollenweider, P., 2007. Endothelial nitric oxide synthase (eNOS) knockout mice have defective mitochondrial β-oxidation. *Diabetes*, 56(11), pp.2690–2696.

Lei, B., and Yao, G., 2006. Spectral attenuation of the mouse, rat, pig and human lenses from wavelengths 360nm to 1020nm. *Experimental Eye Research*, 83(3), pp.610–614.

Leist, M., Ghezzi, P., Grasso, G., Bianchi, R., Villa, P., Fratelli, M., Savino, C., Bianchi, M., Nielsen, J., Gerwien, J., and others 2004. Derivatives of erythropoietin that are tissue protective but not erythropoietic. *Science*, 305(5681), pp.239–242.

Levin, L.A., Beck, R.W., Joseph, M.P., Seiff, S., Kraker, R., Group, I.O.N.T.S., and others 1999. The treatment of traumatic optic neuropathy: the international optic nerve trauma study. *Ophthalmology*, 106(7), pp.1268–1277.

Liang, F.Q., and Godley, B.F., 2003. Oxidative stress-induced mitochondrial DNA damage in human retinal pigment epithelial cells: a possible mechanism for RPE aging and age-related macular degeneration. *Experimental Eye Research*, 76(4), pp.397–403.

Liang, L.P., and Patel, M., 2004. Mitochondrial oxidative stress and increased seizure susceptibility in Sod2-/+ mice. *Free Radical Biology and Medicine*, 36(5), pp.542–554.

Libby, R.T., Gould, D.B., Anderson, M.G., and John, S.W., 2005. Complex genetics of glaucoma susceptibility. *Annual Review of Genomics and Human Genetics*, 6(1), p.15.

Lifshitz, J., Sullivan, P.G., Hovda, D.A., Wieloch, T., and McIntosh, T.K., 2004. Mitochondrial damage and dysfunction in traumatic brain injury. *Mitochondrion*, 4(5), pp.705–713.

Li, J., McQuade, T., Siemer, A.B., Napetschnig, J., Moriwaki, K., Hsiao, Y.S., Damko, E., Moquin, D., Walz, T., McDermott, A., and others 2012. The RIP1/RIP3 necrosome forms a functional amyloid signaling complex required for programmed necrosis. *Cell*, 150(2), pp.339–350.

Lindqvist, N., Liu, Q., Zajadacz, J., Franze, K., and Reichenbach, A., 2010. Retinal glial (müller) cells: sensing and responding to tissue stretch. *Investigative Ophthalmology & Visual Science*, 51(3), pp.1683–1690.

Li, Q., Zemel, E., Miller, B., and Perlman, I., 2002. Early retinal damage in experimental diabetes: electroretinographical and morphological observations. *Experimental Eye Research*, 74(5), pp.615–625.

Li, Y., Semaan, S.J., Schlamp, C.L., and Nickells, R.W., 2007. Dominant inheritance of retinal ganglion cell resistance to optic nerve crush in mice. *BMC Neuroscience*, 8(1), p.19.

Li, Z., Tso, M., Wang, H., and Organisciak, D., 1985. Amelioration of photic injury in rat retina by ascorbic acid: a histopathologic study. *Investigative Ophthalmology & Visual Science*, 26(11), pp.1589–1598.

Lodge, P.A., and Sriram, S., 1996. Regulation of microglial activation by TGF-beta, IL-10, and CSF-1. *Journal of Leukocyte Biology*, 60(4), pp.502–508.

Louboutin, J.P., Wang, L., and Wilson, J.M., 2005. Gene transfer into skeletal muscle using novel AAV serotypes. *The Journal of Gene Medicine*, 7(4), pp.442–451.

Lu, D., Mahmood, A., Qu, C., Goussev, A., Schallert, T., and Chopp, M., 2005. Erythropoietin enhances neurogenesis and restores spatial memory in rats after traumatic brain injury. *Journal of Neurotrauma*, 22(9), pp.1011–1017.

Maeda, N., Hagihara, H., Nakata, Y., Hiller, S., Wilder, J., and Reddick, R., 2000. Aortic wall damage in mice unable to synthesize ascorbic acid. *Proceedings of the National Academy of Sciences*, 97(2), pp.841–846.

Maffei, L., Fiorentini, A., Bisti, S., and Holländer, H., 1985. Pattern ERG in the monkey after section of the optic nerve. *Experimental Brain Research*, 59(2), pp.423–425.

Mark, R.J., Lovell, M.A., Markesbery, W.R., Uchida, K., and Mattson, M.P., 1997. A role for 4-hydroxynonenal, an aldehydic product of lipid peroxidation, in disruption of ion homeostasis and neuronal death induced by amyloid β-peptide. *Journal of Neurochemistry*, 68(1), pp.255–264.

Massey, S.C., O'Brien, J.J., Trexler, E.B., Li, W., Keung, J.W., Mills, S.L., and O'Brien, J., 2003. Multiple neuronal connexins in the mammalian retina. *Cell Communication & Adhesion*, 10(4-6), pp.425–430.

Melki, S., Todani, A., and Cherfan, G., 2014. An implantable intraocular pressure transducer: initial safety outcomes. *JAMA Ophthalmology*, 132(10), pp.1221–1225.

Mervin, K., Valter, K., Maslim, J., Lewis, G., Fisher, S., and Stone, J., 1999. Limiting photoreceptor death and deconstruction during experimental retinal detachment: the value of oxygen supplementation. *American Journal of Ophthalmology*, 128(2), pp.155–164.

Mohan, K., Kecova, H., Hernandez-Merino, E., Kardon, R.H., and Harper, M.M., 2013. Retinal ganglion cell damage in an experimental rodent model of blast-mediated traumatic brain injury. *Investigative Ophthalmology & Visual Science*, 54(5), pp.3440–3450.

Morishita, E., Masuda, S., Nagao, M., Yasuda, Y., and Sasaki, R., 1996. Erythropoietin receptor is expressed in rat hippocampal and cerebral cortical neurons, and erythropoietin prevents in vitro glutamate-induced neuronal death. *Neuroscience*, 76(1), pp.105–116.

Moriwaki, K., and Chan, F.K.M., 2013. RIP3: a molecular switch for necrosis and inflammation. *Genes & Development*, 27(15), pp.1640–1649.

Nakazawa, T., Matsubara, A., Noda, K., Hisatomi, T., She, H., Skondra, D., Miyahara, S., Sobrin, L., Thomas, K.L., Chen, D.F., and others 2006. Characterization of cytokine responses to retinal detachment in rats. *Molecular Vision*, 12(8), p.67.

Nauseef, W.M., 2008. Biological roles for the NOX family NADPH oxidases. *Journal of Biological Chemistry*, 283(25), pp.16961–16965.

Neufeld, A.H., Sawada, A., and Becker, B., 1999. Inhibition of nitric-oxide synthase 2 by aminoguanidine provides neuroprotection of retinal ganglion cells in a rat model of chronic glaucoma. *Proceedings of the National Academy of Sciences*, 96(17), pp.9944–9948.

Niki, E., Yoshida, Y., Saito, Y., and Noguchi, N., 2005. Lipid peroxidation: mechanisms, inhibition, and biological effects. *Biochemical and Biophysical Research Communications*, 338(1), pp.668–676.

Ozer, P.A., Yalvac, I.S., Satana, B., Eksioglu, U., and Duman, S., 2007. Incidence and risk factors in secondary glaucomas after blunt and penetrating ocular trauma. *Journal of Glaucoma*, 16(8), pp.685–690.

Pacher, P., Beckman, J.S., and Liaudet, L., 2007. Nitric oxide and peroxynitrite in health and disease. *Physiological Reviews*, 87(1), pp.315–424.

Pal-Ghosh, S., Tadvalkar, G., Jurjus, R.A., Zieske, J.D., and Stepp, M.A., 2008. BALB/c and C57BL6 mouse strains vary in their ability to heal corneal epithelial debridement wounds. *Experimental Eye Research*, 87(5), pp.478–486.

Parganas, E., Wang, D., Stravopodis, D., Topham, D.J., Marine, J.C., Teglund, S., Vanin, E.F., Bodner, S., Colamonici, O.R., van Deursen, J.M., and others, 1998. Jak2 is essential for signaling through a variety of cytokine receptors. *Cell*, 93(3), pp.385–395.

Paschon, V., Higa, G.S.V., Resende, R.R., Britto, L.R.G., and Kihara, A.H., 2012. Blocking of connexin-mediated communication promotes neuroprotection during acute degeneration induced by mechanical trauma. *PLoS One*, 7(9), p.e45449.

Peirce, J.L., Lu, L., Gu, J., Silver, L.M., and Williams, R.W., 2004. A new set of BXD recombinant inbred lines from advanced intercross populations in mice. *BMC Genetics*, 5(1), p.1.

Peng, W., Xing, Z., Yang, J., Wang, Y., Wang, W., and Huang, W., 2014. The efficacy of erythropoietin in treating experimental traumatic brain injury: a systematic review of controlled trials in animal models: A review. *Journal of Neurosurgery*, 121(3), pp.653–664.

Pennesi, M.E., Neuringer, M., and Courtney, R.J., 2012. Animal models of age related macular degeneration. *Molecular Aspects of Medicine*, 33(4), pp.487–509.

Petersen, D.R., and Doorn, J.A., 2004. Reactions of 4-hydroxynonenal with proteins and cellular targets. *Free Radical Biology and Medicine*, 37(7), pp.937–945.

Peyman, G., and Bok, D., 1972. Peroxidase diffusion in the normal and laser-coagulated primate retina. *Investigative Ophthalmology*, 11(1), pp.35–45.

Phillips, B.N., Chun, D.W., and Colyer, M., 2013. Closed globe macular injuries after blasts in combat. *Retina*, 33(2), pp.371–379.

Plant, T.D., Zöllner, C., Kepura, F., Mousa, S.S., Eichhorst, J., Schaefer, M., Furkert, J., Stein, C., and Oksche, A., 2007. Endothelin potentiates TRPV1 via ET A receptor-mediated activation of protein kinase C. *Molecular Pain*, 3(1), p.1.

Por, E.D., Choi, J.H., and Lund, B.J., 2016. Low-Level Blast Exposure Increases Transient Receptor Potential Vanilloid 1 (TRPV1) Expression in the Rat Cornea. *Current Eye Research*, pp.1–8.

Pousset, F., Cremona, S., Dantzer, R., Kelley, K., and Parnet, P., 1999. Interleukin-4 and interleukin-10 regulate IL1-β induced mouse primary astrocyte activation: A comparative study. *Glia*, 26(1), pp.12–21.

Prusky, G.T., Silver, B.D., Tschetter, W.W., Alam, N.M., and Douglas, R.M., 2008. Experience-dependent plasticity from eye opening enables lasting, visual cortex-dependent enhancement of motion vision. *The Journal of Neuroscience*, 28(39), pp.9817–9827.

Rapaport, D., and Stone, J., 1984. The area centralis of the retina in the cat and other mammals: focal point for function and development of the visual system. *Neuroscience*, 11(2), pp.289–301.

Readnower, R.D., Chavko, M., Adeeb, S., Conroy, M.D., Pauly, J.R., McCarron, R.M., and Sullivan, P.G., 2010. Increase in blood–brain barrier permeability, oxidative stress, and activated microglia in a rat model of blast-induced traumatic brain injury. *Journal of Neuroscience Research*, 88(16), pp.3530–3539.

Rex, T.S., Allocca, M., Domenici, L., Surace, E.M., Maguire, A.M., Lyubarsky, A., Cellerino, A., Bennett, J., and Auricchio, A., 2004. Systemic but not intraocular Epo gene transfer protects the retina from light-and genetic-induced degeneration. *Molecular Therapy*, 10(5), pp.855–861.

Rex, T.S., Wong, Y., Kodali, K., and Merry, S., 2009. Neuroprotection of photoreceptors by direct delivery of erythropoietin to the retina of the retinal degeneration slow mouse. *Experimental Eye Research*, 89(5), pp.735–740.

Robison, W., Kuwabara, T., and Bieri, J., 1979. Vitamin E deficiency and the retina: photoreceptor and pigment epithelial changes. *Investigative Ophthalmology & Visual Science*, 18(7), pp.683–690.

Rokicki, W., Żaba, M., Wyględowska-Promieńska, D., Kabiesz, A., Reichman-Warmusz, E., Brzozowa, M., Majewski, W., and Wojnicz, R., 2015. Inducible and endothelial nitric synthetase expression and nitrotyrosine accumulation in iris vasculature of patients with primary open-angle glaucoma: a pilot study. *Medical Science Monitor: International Medical Journal of Experimental and Clinical Research*, 21, p.76.

Rosenbaum, J.T., Howes Jr, E., and English, D., 1985. Ascorbate in aqueous humor protects against myeloperoxidase-induced oxidation. *The American Journal of Pathology*, 120(2), p.244.

Rossi, T., Boccassini, B., Esposito, L., Clemente, C., Iossa, M., Placentino, L., and Bonora, N., 2012. Primary blast injury to the eye and orbit: finite element modeling. *Investigative Ophthalmology & Visual Science*, 53(13), pp.8057–8066.

Samardzic, K., Samardzic, J., Janjetovic, Z., Samardzic, I., Sekelj, S., and Latic-Hodzic, L., 2012. Traumatic optic neuropathy-to treat or to observe? *Acta Informatica Medica*, 20(2), p.131.

Sandbach, J.M., Coscun, P.E., Grossniklaus, H.E., Kokoszka, J.E., Newman, N.J., and Wallace, D.C., 2001. Ocular pathology in mitochondrial superoxide dismutase (Sod2)–deficient mice. *Investigative Ophthalmology & Visual Science*, 42(10), pp.2173–2178.

Sanders, SP 2016. Ocular hypotony: background, pathophysiology, epidemiology. *Medscape*. 6 May.

Sappington, R.M., and Calkins, D.J., 2008. Contribution of TRPV1 to microglia-derived IL-6 and NFκB translocation with elevated hydrostatic pressure. *Investigative Ophthalmology & Visual Science*, 49(7), pp.3004–3017.

Sarrazin, L., Averbukh, E., Halpert, M., Hemo, I., and Rumelt, S., 2004. Traumatic pediatric retinal detachment: a comparison between open and closed globe injuries. *American Journal of Ophthalmology*, 137(6), pp.1042–1049.

Sawada, M., Suzumura, A., Hosoya, H., Marunouchi, T., and Nagatsu, T., 1999. Interleukin-10 inhibits both production of cytokines and expression of cytokine receptors in microglia. *Journal of Neurochemistry*, 72(4), pp.1466–1471.

Schilling, T., and Eder, C., 2009. Importance of the non-selective cation channel TRPV1 for microglial reactive oxygen species generation. *Journal of Neuroimmunology*, 216(1), pp.118–121.

Schraermeyer, U., and Heimann, K., 1999. Current understanding on the role of retinal pigment epithelium and its pigmentation. *Pigment Cell Research*, 12(4), pp.219–236.

Scott, R., 2011. The injured eye. *Philosophical Transactions of the Royal Society B: Biological Sciences*, 366(1562), pp.251–260.

Seddon, J.M., Ajani, U.A., Sperduto, R.D., Hiller, R., Blair, N., Burton, T.C., Farber, M.D., Gragoudas, E.S., Haller, J., Miller, D.T., and others 1994. Dietary carotenoids, vitamins A, C, and E, and advanced age-related macular degeneration. *JAMA*, 272(18), pp.1413–1420.

Semenza, G.L., 2001. HIF-1, O 2, and the 3 PHDs: how animal cells signal hypoxia to the nucleus. *Cell*, 107(1), pp.1–3.

Sennlaub, F., Courtois, Y., and Goureau, O., 2002. Inducible nitric oxide synthase mediates retinal apoptosis in ischemic proliferative retinopathy. *The Journal of Neuroscience*, 22(10), pp.3987–3993.

Sharma, T.P., McDowell, C.M., Liu, Y., Wagner, A.H., Thole, D., Faga, B.P., Wordinger, R.J., Braun, T.A., and Clark, A.F., 2014. Optic nerve crush induces spatial and temporal gene expression patterns in retina and optic nerve of BALB/cJ mice. *Molecular Neurodegeneration*, 9(1), p.1.

Shen, Y., Heimel, J.A., Kamermans, M., Peachey, N.S., Gregg, R.G., and Nawy, S., 2009. A transient receptor potential-like channel mediates synaptic transmission in rod bipolar cells. *The Journal of Neuroscience*, 29(19), pp.6088–6093.

Singh, I.N., Sullivan, P.G., Deng, Y., Mbye, L.H., and Hall, E.D., 2006. Time course of post-traumatic mitochondrial oxidative damage and dysfunction in a mouse model of focal traumatic brain injury: implications for neuroprotective therapy. *Journal of Cerebral Blood Flow & Metabolism*, 26(11), pp.1407–1418.

Sipperley, J.O., Quigley, H.A., and Gass, J.D.M., 1978. Traumatic retinopathy in primates: the explanation of commotio retinae. *Archives of Ophthalmology*, 96(12), pp.2267–2273.

Sirén, A.L., Fratelli, M., Brines, M., Goemans, C., Casagrande, S., Lewczuk, P., Keenan, S., Gleiter, C., Pasquali, C., Capobianco, A., and others, 2001a. Erythropoietin prevents neuronal apoptosis after cerebral ischemia and metabolic stress. *Proceedings of the National Academy of Sciences*, 98(7), pp.4044–4049.

Sirén, A.L., Knerlich, F., Poser, W., Gleiter, C.H., Brück, W., and Ehrenreich, H., 2001b. Erythropoietin and erythropoietin receptor in human ischemic/hypoxic brain. *Acta Neuropathologica*, 101(3), pp.271–276.

Smith, J.A., 1994. Neutrophils, host defense, and inflammation: a double-edged sword. *Journal of Leukocyte Biology*, 56(6), pp.672–686.

Steinsapir, K.D., and Goldberg, R.A., 1994. Traumatic optic neuropathy. *Survey of Ophthalmology*, 38(6), pp.487–518.

Stoyanovsky, D.A., Goldman, R., Darrow, R.M., Organisciak, D.T., and Kagan, V.E., 1995. Endogenous ascorbate regenerates vitamin E in the retina directly and in combination with exogenous dihydrolipoic acid. *Current Eye Research*, 14(3), pp.181–189.

Strauss, O., 2005. The retinal pigment epithelium in visual function. *Physiological Reviews*, 85(3), pp.845–881.

Streilein, J.W., 2003. Ocular immune privilege: therapeutic opportunities from an experiment of nature. *Nature Reviews Immunology*, 3(11), pp.879–889.

Strich, S., 1961. Shearing of nerve fibres as a cause of brain damage due to head injury: a pathological study of twenty cases. *The Lancet*, 278(7200), pp.443–448.

Striedinger, K., Petrasch-Parwez, E., Zoidl, G., Napirei, M., Meier, C., Eysel, U.T., and Dermietzel, R., 2005. Loss of connexin36 increases retinal cell vulnerability to secondary cell loss. *European Journal of Neuroscience*, 22(3), pp.605–616.

Sullivan, T.A., Geisert, E.E., Hines-Beard, J., and Rex, T.S., 2011a. Systemic adeno-associated virus-mediated gene therapy preserves retinal ganglion cells and visual function in DBA/2J glaucomatous mice. *Human GeneTherapy*, 22(10), pp.1191–1200.

Sullivan, T.A., Geisert, E.E., Templeton, J.P., and Rex, T.S., 2012. Dose-dependent treatment of optic nerve crush by exogenous systemic mutant erythropoietin. *Experimental Eye Research*, 96(1), pp.36–41.

Sullivan, T., Geisert, E., and Rex, T., 2010. Systemic AAV-Mediated Gene Therapy Protects Retinal Ganglion Cells in DBA/2J Glaucomatous Mice. *Investigative Ophthalmology & Visual Science*, 51(13), pp.5191–5191.

Sullivan, T., Kodali, K., and Rex, T.S., 2011b. Systemic gene delivery protects the photoreceptors in the retinal degeneration slow mouse. *Neurochemical Research*, 36(4), pp.613–618.

Sun, B., Rizzo, L.V., Sun, S.H., Chan, C.C., Wiggert, B., Wilder, R.L., and Caspi, R.R., 1997. Genetic susceptibility to experimental autoimmune uveitis involves more than a predisposition to generate a T helper-1-like or a T helper-2-like response. *The Journal of Immunology*, 159(2), pp.1004–1011.

Szel, A., Röhlich, P., Mieziewska, K., Aguirre, G., and Van Veen, T., 1993. Spatial and temporal differences between the expression of short-and middle-wave sensitive cone pigments in the mouse retina: A developmental study. *Journal of Comparative Neurology*, 331(4), pp.564–577.

Tan, C.C., Eckardt, K., Firth, J., and Ratcliffe, P., 1992. Feedback modulation of renal and hepatic erythropoietin mRNA in response to graded anemia and hypoxia. *American Journal of Physiology-Renal Physiology*, 263(3), pp.F474–F481.

Tanito, M., Elliott, M.H., Kotake, Y., and Anderson, R.E., 2005. Protein modifications by 4-hydroxynonenal and 4-hydroxyhexenal in light-exposed rat retina. *Investigative Ophthalmology & Visual Science*, 46(10), pp.3859–3868.

Tansley, K., 1956. Comparison of the lamina cribrosa in mammalian species with good and with indifferent vision. *The British Journal of Ophthalmology*, 40(3), p.178.

Taylor, W., and Smith, R., 2012. The role of starburst amacrine cells in visual signal processing. *Visual Neuroscience*, 29(01), pp.73–81.

Templeton, J.P., Nassr, M., Vazquez-Chona, F., Freeman-Anderson, N.E., Orr, W.E.,

Williams, R.W., and Geisert, E.E., 2009. Differential response of C57BL/6J mouse and DBA/2J mouse to optic nerve crush. *BMC Neuroscience*, 10(1), p.1.

Tezel, G., 2006. Oxidative stress in glaucomatous neurodegeneration: mechanisms and consequences. *Progress in Retinal and Eye Research*, 25(5), pp.490–513.

Thach, A.B., Johnson, A.J., Carroll, R.B., Huchun, A., Ainbinder, D.J., Stutzman, R.D., Blaydon, S.M., DeMartelaere, S.L., Mader, T.H., Slade, C.S., and others 2008. Severe eye injuries in the war in Iraq, 2003–2005. *Ophthalmology*, 115(2), pp.377–382.

Tong, D., and Verkman, AS., 2004. Aquaporin-4 gene disruption in mice protects against impaired retinal function and cell death after ischemia. *Investigative Ophthalmology & Visual Science*, 45(12), pp.4477–4483.

Topper, J.N., Cai, J., Falb, D., and Gimbrone, M.A., 1996. Identification of vascular endothelial genes differentially responsive to fluid mechanical stimuli: cyclooxygenase-2, manganese superoxide dismutase, and endothelial cell nitric oxide synthase are selectively up-regulated by steady laminar shear stress. *Proceedings of the National Academy of Sciences*, 93(19), pp.10417–10422.

Traub, O., and Berk, B.C., 1998. Laminar shear stress mechanisms by which endothelial cells transduce an atheroprotective force. *Arteriosclerosis, Thrombosis, and Vascular Biology*, 18(5), pp.677–685.

Trichonas, G., Murakami, Y., Thanos, A., Morizane, Y., Kayama, M., Debouck, C.M., Hisatomi, T., Miller, J.W., and Vavvas, D.G., 2010. Receptor interacting protein kinases mediate retinal detachment-induced photoreceptor necrosis and compensate for inhibition of apoptosis. *Proceedings of the National Academy of Sciences*, 107(50), pp.21695–21700.

Tsai, J.C., Wu, L., Worgul, B., Forbes, M., and Cao, J., 2005. Intravitreal administration of erythropoietin and preservation of retinal ganglion cells in an experimental rat model of glaucoma. *Current Eye Research*, 30(11), pp.1025–1031.

Tsakiri, N., Kimber, I., Rothwell, N.J., and Pinteaux, E., 2008. Differential effects of interleukin-1 alpha and beta on interleukin-6 and chemokine synthesis in neurons. *Molecular and Cellular Neuroscience*, 38(2), pp.259–265.

Tyurin, V.A., Tyurina, Y.Y., Borisenko, G.G., Sokolova, T.V., Ritov, V.B., Quinn, P.J., Rose, M., Kochanek, P., Graham, S.H., and Kagan, V.E., 2000. Oxidative stress following traumatic brain injury in rats. *Journal of Neurochemistry*, 75(5), pp.2178–2189.

Vatassery, G.T., Lai, J.C., DeMaster, E.G., Smith, W., and Quach, H.T., 2004. Oxidation of vitamin E and vitamin C and inhibition of brain mitochondrial oxidative phosphorylation by peroxynitrite. *Journal of Neuroscience Research*, 75(6), pp.845–853.

de Waal Malefyt, R., Abrams, J., Bennett, B., Figdor, C.G., and De Vries, J.E., 1991. Interleukin 10 (IL-10) inhibits cytokine synthesis by human monocytes: an autoregulatory role of IL-10 produced by monocytes. *The Journal of Experimental Medicine*, 174(5), pp.1209–1220.

Wang, H.C.H., Choi, J.H., Greene, W.A., Plamper, M.L., Cortez, H.E., Chavko, M., Li, Y., Dalle Lucca, J.J., and Johnson, A.J., 2014. Pathophysiology of blast-induced ocular trauma with apoptosis in the retina and optic nerve. *Military Medicine*, 179(8S), pp.34–40.

Wang, Q., Pfister, F., Dorn-Beineke, A., vom Hagen, F., Lin, J., Feng, Y., and Hammes, H.P., 2010. Low-dose erythropoietin inhibits oxidative stress and early vascular changes in the experimental diabetic retina. *Diabetologia*, 53(6), pp.1227–1238.

Warner, N., and Eggenberger, E., 2010. Traumatic optic neuropathy: a review of the current literature. *Current Opinion in Ophthalmology*, 21(6), pp.459–462.

Weichel, E.D., and Colyer, M.H., 2008. Combat ocular trauma and systemic injury. *Current Opinion in Ophthalmology*, 19(6), pp.519–525.

Weichel, E.D., Colyer, M.H., Bautista, C., Bower, K.S., and French, L.M., 2009. Traumatic brain injury associated with combat ocular trauma. *The Journal of Head Trauma Rehabilitation*, 24(1), pp.41–50.

Weichel, E.D., Colyer, M.H., Ludlow, S.E., Bower, K.S., and Eiseman, A.S., 2008. Combat ocular trauma visual outcomes during Operations Iraqi and Enduring Freedom. *Ophthalmology*, 115(12), pp.2235–2245.

Weishaupt, J.H., Rohde, G., Pölking, E., Siren, A.L., Ehrenreich, H., and Bähr, M., 2004. Effect of erythropoietin axotomy-induced apoptosis in rat retinal ganglion cells. *Investigative Ophthalmology & Visual Science*, 45(5), pp.1514–1522.

Weitlauf, C., Ward, N.J., Lambert, W.S., Sidorova, T.N., Ho, K.W., Sappington, R.M., and Calkins, D.J., 2014. Short-term increases in transient receptor potential vanilloid-1 mediate stress-induced enhancement of neuronal excitation. *The Journal of Neuroscience*, 34(46), pp.15369–15381.

Wenzel, A., Remé, C.E., Williams, T.P., Hafezi, F., and Grimm, C., 2001. The Rpe65 Leu450Met variation increases retinal resistance against light-induced degeneration by slowing rhodopsin regeneration. *The Journal of Neuroscience*, 21(1), pp.53–58.

Wetsel, R., Fleischer, D.T., and Haviland, D., 1990. Deficiency of the murine fifth complement component (C5). A 2-base pair gene deletion in a 5’-exon. *Journal of Biological Chemistry*, 265(5), pp.2435–2440.

Wilhelm, B.T., Landry, J.R., Takei, F., and Mager, D.L., 2003. Transcriptional control of murine CD94 gene: differential usage of dual promoters by lymphoid cell types. *The Journal of Immunology*, 171(8), pp.4219–4226.

Wolf, A., Eulenfeld, R., Gäbler, K., Rolvering, C., Haan, S., Behrmann, I., Denecke, B., Haan, C., and Schaper, F., 2013. JAK2-V617F-induced MAPK activity is regulated by PI3K and acts synergistically with PI3K on the proliferation of JAK2-V617F-positive cells. *JAK-STAT*, 2(3), p.e24574.

Woodford, B.J., Tso, M., and Lam, K., 1983. Reduced and oxidized ascorbates in guinea pig retina under normal and light-exposed conditions. *Investigative Ophthalmology & Visual Science*, 24(7), pp.862–867.

Xia, T., Bauza, A.M., Soni, N., Zarbin, M.A., Langer, P.D. and Bhagat, N., 2015. Open globe injuries requiring pars plana vitrectomy at an urban hospital: retrospective review of 10-year experience. *Investigative Ophthalmology & Visual Science*, *56*(7), pp.6041-6041.

Xie, Z., Wu, X., Qiu, Q., Gong, Y., Song, Y., Gu, Q., and Li, C., 2007. Expression pattern of erythropoietin and erythropoietin receptor in experimental model of retinal detachment. *Current Eye Research*, 32(9), pp.757–764.

Xiong, Y., Gu, Q., Peterson, P., Muizelaar, J.P., and Lee, C., 1997. Mitochondrial dysfunction and calcium perturbation induced by traumatic brain injury. *Journal of Neurotrauma*, 14(1), pp.23–34.

Xiong, Y., Mahmood, A., Meng, Y., Zhang, Y., Qu, C., Schallert, T., and Chopp, M., 2010. Delayed administration of erythropoietin reduces hippocampal cell loss, enhances angiogenesis and neurogenesis, and improves functional outcome following traumatic brain injury in rats: comparison of treatment with single dose and triple dose. *Journal of Neurosurgery*, 113(3), p.598.

Yatsiv, I., Grigoriadis, N., Simeonidou, C., Stahel, P.F., Schmidt, O.I., Alexandrovitch, A., Tsenter, J., and Shohami, E., 2005. Erythropoietin is neuroprotective, improves functional recovery, and reduces neuronal apoptosis and inflammation in a rodent model of experimental closed head injury. *The FASEB Journal*, 19(12), pp.1701–1703.

Yazihan, N., Uzuner, K., Salman, B., Vural, M., Koken, T., and Arslantas, A., 2008. Erythropoietin improves oxidative stress following spinal cord trauma in rats. *Injury*, 39(12), pp.1408–1413.

Yin, J., and Kuebler, W.M., 2010. Mechanotransduction by TRP channels: general concepts and specific role in the vasculature. *Cell Biochemistry and Biophysics*, 56(1), pp.1–18.

Yonekawa, Y., Hacker, H.D., Lehman, R.E., Beal, C.J., Veldman, P.B., Vyas, N.M.,

Shah, A.S., Wu, D., Eliott, D., Gardiner, M.F., and others 2014. Ocular blast injuries in mass-casualty incidents: the Marathon bombing in Boston, Massachusetts, and the fertilizer plant explosion in West, Texas. *Ophthalmology*, 121(9), pp.1670–1676.

Yoon, J.J., Green, C.R., O'Carroll, S.J., and Nicholson, L.F., 2010. Dose-dependent protective effect of connexin43 mimetic peptide against neurodegeneration in an ex vivo model of epileptiform lesion. *Epilepsy Research*, 92(2), pp.153–162.

Yoshida, K., Watanabe, D., Ishikane, H., Tachibana, M., Pastan, I., and Nakanishi, S., 2001. A key role of starburst amacrine cells in originating retinal directional selectivity and optokinetic eye movement. *Neuron*, 30(3), pp.771–780.

Zhang, D.W., Shao, J., Lin, J., Zhang, N., Lu, B.J., Lin, S.C., Dong, M.Q., and Han, J., 2009. RIP3, an energy metabolism regulator that switches TNF-induced cell death from apoptosis to necrosis. *Science*, 325(5938), pp.332–336.

Zheng, L., Du, Y., Miller, C., Gubitosi-Klug, R., Kern, T., Ball, S., and Berkowitz, B., 2007. Critical role of inducible nitric oxide synthase in degeneration of retinal capillaries in mice with streptozotocin-induced diabetes. *Diabetologia*, 50(9), pp.1987–1996.

Zhou, H., Chen, L., Gao, X., Luo, B., and Chen, J., 2012. Moderate traumatic brain injury triggers rapid necrotic death of immature neurons in the hippocampus. *Journal of Neuropathology & Experimental Neurology*, 71(4), pp.348–359.

Zhu, L., Zhong, M., Elder, G.A., Sano, M., Holtzman, D.M., Gandy, S., Cardozo, C., Haroutunian, V., Robakis, N.K., and Cai, D., 2015. Phospholipid dysregulation contributes to ApoE4-associated cognitive deficits in Alzheimer's disease pathogenesis. *Proceedings of the National Academy of Sciences*, 112(38), pp.11965–11970.

Zou, Y., Kan, E.M., Lu, J., Ng, K.C., Tan, M.H., Yao, L., and Ling, E.A., 2013. Primary blast injury-induced lesions in the retina of adult rats. *Journal of Neuroinflammation*, 10(1), p.1186.